Universidad de la República

Tesis de Maestría

Coding of Multichannel Signals with Irregular Sampling Rates and Data Gaps (Appendix)

Autor:
Pablo Cerveñansky

Supervisores:
Álvaro Martín
Gadiel Seroussi

Núcleo de Teoría de la Información
Facultad de Ingeniería

Introduction

This document includes each plot figure generated from the experimental results obtained in our work. In **Appendix A** we present the figures corresponding to Section 4.2 (Comparison of Masking and Non-Masking Variants). In **Appendix B** we present the figures corresponding to Section 4.3 (Window Size Parameter). Finally, in **Appendix C** we present the figures corresponding to Section 4.4 (Algorithm Compression Performance).

Table of Contents

Introduction **ii**

Table of Contents **ii**

List of Figures **iv**

A Figures: Comparison of Masking and Non-Masking Variants **1**

B Figures: Window Size Parameter **23**

C Figures: Algorithm Compression Performance **49**

List of Figures

A.1 CR and RD plots for variants a_M and a_{NM}, for each algorithm $a \in A_M$, for the data type "VWC" of the dataset IRKIS. 2

A.2 CR and RD plots for variants a_M and a_{NM}, for each algorithm $a \in A_M$, for the data type "SST" of the dataset SST. In the RD plot for algorithm PCA we highlight with a red circle the marker for the maximum value (50.78%) obtained for all the tested CAIs. 3

A.3 CR and RD plots for variants a_M and a_{NM}, for each algorithm $a \in A_M$, for the data type "Velocity" of the dataset ADCP. 4

A.4 CR and RD plots for variants a_M and a_{NM}, for each algorithm $a \in A_M$, for the data type "GHI" of the dataset Solar. 5

A.5 CR and RD plots for variants a_M and a_{NM}, for each algorithm $a \in A_M$, for the data type "DNI" of the dataset Solar. 6

A.6 CR and RD plots for variants a_M and a_{NM}, for each algorithm $a \in A_M$, for the data type "DHI" of the dataset Solar. 7

A.7 CR and RD plots for variants a_M and a_{NM}, for each algorithm $a \in A_M$, for the data type "Latitude" of the dataset ElNino. 8

A.8 CR and RD plots for variants a_M and a_{NM}, for each algorithm $a \in A_M$, for the data type "Longitude" of the dataset ElNino. 9

A.9 CR and RD plots for variants a_M and a_{NM}, for each algorithm $a \in A_M$, for the data type "Zon. Wind" of the dataset ElNino. 10

A.10 CR and RD plots for variants a_M and a_{NM}, for each algorithm $a \in A_M$, for the data type "Mer. Wind" of the dataset ElNino. 11

A.11 CR and RD plots for variants a_M and a_{NM}, for each algorithm $a \in A_M$, for the data type "Humidity" of the dataset ElNino. 12

A.12 CR and RD plots for variants a_M and a_{NM}, for each algorithm $a \in A_M$, for the data type "Air Temp." of the dataset ElNino. 13

A.13 CR and RD plots for variants a_M and a_{NM}, for each algorithm $a \in A_M$, for the data type "Sea Temp." of the dataset ElNino. 14

A.14 CR and RD plots for variants a_M and a_{NM}, for each algorithm $a \in A_M$, for the data type "Latitude" of the dataset Hail. 15

A.15 CR and RD plots for variants a_M and a_{NM}, for each algorithm $a \in A_M$, for the data type "Longitude" of the dataset Hail. 16

A.16 CR and RD plots for variants a_M and a_{NM}, for each algorithm $a \in A_M$, for the data type "Size" of the dataset Hail. 17

A.17 CR and RD plots for variants a_M and a_{NM}, for each algorithm $a \in A_M$, for the data type "Latitude" of the dataset Tornado. 18

A.18 CR and RD plots for variants a_M and a_{NM}, for each algorithm $a \in A_M$, for the data type "Longitude" of the dataset Tornado. In the RD plot for algorithm APCA we highlight with a blue circle the marker for the minimum value (-0.29%) obtained for all the tested CAIs. 19

A.19 CR and RD plots for variants a_M and a_{NM}, for each algorithm $a \in A_M$, for the data type "Latitude" of the dataset Wind. 20

A.20 CR and RD plots for variants a_M and a_{NM}, for each algorithm $a \in A_M$, for the data type "Longitude" of the dataset Wind. 21

A.21 CR and RD plots for variants a_M and a_{NM}, for each algorithm $a \in A_M$, for the data type "Speed" of the dataset Wind. 22

B.1 Plots of w^*_{global}, w^*_{local}, and the RD between $c_{<a_v,w^*_{global},e>}$ and $c_{<a_v,w^*_{local},e>}$, as a function of the error parameter e, obtained for the data type "VWC" of the file "irkis-1202.csv" of the dataset IRKIS. 24

B.2 Plots of w^*_{global}, w^*_{local}, and the RD between $c_{<a_v,w^*_{global},e>}$ and $c_{<a_v,w^*_{local},e>}$, as a function of the error parameter e, obtained for the data type "VWC" of the file "irkis-1203.csv" of the dataset IRKIS. In the RD plot for variant PCA_M we highlight with a red circle the marker for the maximum value (10.6%) obtained for all the tested CAIs. 25

B.3 Plots of w^*_{global}, w^*_{local}, and the RD between $c_{<a_v,w^*_{global},e>}$ and $c_{<a_v,w^*_{local},e>}$, as a function of the error parameter e, obtained for the data type "VWC" of the file "irkis-1204.csv" of the dataset IRKIS. 26

B.4 Plots of w^*_{global}, w^*_{local}, and the RD between $c_{<a_v,w^*_{global},e>}$ and $c_{<a_v,w^*_{local},e>}$, as a function of the error parameter e, obtained for the data type "VWC" of the file "irkis-1205.csv" of the dataset IRKIS. 27

B.5 Plots of w^*_{global}, w^*_{local}, and the RD between $c_{<a_v,w^*_{global},e>}$ and $c_{<a_v,w^*_{local},e>}$, as a function of the error parameter e, obtained for the data type "VWC" of the file "irkis-222.csv" of the dataset IRKIS. 28

B.6 Plots of w^*_{global}, w^*_{local}, and the RD between $c_{<a_v,w^*_{global},e>}$ and $c_{<a_v,w^*_{local},e>}$, as a function of the error parameter e, obtained for the data type "VWC" of the file "irkis-333.csv" of the dataset IRKIS. 29

B.7 Plots of w^*_{global}, w^*_{local}, and the RD between $c_{<a_v,w^*_{global},e>}$ and $c_{<a_v,w^*_{local},e>}$, as a function of the error parameter e, obtained for the data type "VWC" of the file "irkis-SLF2.csv" of the dataset IRKIS. 30

B.8 Plots of w^*_{global}, w^*_{local}, and the RD between $c_{<a_v,w^*_{global},e>}$ and $c_{<a_v,w^*_{local},e>}$, as a function of the error parameter e, obtained for the data type "SST" of the file "sst-01-2017.csv" of the dataset SST. 31

B.9 Plots of w^*_{global}, w^*_{local}, and the RD between $c_{<a_v,w^*_{global},e>}$ and $c_{<a_v,w^*_{local},e>}$, as a function of the error parameter e, obtained for the data type "SST" of the file "sst-02-2017.csv" of the dataset SST. 32

B.10 Plots of w^*_{global}, w^*_{local}, and the RD between $c_{<a_v,w^*_{global},e>}$ and $c_{<a_v,w^*_{local},e>}$, as a function of the error parameter e, obtained for the data type "SST" of the file "sst-03-2017.csv" of the dataset SST. 33

B.11 Plots of w^*_{global}, w^*_{local}, and the RD between $c_{<a_v,w^*_{global},e>}$ and $c_{<a_v,w^*_{local},e>}$, as a function of the error parameter e, obtained for the data type "Velocity" of the file "adcp-01-2015.csv" of the dataset SST. 34

B.12 Plots of w^*_{global}, w^*_{local}, and the RD between $c_{<a_v,w^*_{global},e>}$ and $c_{<a_v,w^*_{local},e>}$, as a function of the error parameter e, obtained for the data type "Velocity" of the file "adcp-02-2015.csv" of the dataset SST. 35

B.13 Plots of w^*_{global}, w^*_{local}, and the RD between $c_{<a_v,w^*_{global},e>}$ and $c_{<a_v,w^*_{local},e>}$, as a function of the error parameter e, obtained for the data type "Velocity" of the file "adcp-03-2015.csv" of the dataset SST. 36

B.14 Plots of w^*_{global}, w^*_{local}, and the RD between $c_{<a_v,w^*_{global},e>}$ and $c_{<a_v,w^*_{local},e>}$, as a function of the error parameter e, obtained for the data type "GHI" of the file "solar-2011.csv" of the dataset Solar. 37

B.15 Plots of w^*_{global}, w^*_{local}, and the RD between $c_{<a_v,w^*_{global},e>}$ and $c_{<a_v,w^*_{local},e>}$, as a function of the error parameter e, obtained for the data type "DNI" of the file "solar-2011.csv" of the dataset Solar. 38

B.16 Plots of w^*_{global}, w^*_{local}, and the RD between $c_{<a_v,w^*_{global},e>}$ and $c_{<a_v,w^*_{local},e>}$, as a function of the error parameter e, obtained for the data type "DHI" of the file "solar-2011.csv" of the dataset Solar. 39

B.17 Plots of w^*_{global}, w^*_{local}, and the RD between $c_{<a_v,w^*_{global},e>}$ and $c_{<a_v,w^*_{local},e>}$, as a function of the error parameter e, obtained for the data type "GHI" of the file "solar-2012.csv" of the dataset Solar. 40
B.18 Plots of w^*_{global}, w^*_{local}, and the RD between $c_{<a_v,w^*_{global},e>}$ and $c_{<a_v,w^*_{local},e>}$, as a function of the error parameter e, obtained for the data type "DNI" of the file "solar-2012.csv" of the dataset Solar. 41
B.19 Plots of w^*_{global}, w^*_{local}, and the RD between $c_{<a_v,w^*_{global},e>}$ and $c_{<a_v,w^*_{local},e>}$, as a function of the error parameter e, obtained for the data type "DHI" of the file "solar-2012.csv" of the dataset Solar. 42
B.20 Plots of w^*_{global}, w^*_{local}, and the RD between $c_{<a_v,w^*_{global},e>}$ and $c_{<a_v,w^*_{local},e>}$, as a function of the error parameter e, obtained for the data type "GHI" of the file "solar-2013.csv" of the dataset Solar. 43
B.21 Plots of w^*_{global}, w^*_{local}, and the RD between $c_{<a_v,w^*_{global},e>}$ and $c_{<a_v,w^*_{local},e>}$, as a function of the error parameter e, obtained for the data type "DNI" of the file "solar-2013.csv" of the dataset Solar. 44
B.22 Plots of w^*_{global}, w^*_{local}, and the RD between $c_{<a_v,w^*_{global},e>}$ and $c_{<a_v,w^*_{local},e>}$, as a function of the error parameter e, obtained for the data type "DHI" of the file "solar-2013.csv" of the dataset Solar. 45
B.23 Plots of w^*_{global}, w^*_{local}, and the RD between $c_{<a_v,w^*_{global},e>}$ and $c_{<a_v,w^*_{local},e>}$, as a function of the error parameter e, obtained for the data type "GHI" of the file "solar-2014.csv" of the dataset Solar. 46
B.24 Plots of w^*_{global}, w^*_{local}, and the RD between $c_{<a_v,w^*_{global},e>}$ and $c_{<a_v,w^*_{local},e>}$, as a function of the error parameter e, obtained for the data type "DNI" of the file "solar-2014.csv" of the dataset Solar. 47
B.25 Plots of w^*_{global}, w^*_{local}, and the RD between $c_{<a_v,w^*_{global},e>}$ and $c_{<a_v,w^*_{local},e>}$, as a function of the error parameter e, obtained for the data type "DHI" of the file "solar-2014.csv" of the dataset Solar. 48

C.1 CR and window size parameter plots for every evaluated algorithm, for the data type "VWC" of the dataset IRKIS. 50
C.2 CR and window size parameter plots for every evaluated algorithm, for the data type "SST" of the dataset SST. 51
C.3 CR and window size parameter plots for every evaluated algorithm, for the data type "Velocity" of the dataset ADCP. 52
C.4 CR and window size parameter plots for every evaluated algorithm, for the data type "GHI" of the dataset Solar. 53
C.5 CR and window size parameter plots for every evaluated algorithm, for the data type "DNI" of the dataset Solar. 54
C.6 CR and window size parameter plots for every evaluated algorithm, for the data type "DHI" of the dataset Solar. 55
C.7 CR and window size parameter plots for every evaluated algorithm, for the data type "Latitude" of the dataset ElNino. 56
C.8 CR and window size parameter plots for every evaluated algorithm, for the data type "Longitude" of the dataset ElNino. 57
C.9 CR and window size parameter plots for every evaluated algorithm, for the data type "Zon. Wind" of the dataset ElNino. 58
C.10 CR and window size parameter plots for every evaluated algorithm, for the data type "Mer. Wind" of the dataset ElNino. 59
C.11 CR and window size parameter plots for every evaluated algorithm, for the data type "Humidity" of the dataset ElNino. 60
C.12 CR and window size parameter plots for every evaluated algorithm, for the data type "Air Temp." of the dataset ElNino. 61

C.13 CR and window size parameter plots for every evaluated algorithm, for the data type "Sea Temp." of the dataset ElNino. For each error parameter $e \in E$, we use blue circles to highlight the markers for the minimum CR value and the best window size (in the respective plots corresponding to the best coding variant). . 62
C.14 CR and window size parameter plots for every evaluated algorithm, for the data type "Latitude" of the dataset Hail. 63
C.15 CR and window size parameter plots for every evaluated algorithm, for the data type "Longitude" of the dataset Hail. 64
C.16 CR and window size parameter plots for every evaluated algorithm, for the data type "Size" of the dataset Hail. 65
C.17 CR and window size parameter plots for every evaluated algorithm, for the data type "Latitude" of the dataset Tornado. 66
C.18 CR and window size parameter plots for every evaluated algorithm, for the data type "Longitude" of the dataset Tornado. 67
C.19 CR and window size parameter plots for every evaluated algorithm, for the data type "Latitude" of the dataset Wind. 68
C.20 CR and window size parameter plots for every evaluated algorithm, for the data type "Longitude" of the dataset Wind. 69
C.21 CR and window size parameter plots for every evaluated algorithm, for the data type "Speed" of the dataset Wind. 70

Appendix A

Figures: Comparison of Masking and Non-Masking Variants

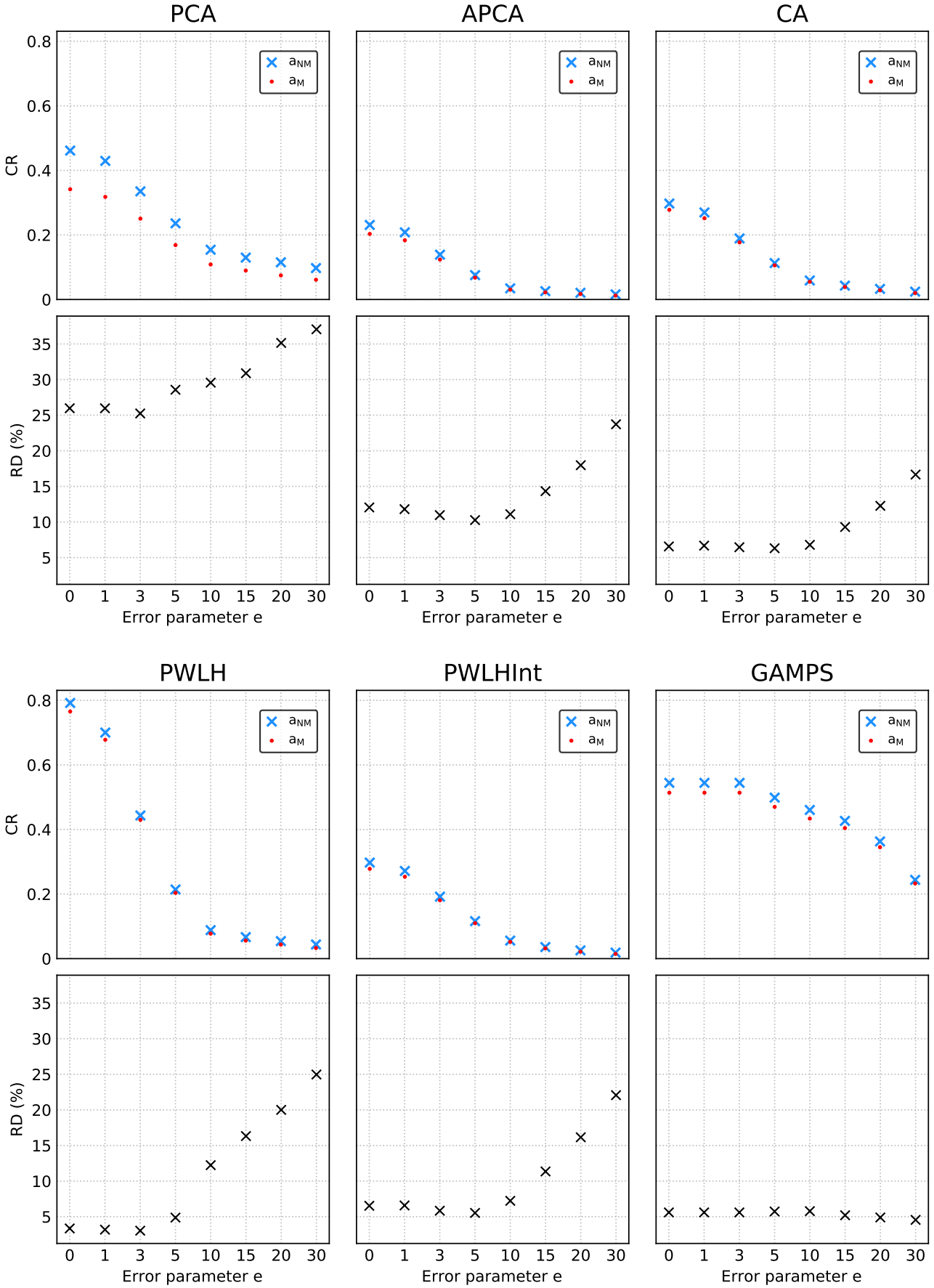

FIGURE A.1: CR and RD plots for variants a_M and a_{NM}, for each algorithm $a \in A_M$, for the data type "VWC" of the dataset IRKIS.

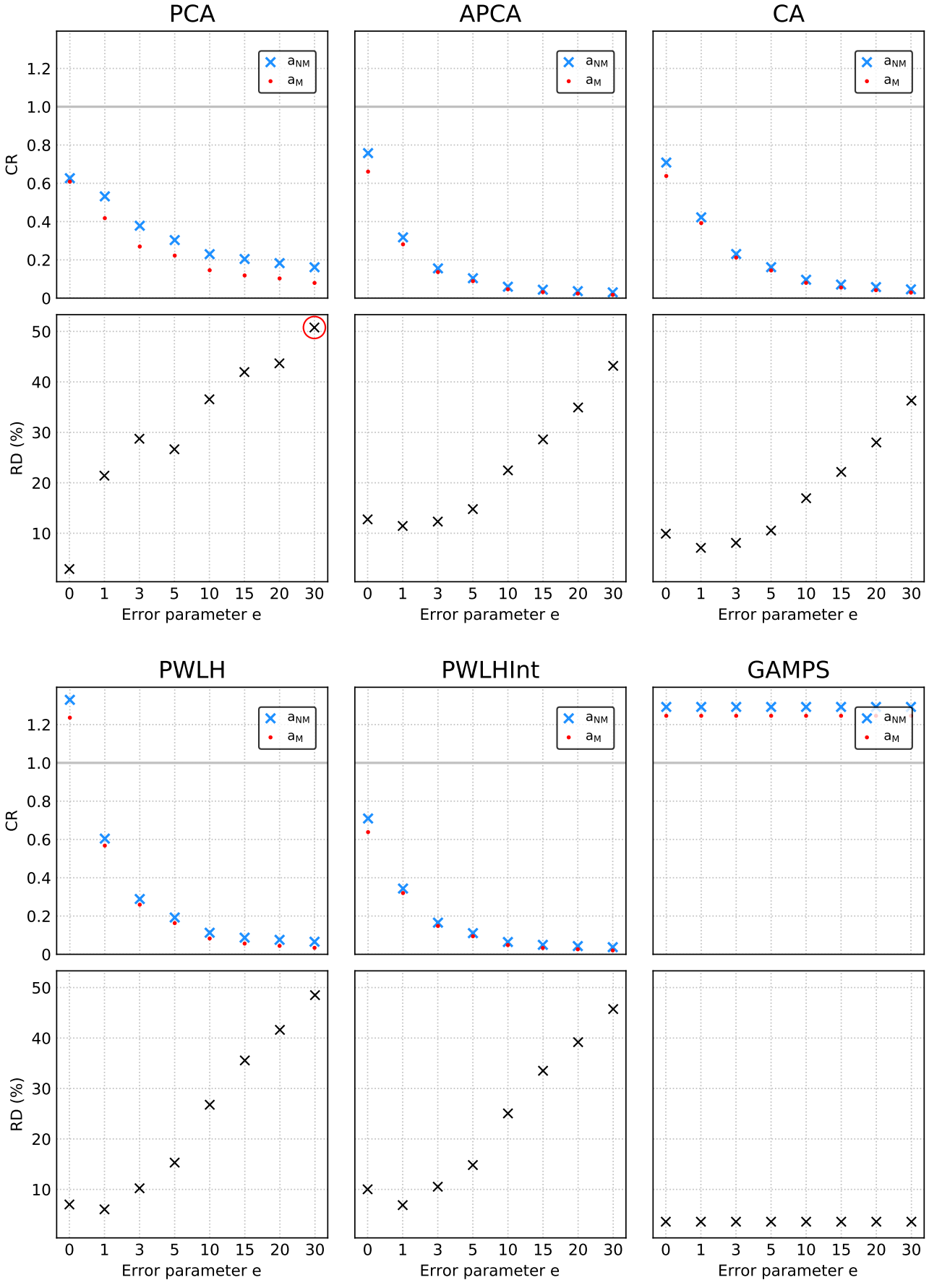

FIGURE A.2: CR and RD plots for variants a_M and a_{NM}, for each algorithm $a \in A_M$, for the data type "SST" of the dataset SST. In the RD plot for algorithm PCA we highlight with a red circle the marker for the maximum value (50.78%) obtained for all the tested CAIs.

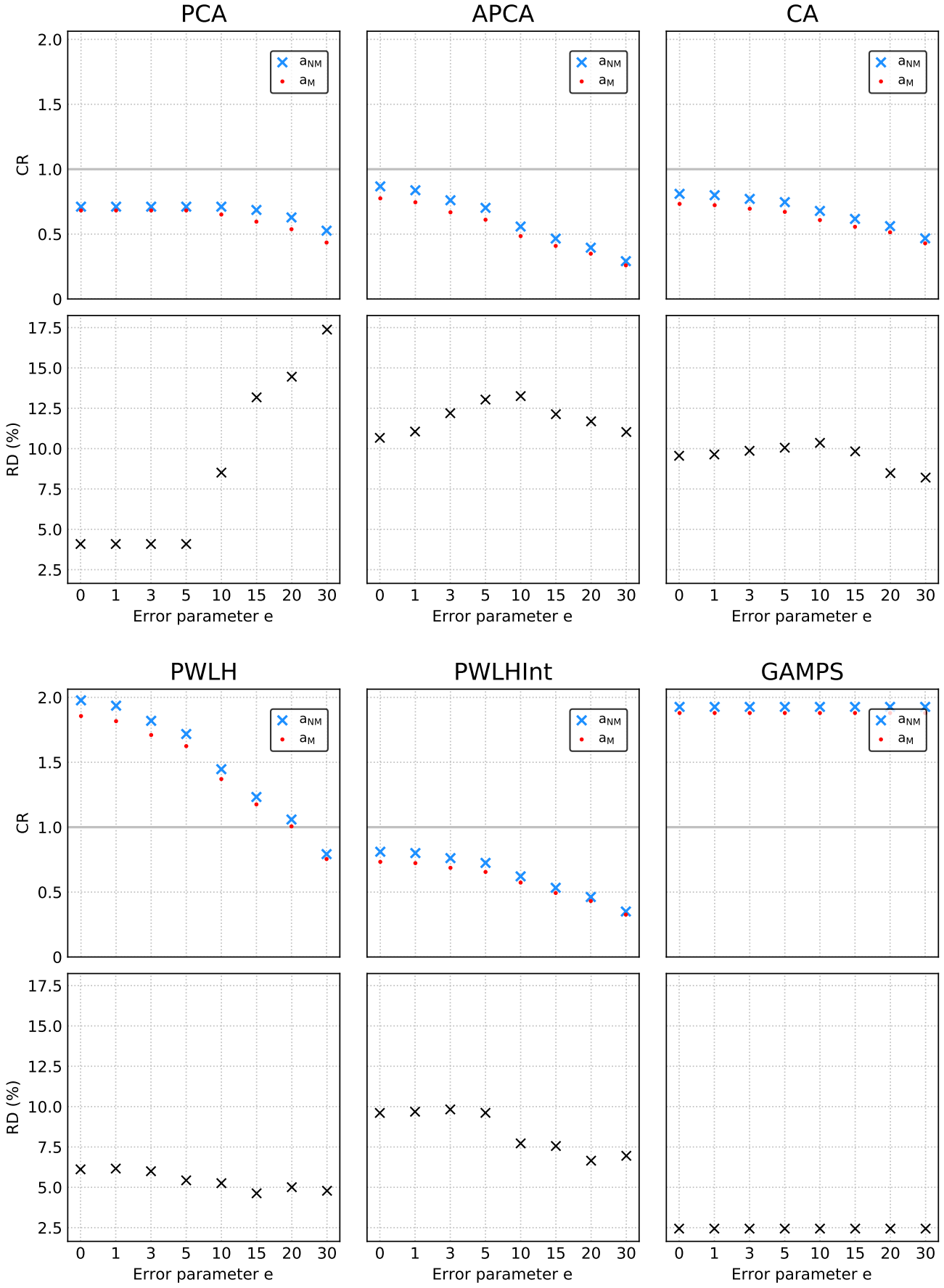

FIGURE A.3: CR and RD plots for variants a_M and a_{NM}, for each algorithm $a \in A_M$, for the data type "Velocity" of the dataset ADCP.

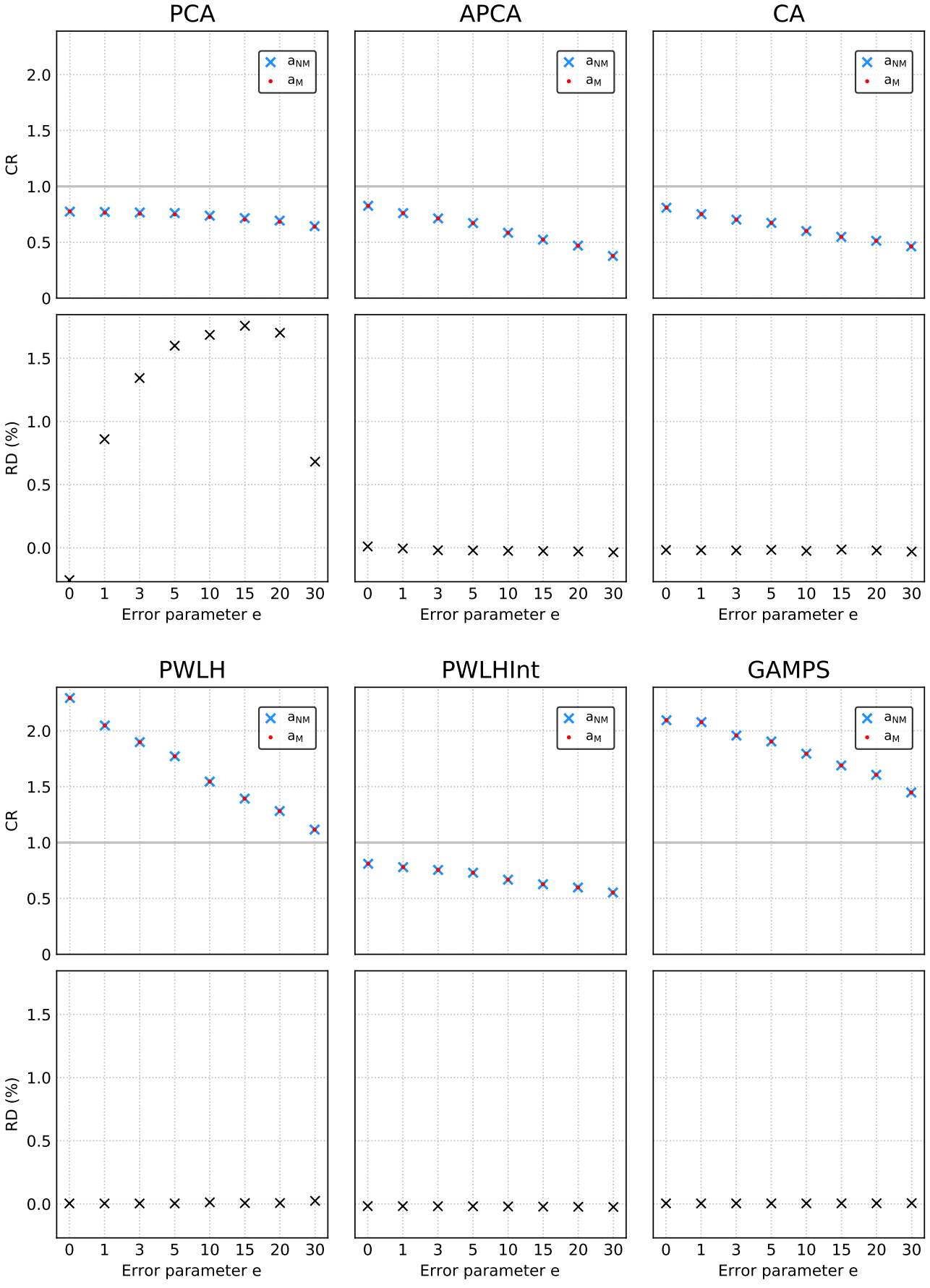

FIGURE A.4: CR and RD plots for variants a_M and a_{NM}, for each algorithm $a \in A_M$, for the data type "GHI" of the dataset Solar.

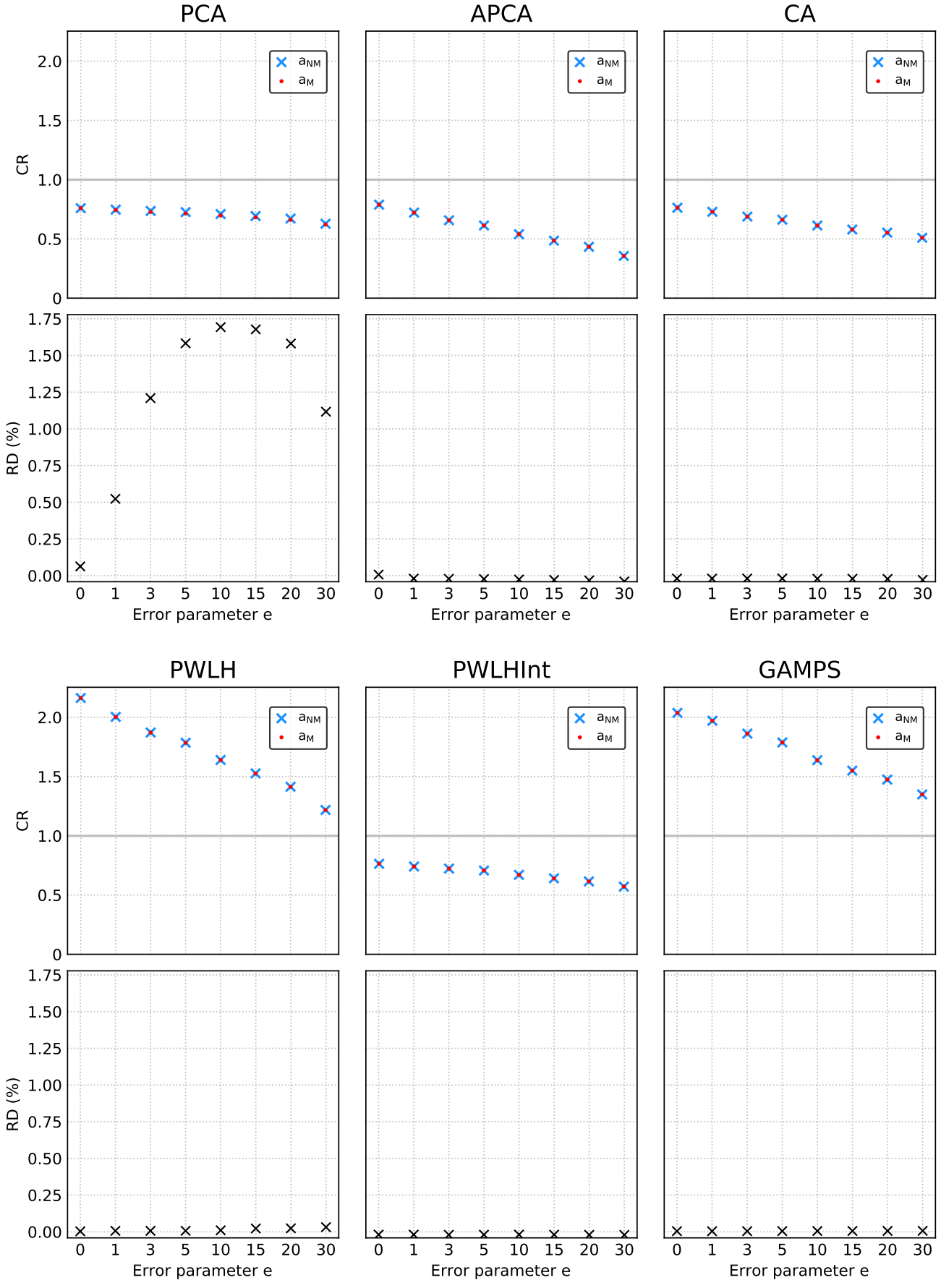

FIGURE A.5: CR and RD plots for variants a_M and a_{NM}, for each algorithm $a \in A_M$, for the data type "DNI" of the dataset Solar.

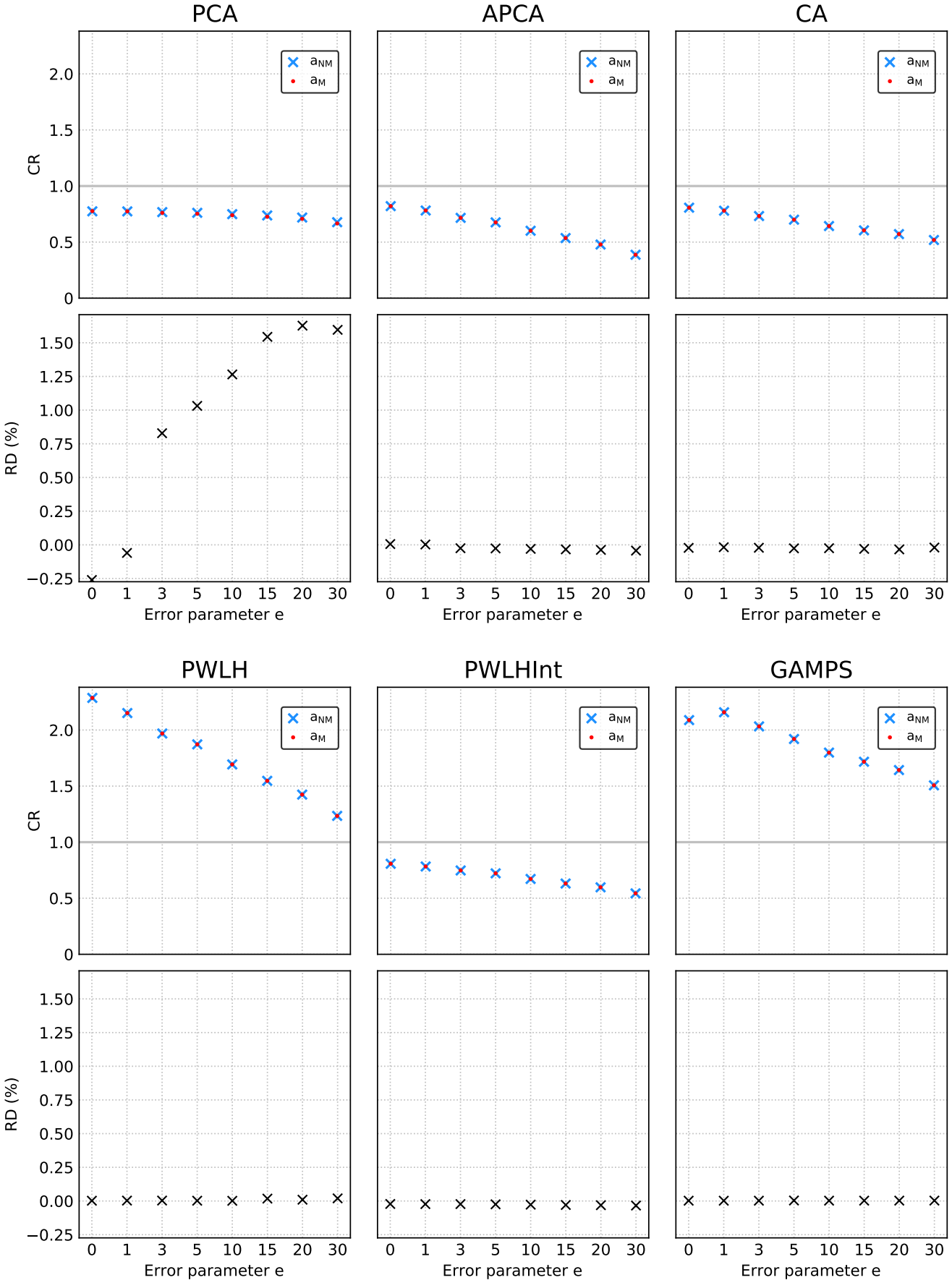

FIGURE A.6: CR and RD plots for variants a_M and a_{NM}, for each algorithm $a \in A_M$, for the data type "DHI" of the dataset Solar.

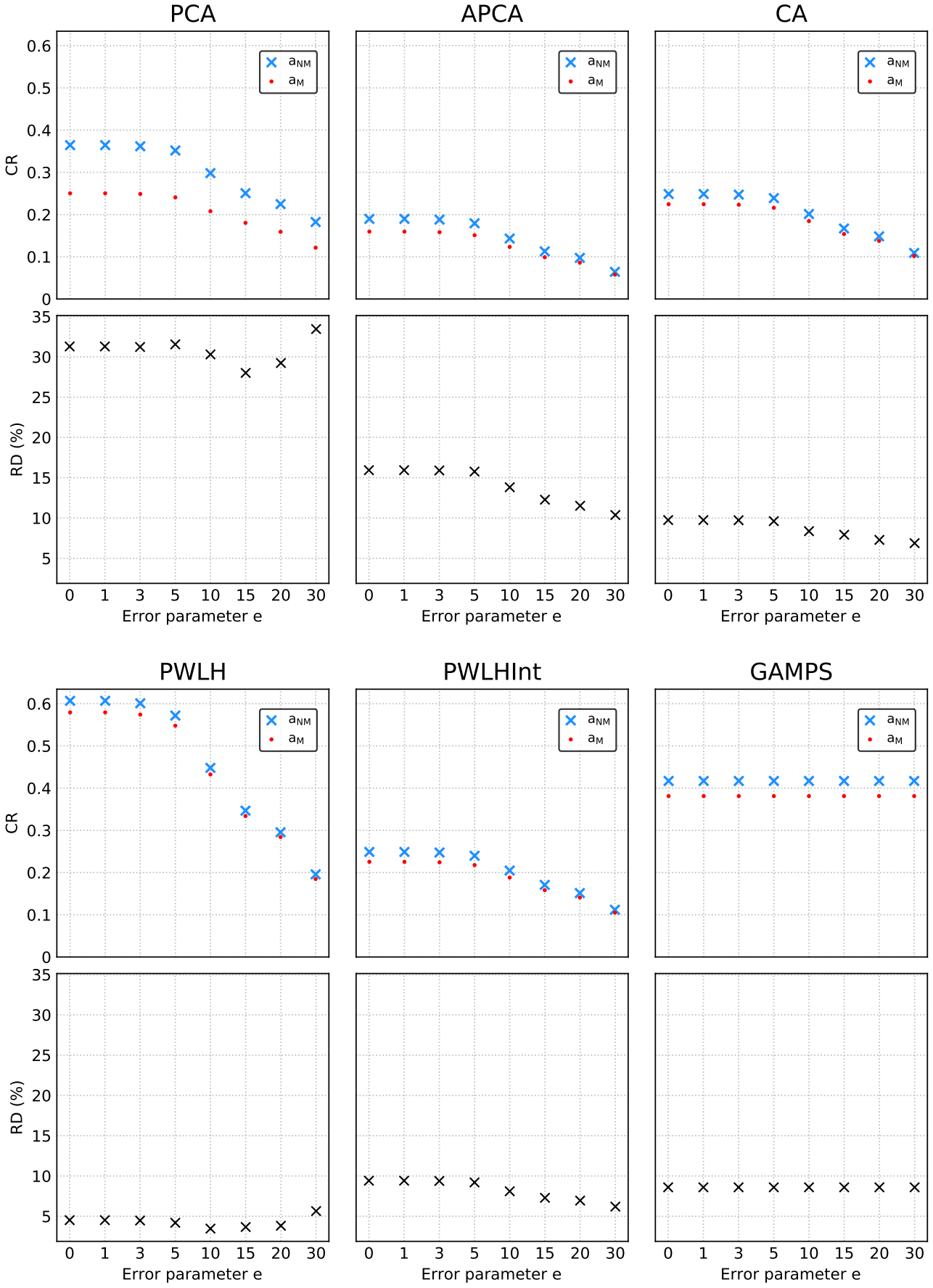

FIGURE A.7: CR and RD plots for variants a_M and a_{NM}, for each algorithm $a \in A_M$, for the data type "Latitude" of the dataset ElNino.

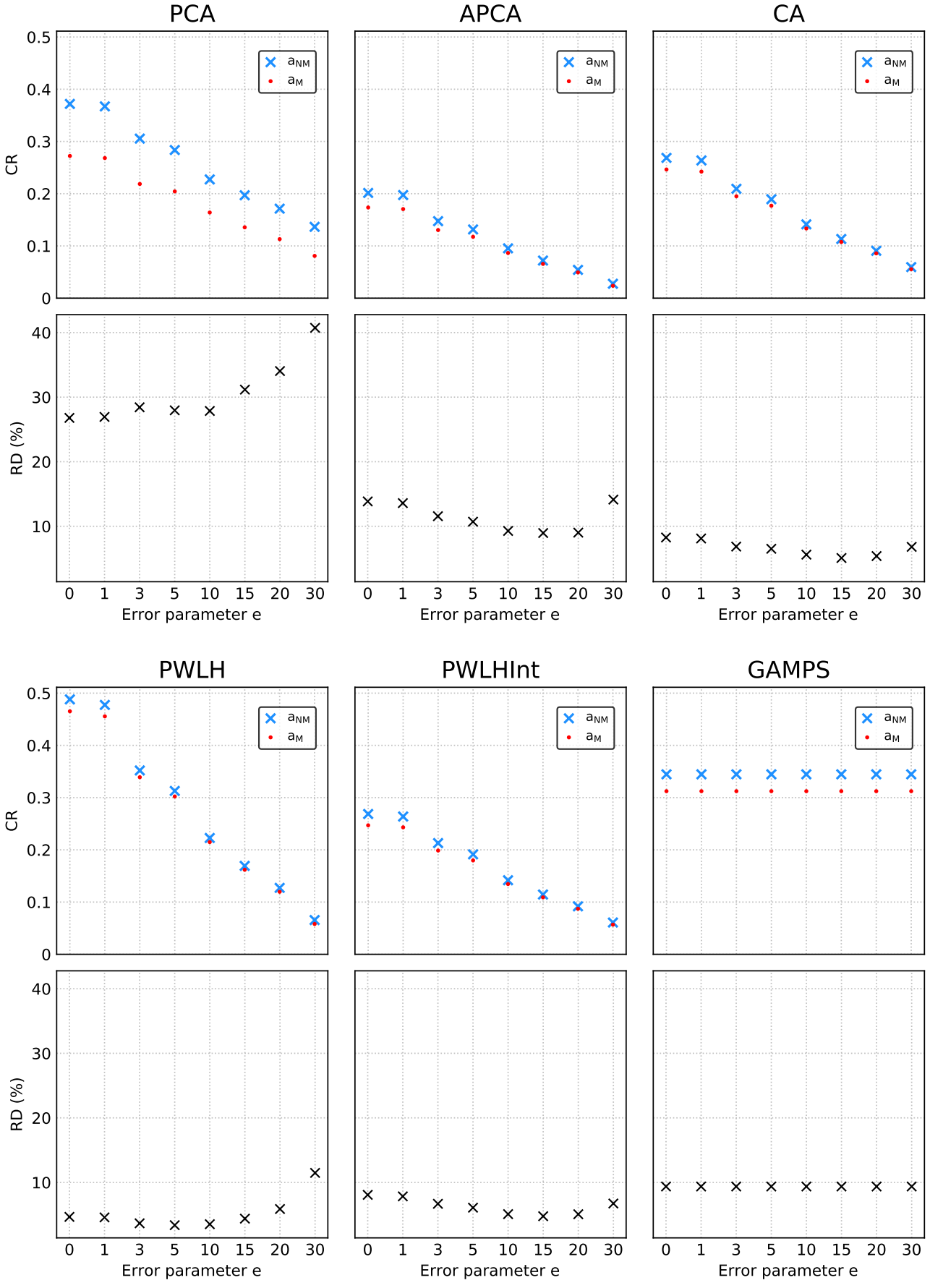

FIGURE A.8: CR and RD plots for variants a_M and a_{NM}, for each algorithm $a \in A_M$, for the data type "Longitude" of the dataset ElNino.

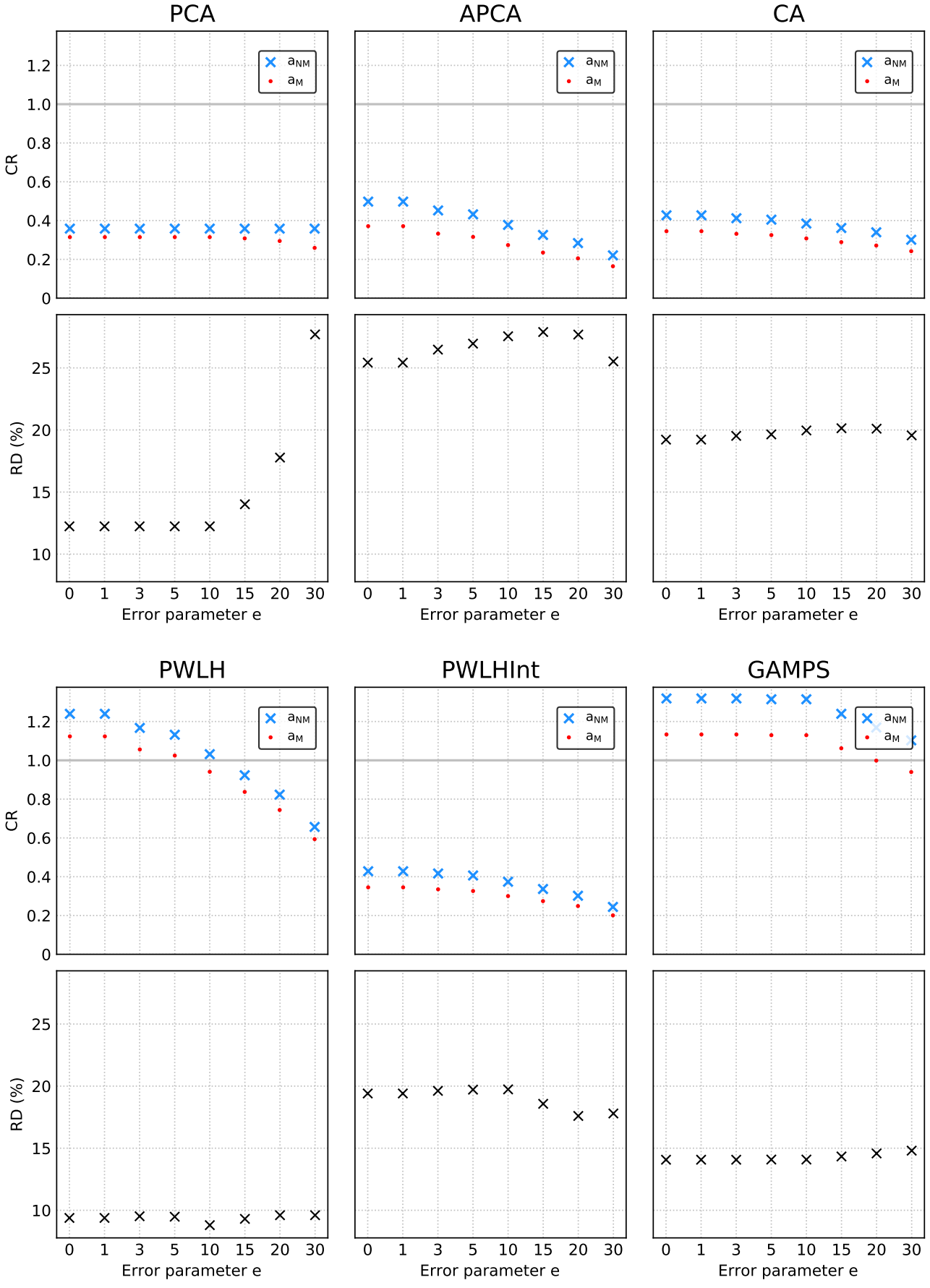

FIGURE A.9: CR and RD plots for variants a_M and a_{NM}, for each algorithm $a \in A_M$, for the data type "Zon. Wind" of the dataset ElNino.

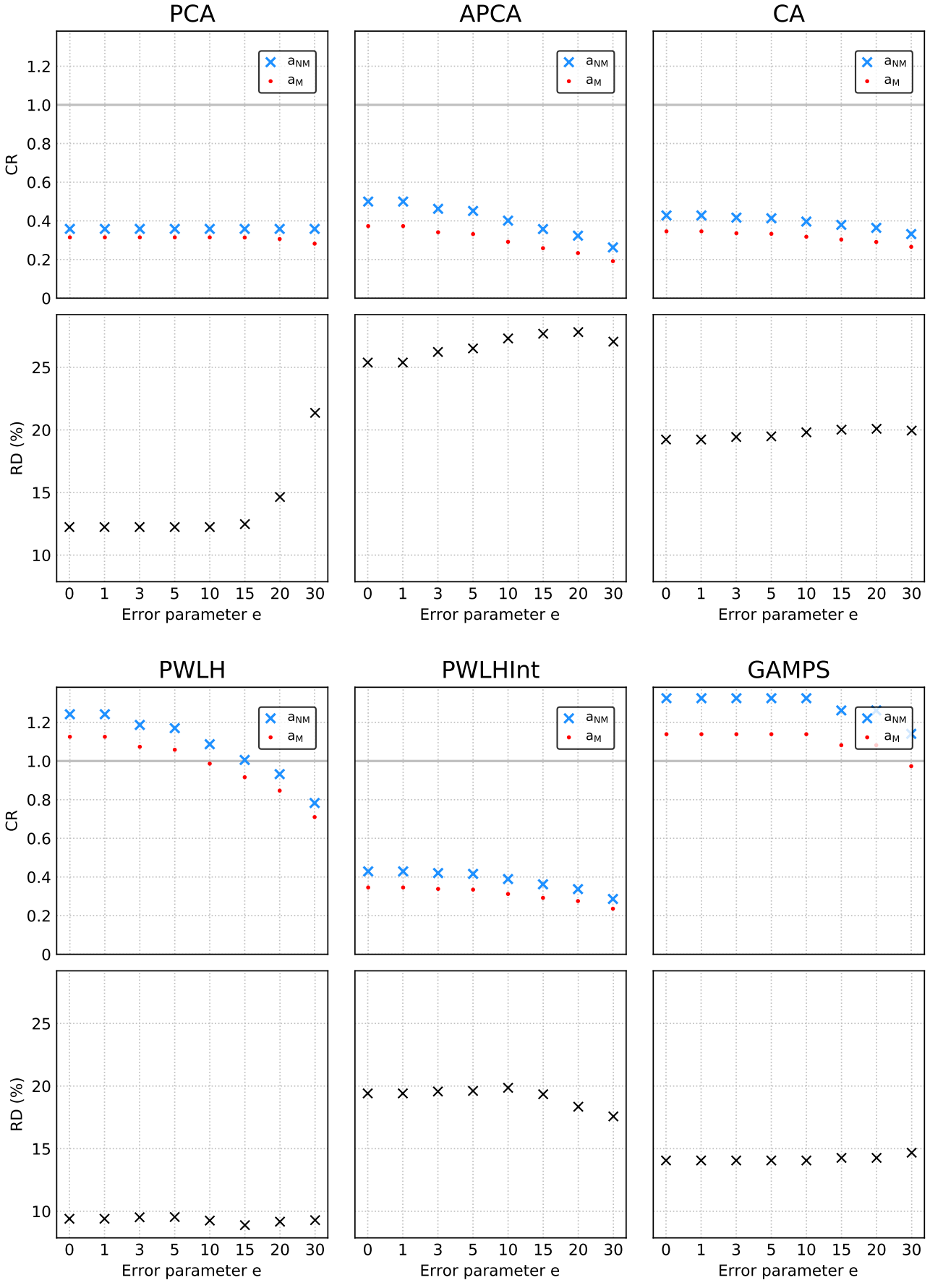

FIGURE A.10: CR and RD plots for variants a_M and a_{NM}, for each algorithm $a \in A_M$, for the data type "Mer. Wind" of the dataset ElNino.

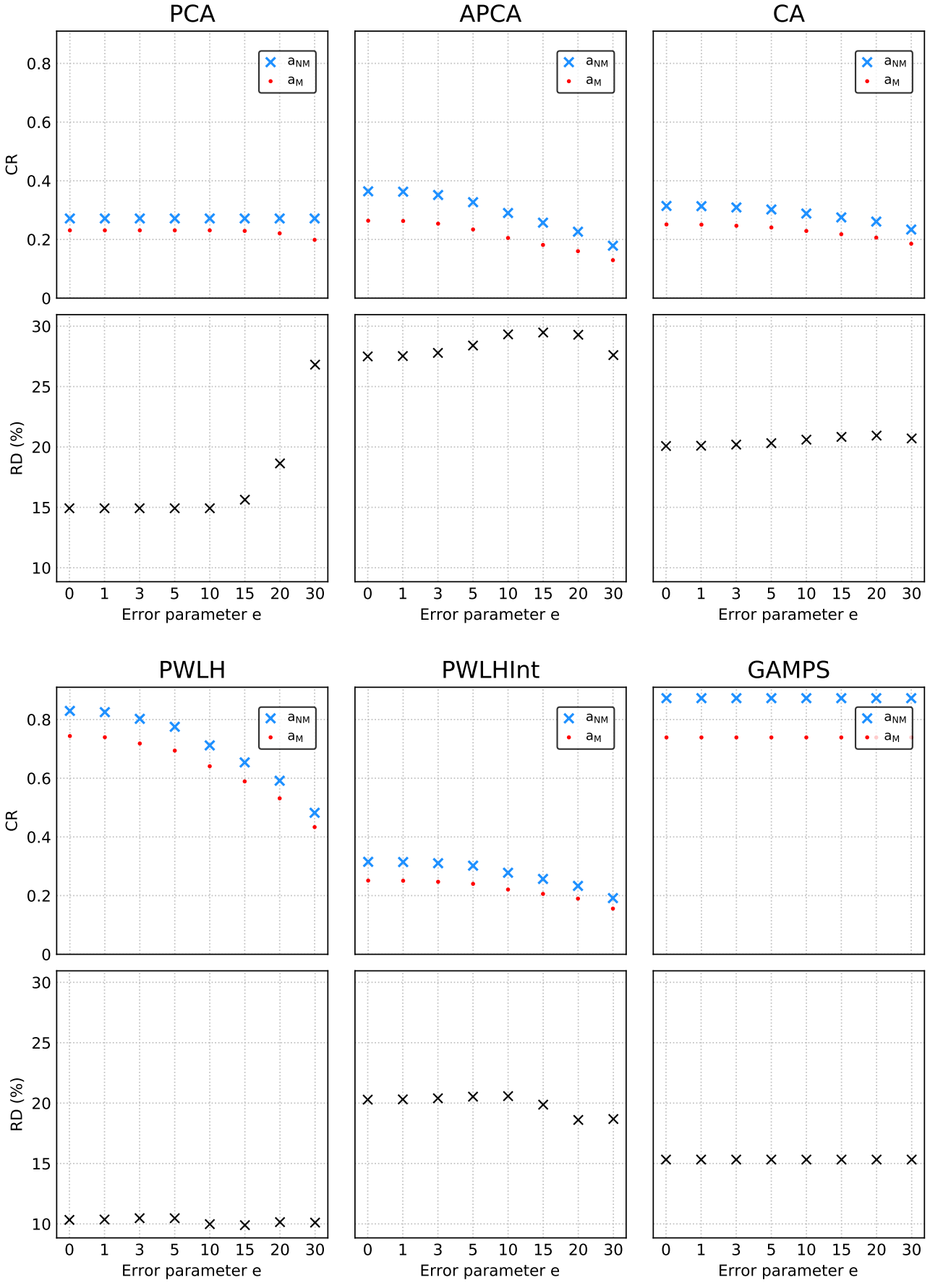

FIGURE A.11: CR and RD plots for variants a_M and a_{NM}, for each algorithm $a \in A_M$, for the data type "Humidity" of the dataset ElNino.

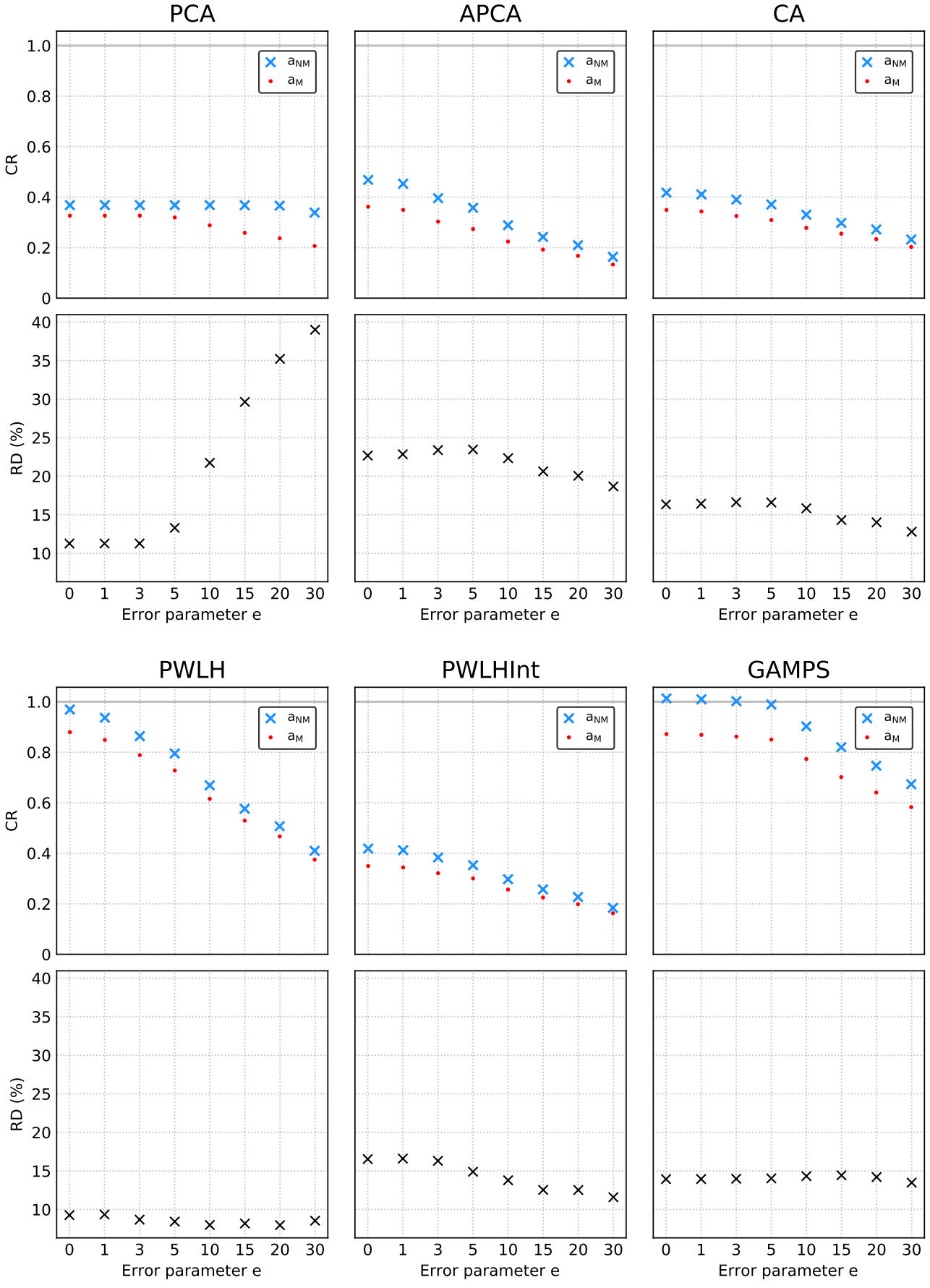

FIGURE A.12: CR and RD plots for variants a_M and a_{NM}, for each algorithm $a \in A_M$, for the data type "Air Temp." of the dataset ElNino.

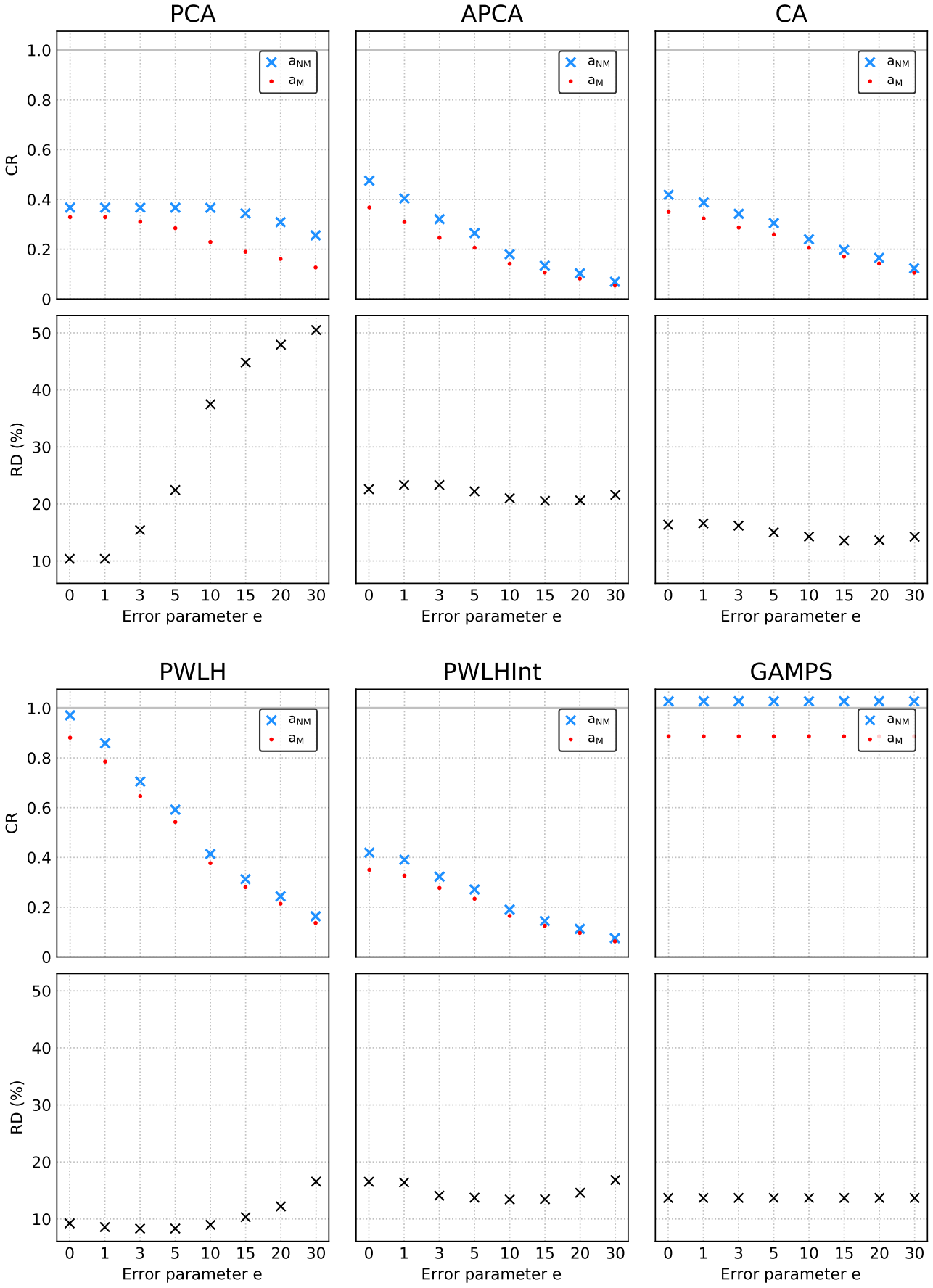

FIGURE A.13: CR and RD plots for variants a_M and a_{NM}, for each algorithm $a \in A_M$, for the data type "Sea Temp." of the dataset ElNino.

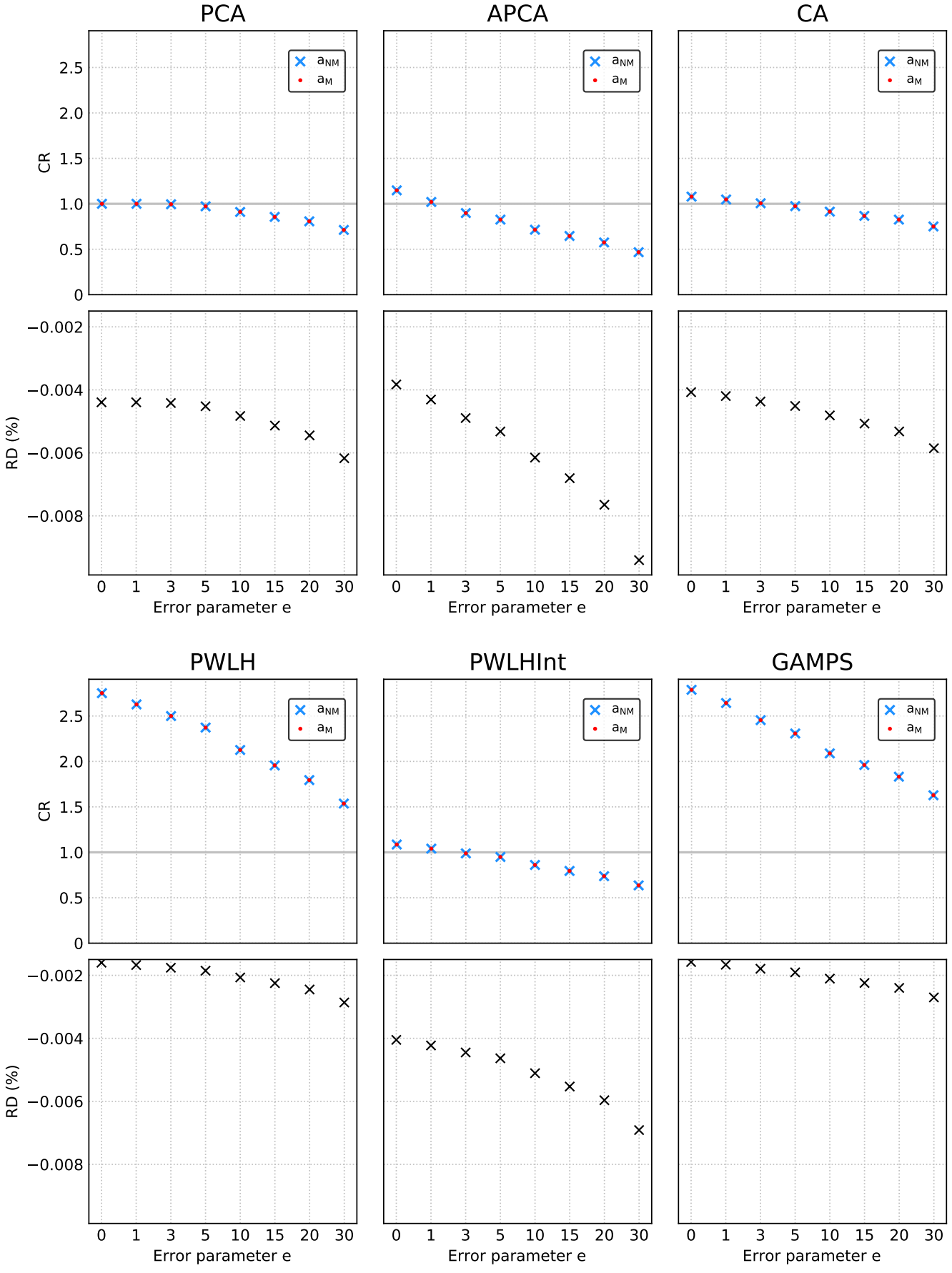

FIGURE A.14: CR and RD plots for variants a_M and a_{NM}, for each algorithm $a \in A_M$, for the data type "Latitude" of the dataset Hail.

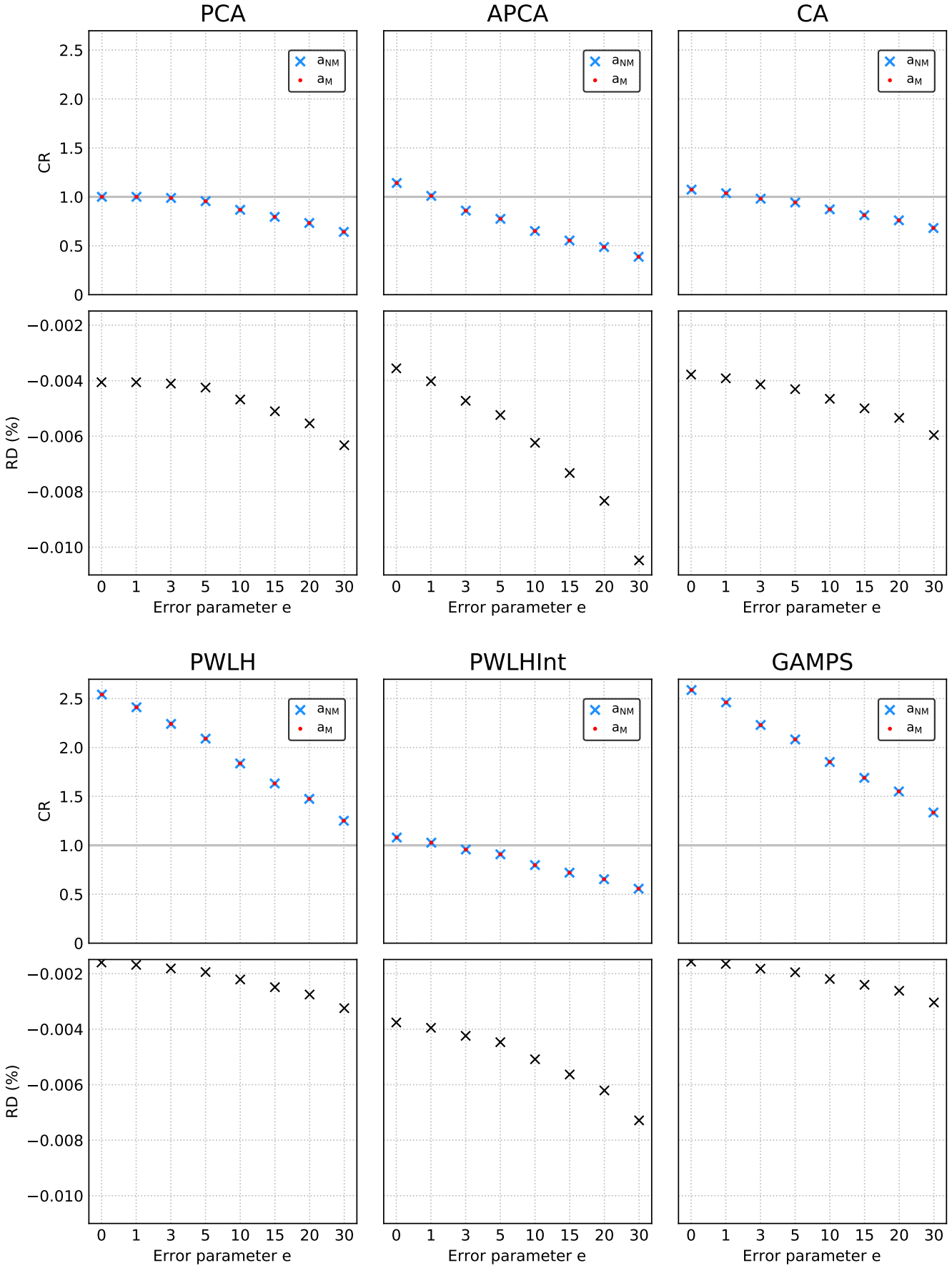

FIGURE A.15: CR and RD plots for variants a_M and a_{NM}, for each algorithm $a \in A_M$, for the data type "Longitude" of the dataset Hail.

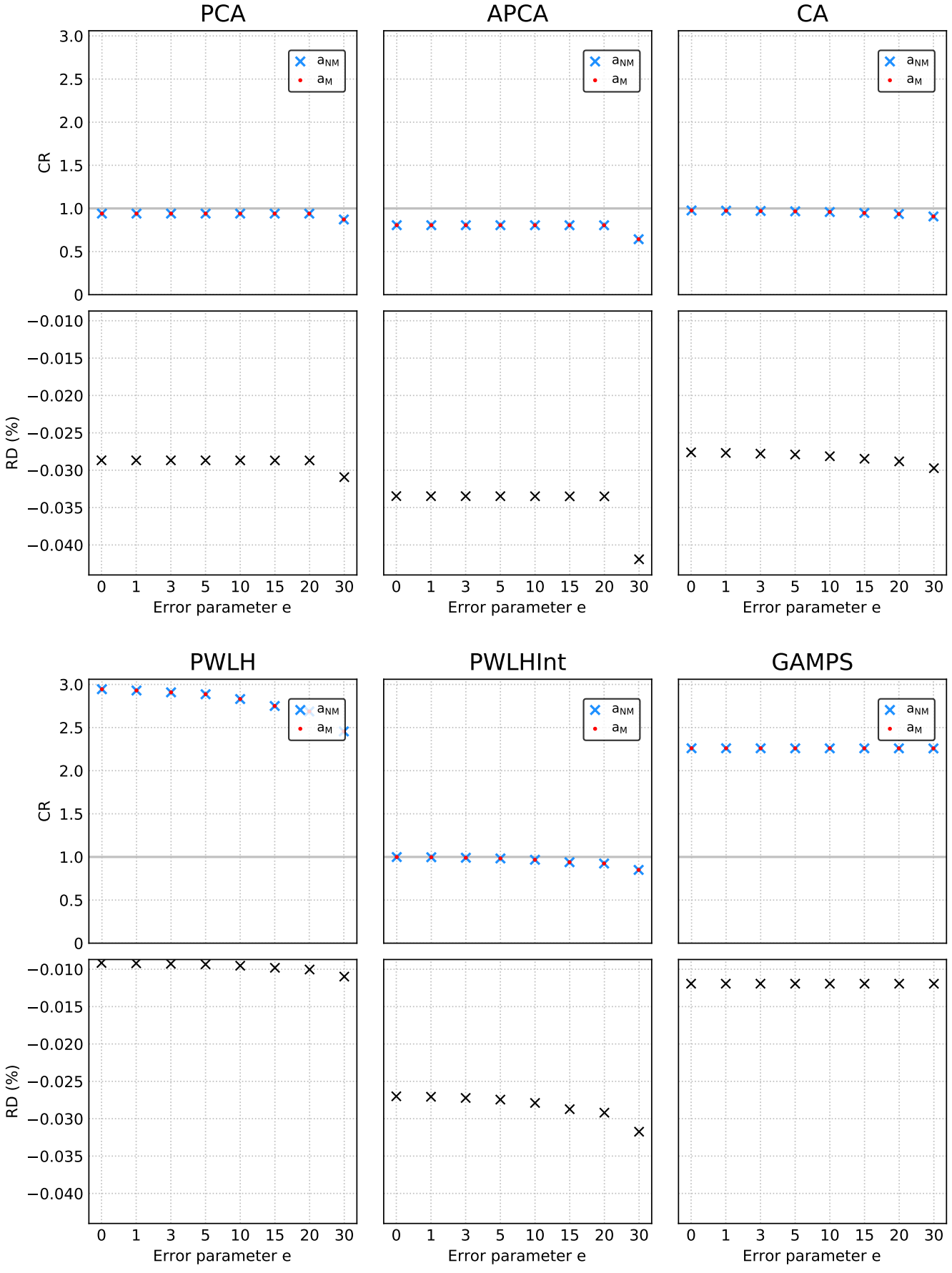

FIGURE A.16: CR and RD plots for variants a_M and a_{NM}, for each algorithm $a \in A_M$, for the data type "Size" of the dataset Hail.

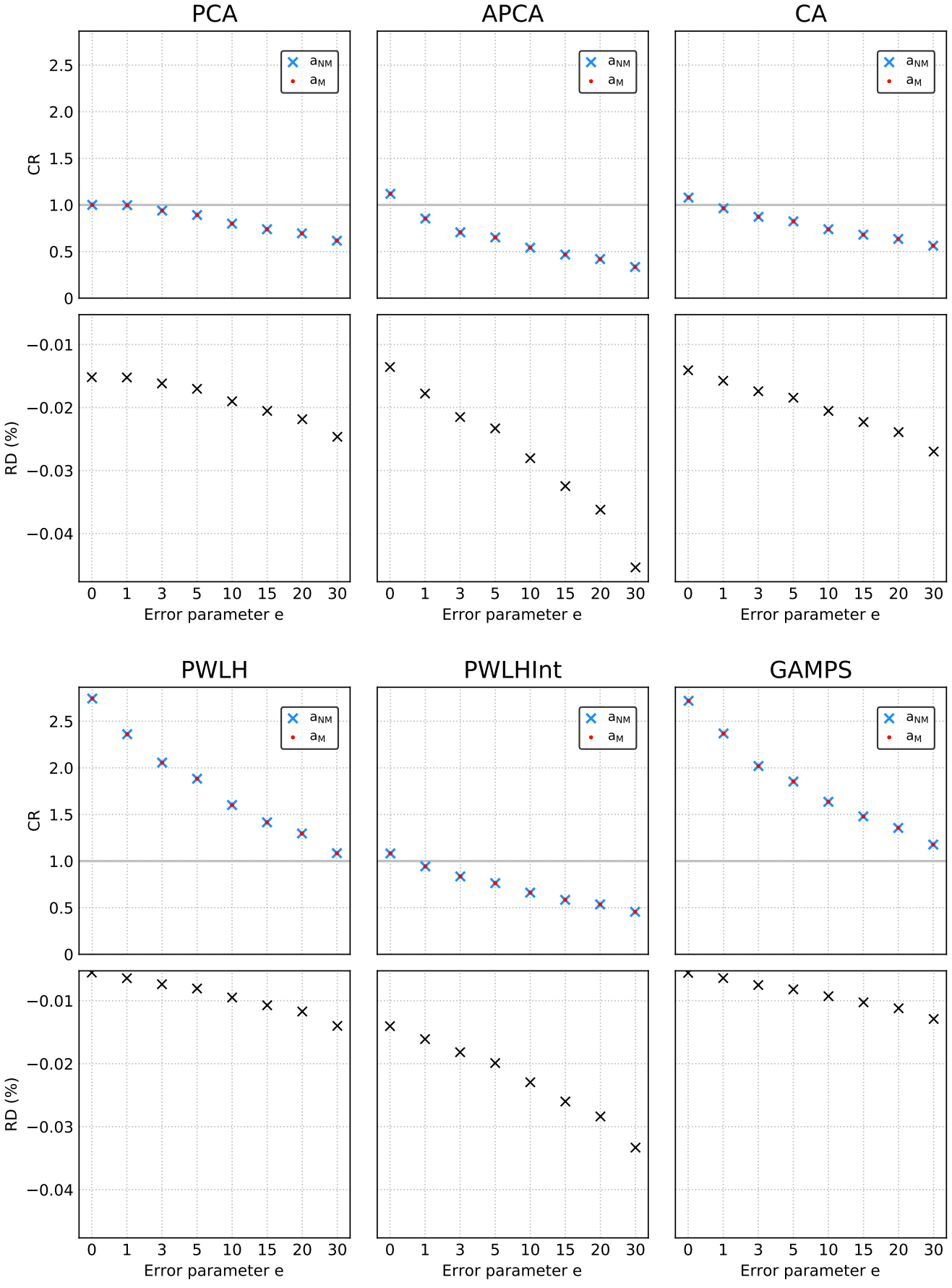

FIGURE A.17: CR and RD plots for variants a_M and a_{NM}, for each algorithm $a \in A_M$, for the data type "Latitude" of the dataset Tornado.

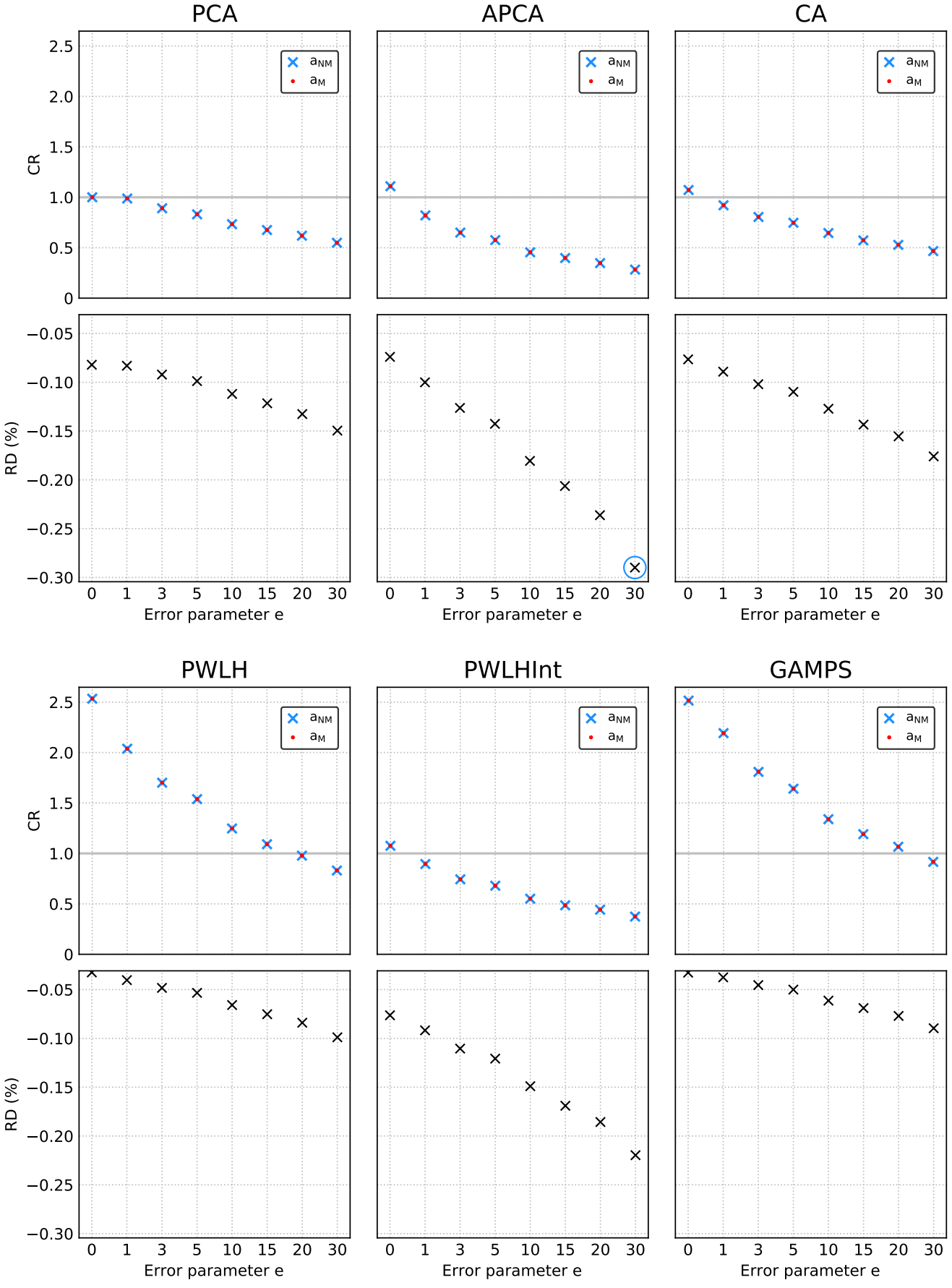

FIGURE A.18: CR and RD plots for variants a_M and a_{NM}, for each algorithm $a \in A_M$, for the data type "Longitude" of the dataset Tornado. In the RD plot for algorithm APCA we highlight with a blue circle the marker for the minimum value (-0.29%) obtained for all the tested CAIs.

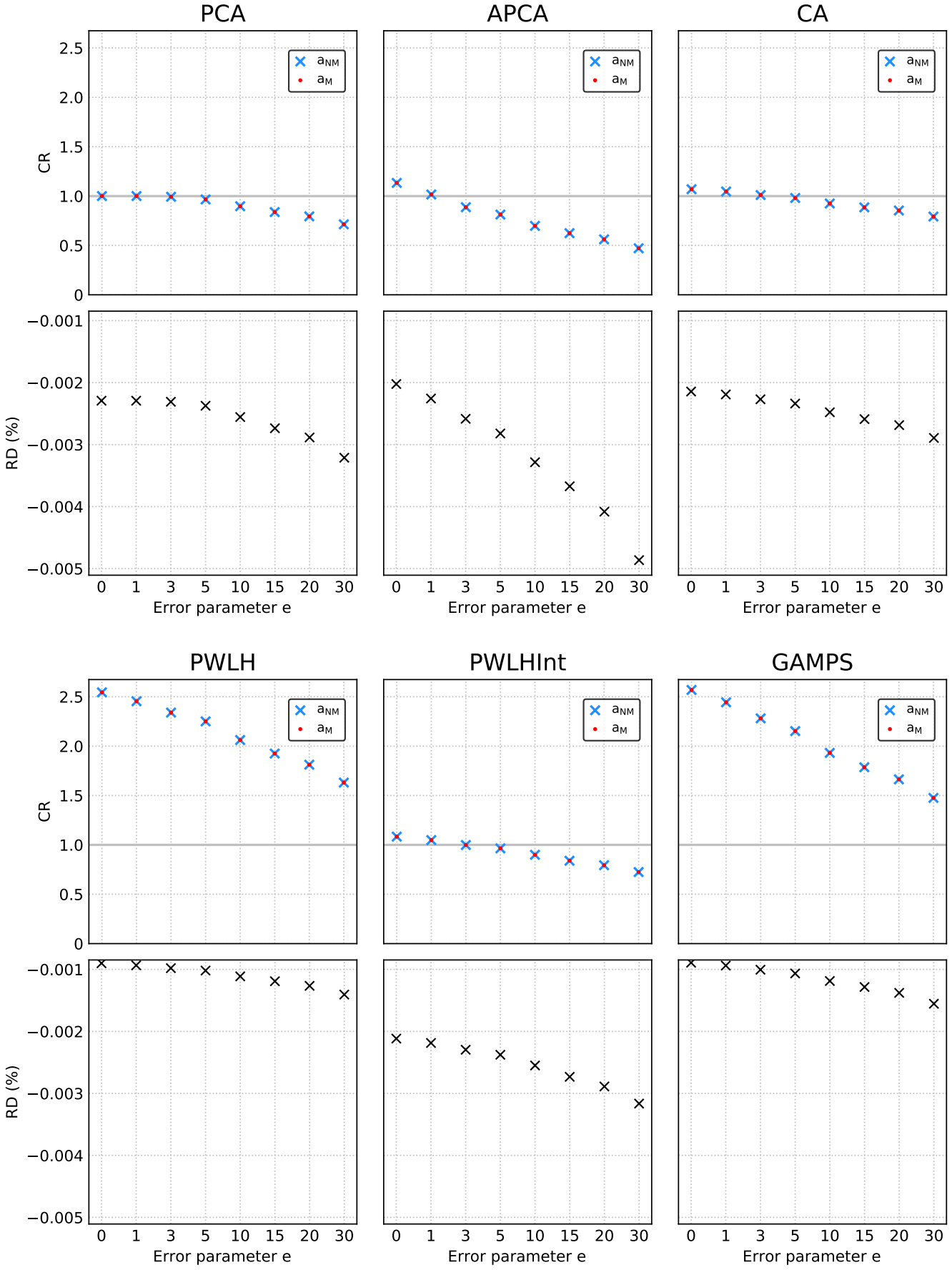

FIGURE A.19: CR and RD plots for variants a_M and a_{NM}, for each algorithm $a \in A_M$, for the data type "Latitude" of the dataset Wind.

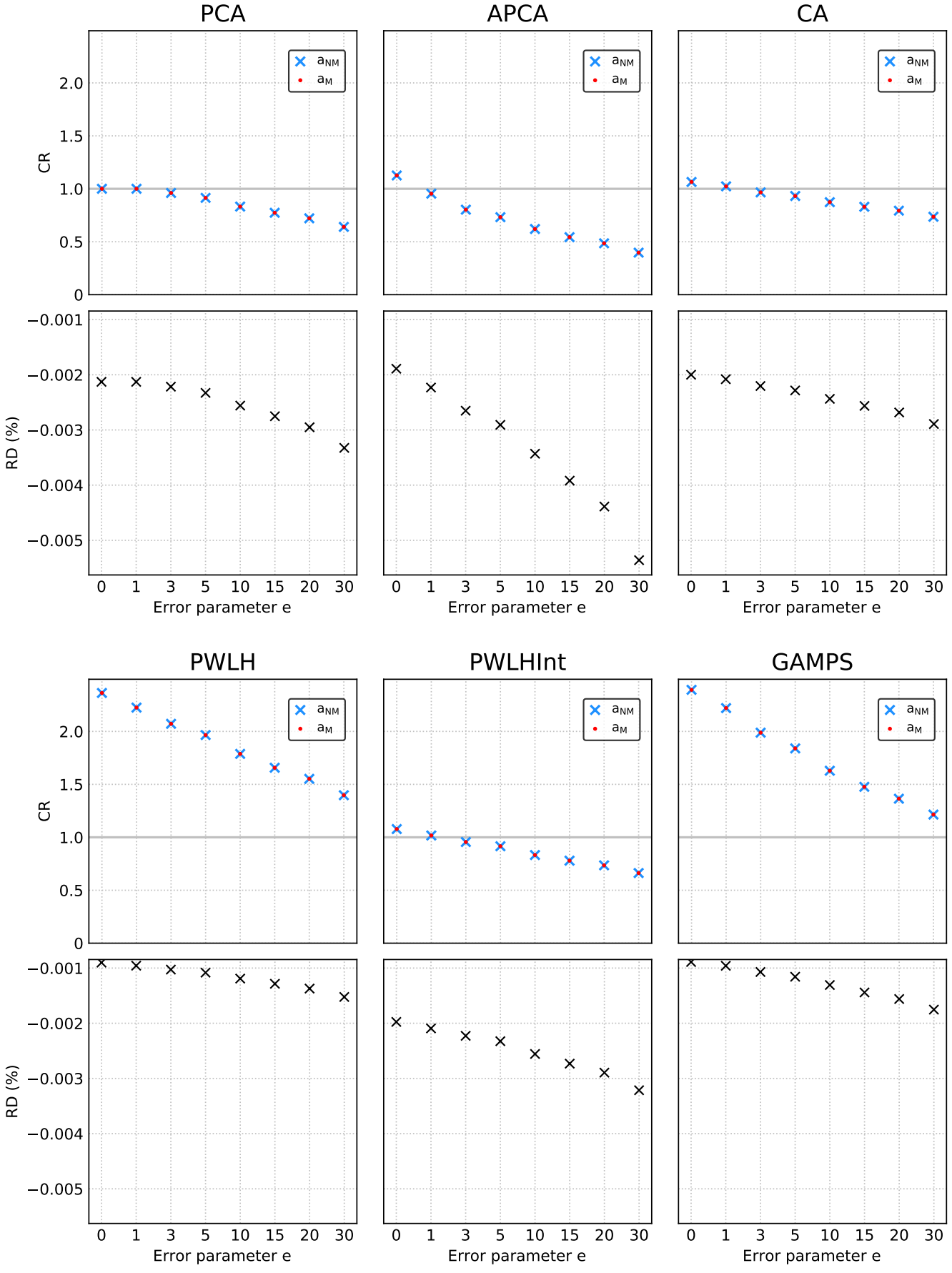

FIGURE A.20: CR and RD plots for variants a_M and a_{NM}, for each algorithm $a \in A_M$, for the data type "Longitude" of the dataset Wind.

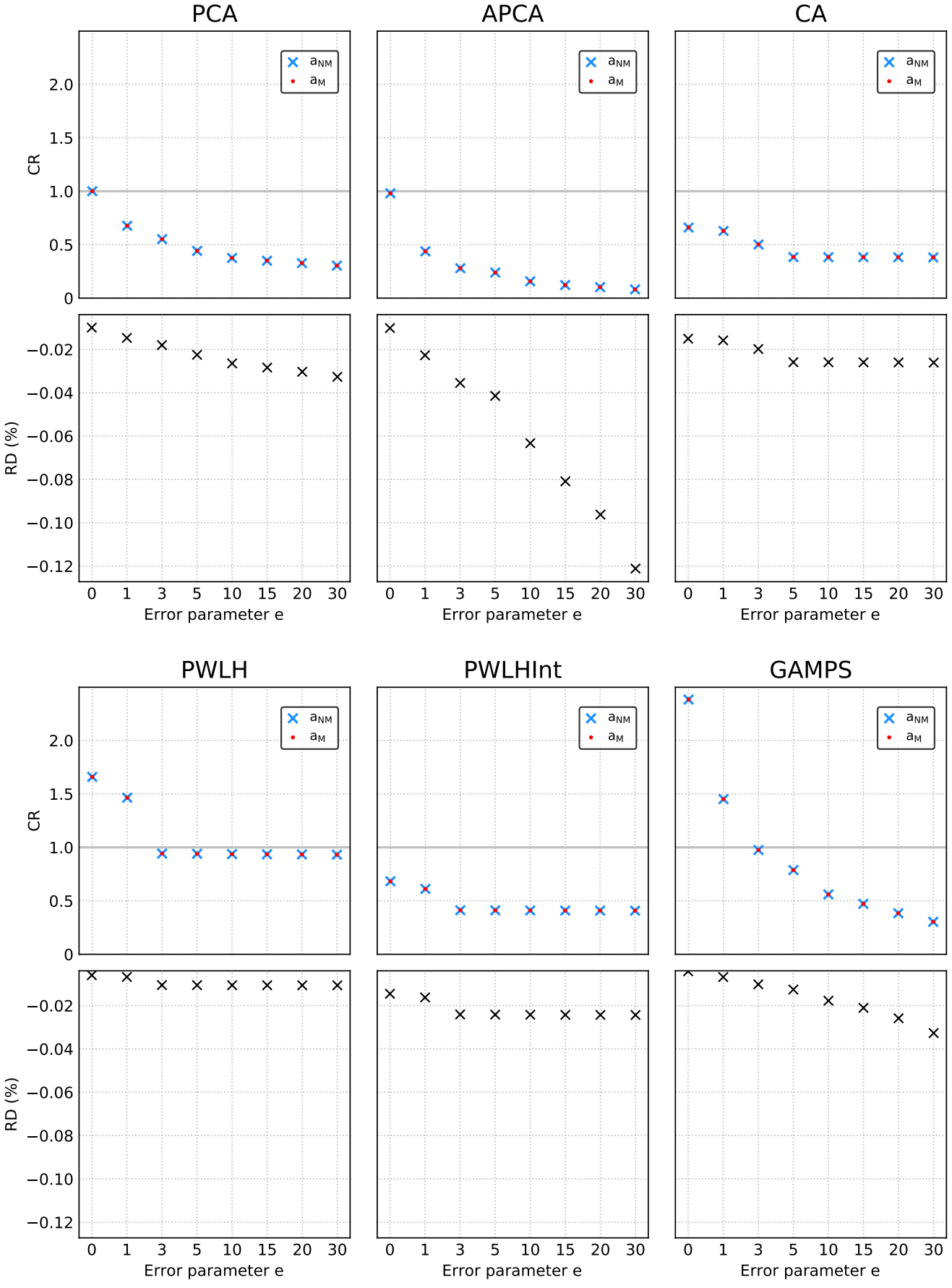

FIGURE A.21: CR and RD plots for variants a_M and a_{NM}, for each algorithm $a \in A_M$, for the data type "Speed" of the dataset Wind.

Appendix B

Figures: Window Size Parameter

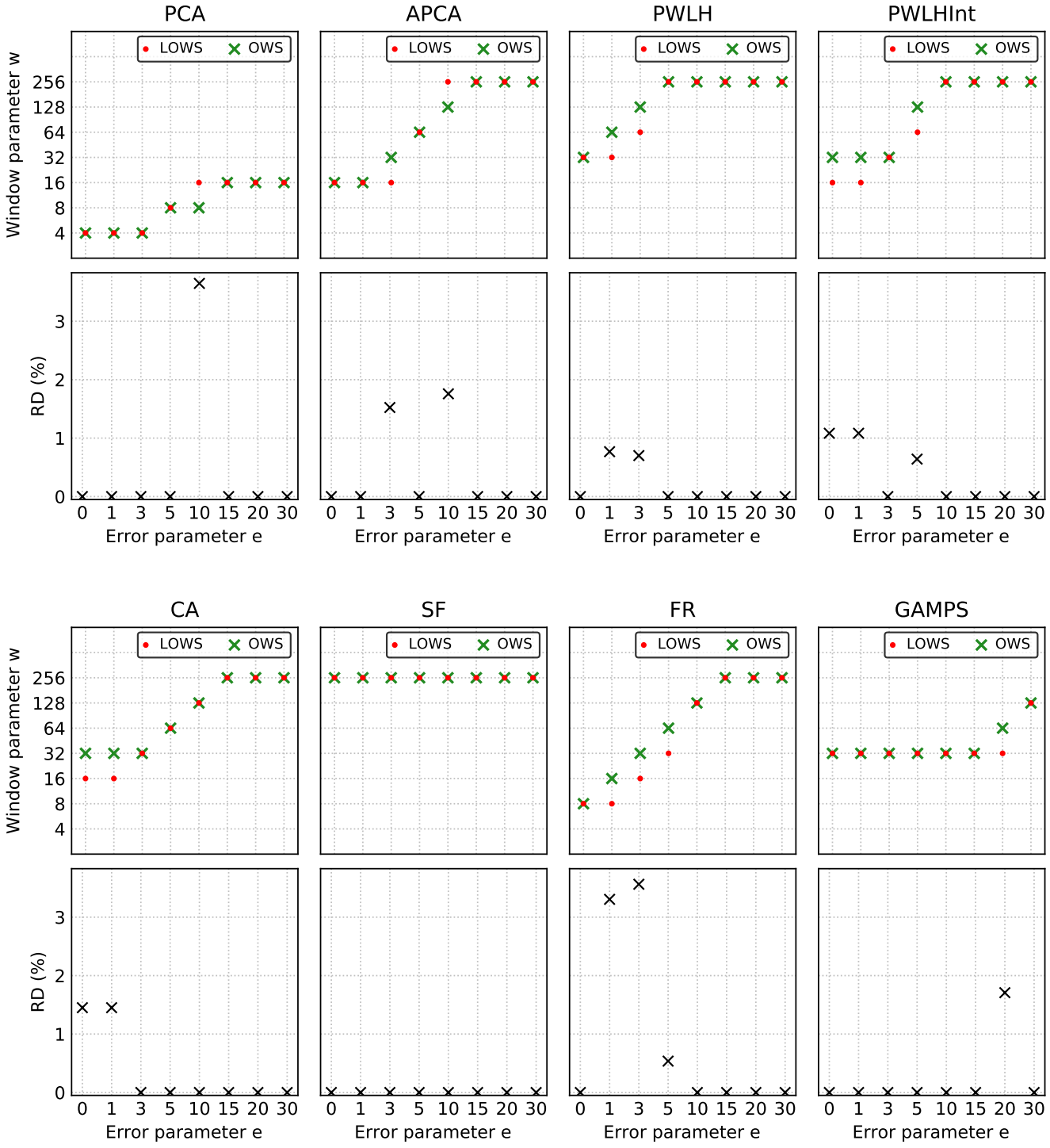

FIGURE B.1: Plots of w^*_{global}, w^*_{local}, and the RD between $c_{<a_v,w^*_{global},e>}$ and $c_{<a_v,w^*_{local},e>}$, as a function of the error parameter e, obtained for the data type "VWC" of the file "irkis-1202.csv" of the dataset IRKIS.

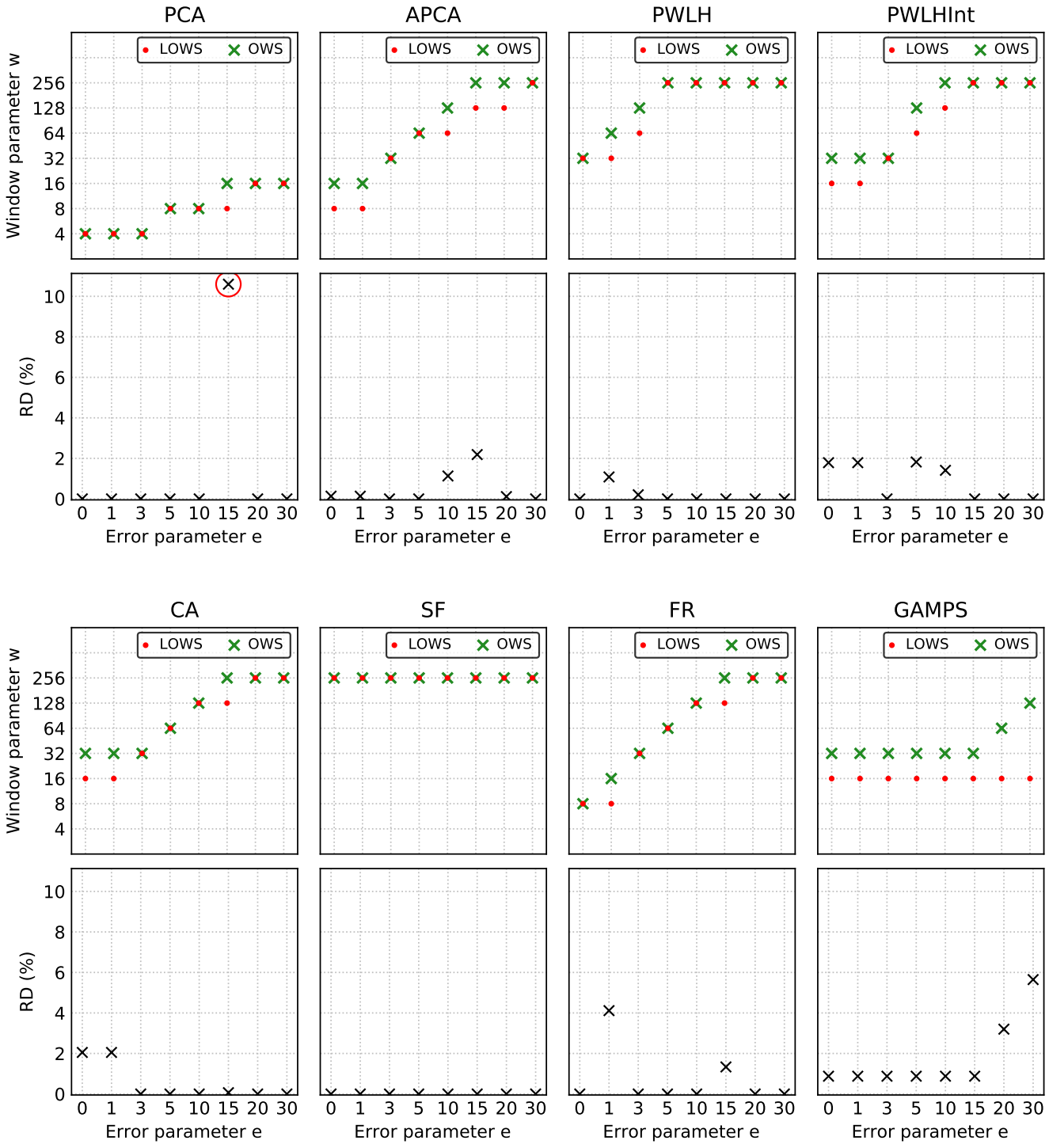

FIGURE B.2: Plots of w^*_{global}, w^*_{local}, and the RD between $c_{<a_v,w^*_{global},e>}$ and $c_{<a_v,w^*_{local},e>}$, as a function of the error parameter e, obtained for the data type "VWC" of the file "irkis-1203.csv" of the dataset IRKIS. In the RD plot for variant PCA$_M$ we highlight with a red circle the marker for the maximum value (10.6%) obtained for all the tested CAIs.

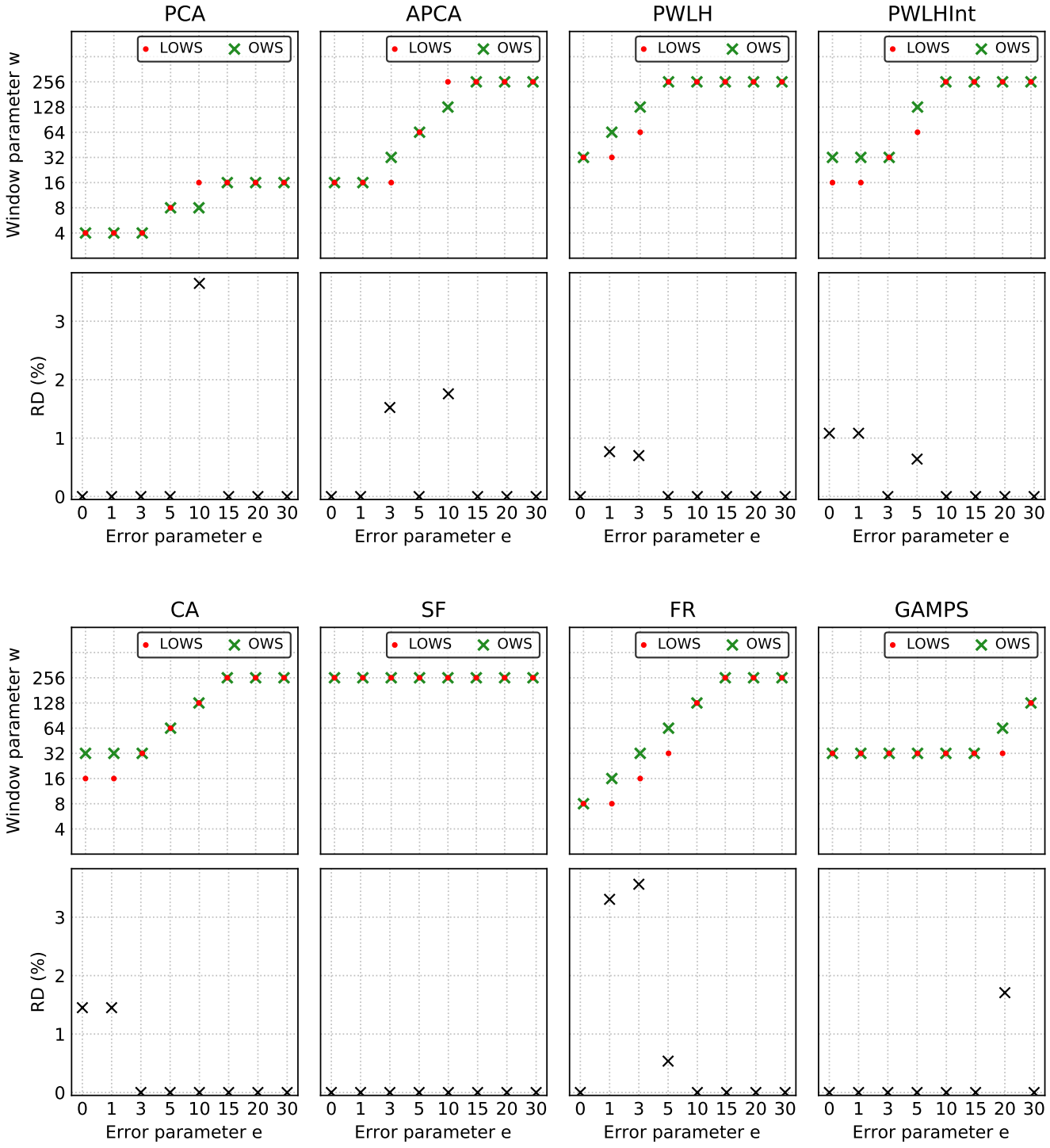

FIGURE B.3: Plots of w^*_{global}, w^*_{local}, and the RD between $c_{<a_v,w^*_{global},e>}$ and $c_{<a_v,w^*_{local},e>}$, as a function of the error parameter e, obtained for the data type "VWC" of the file "irkis-1204.csv" of the dataset IRKIS.

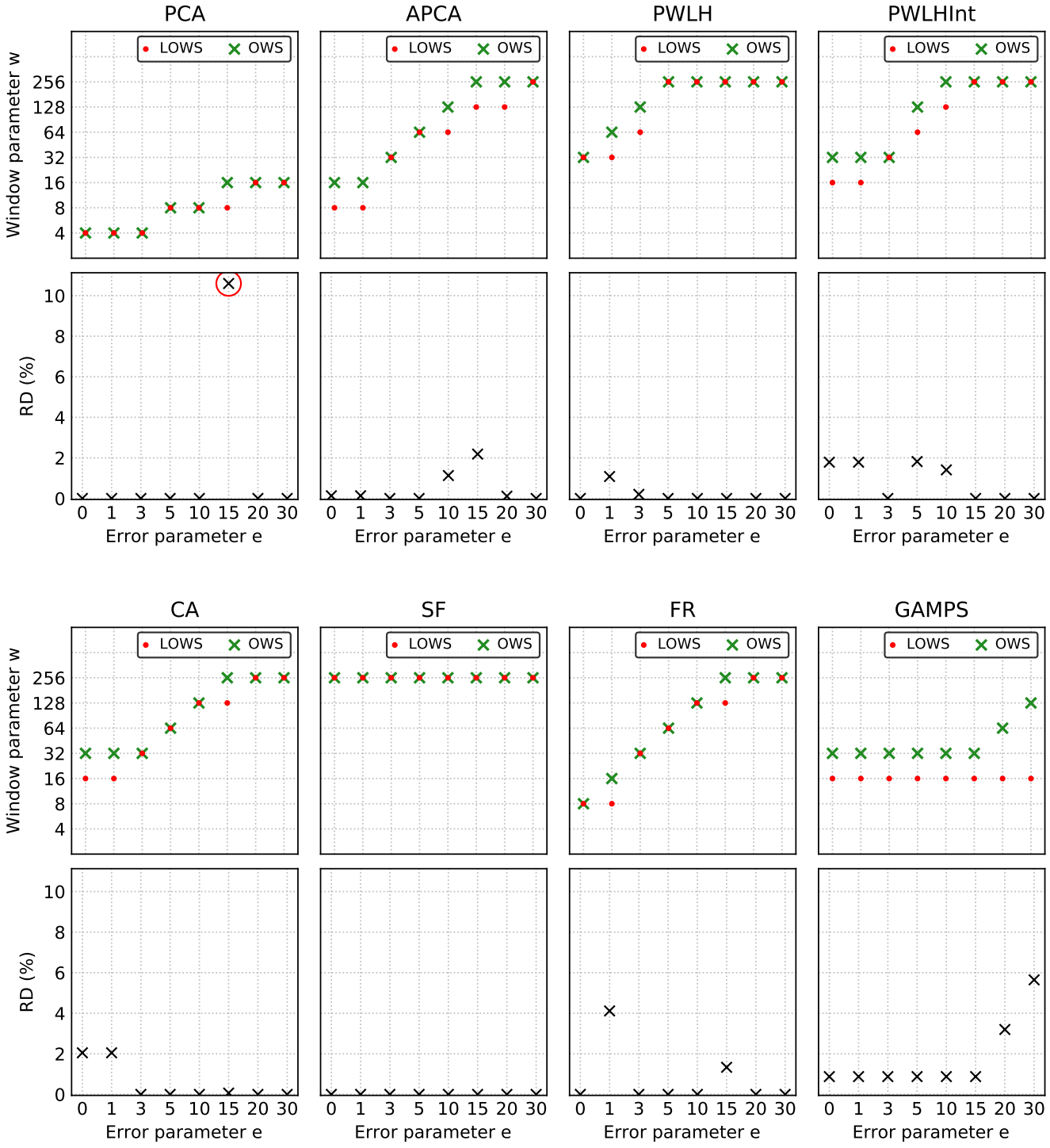

FIGURE B.4: Plots of w^*_{global}, w^*_{local}, and the RD between $c_{<a_v,w^*_{global},e>}$ and $c_{<a_v,w^*_{local},e>}$, as a function of the error parameter e, obtained for the data type "VWC" of the file "irkis-1205.csv" of the dataset IRKIS.

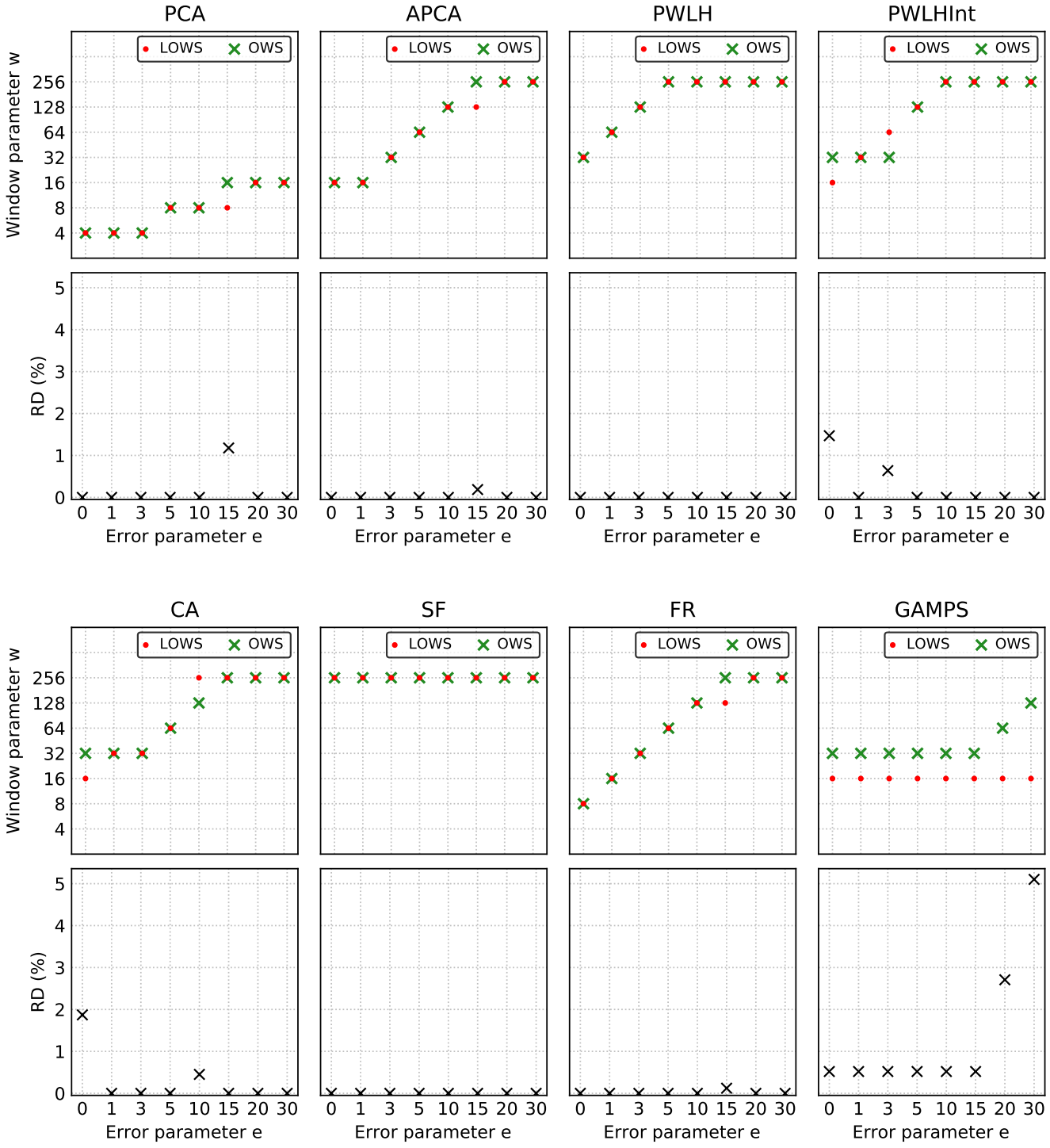

FIGURE B.5: Plots of w^*_{global}, w^*_{local}, and the RD between $c_{<a_v,w^*_{global},e>}$ and $c_{<a_v,w^*_{local},e>}$, as a function of the error parameter e, obtained for the data type "VWC" of the file "irkis-222.csv" of the dataset IRKIS.

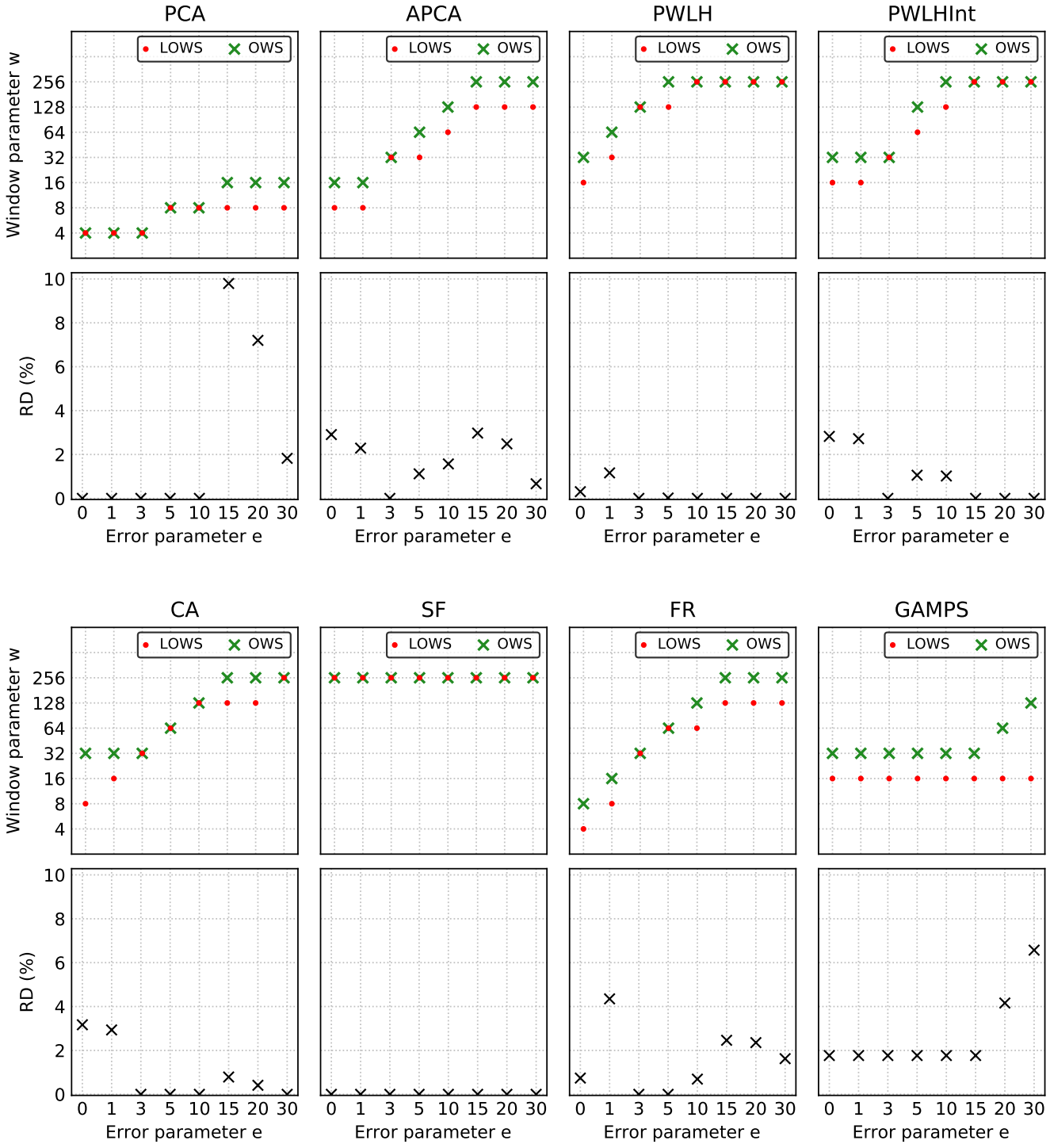

FIGURE B.6: Plots of w^*_{global}, w^*_{local}, and the RD between $c_{<a_v,w^*_{global},e>}$ and $c_{<a_v,w^*_{local},e>}$, as a function of the error parameter e, obtained for the data type "VWC" of the file "irkis-333.csv" of the dataset IRKIS.

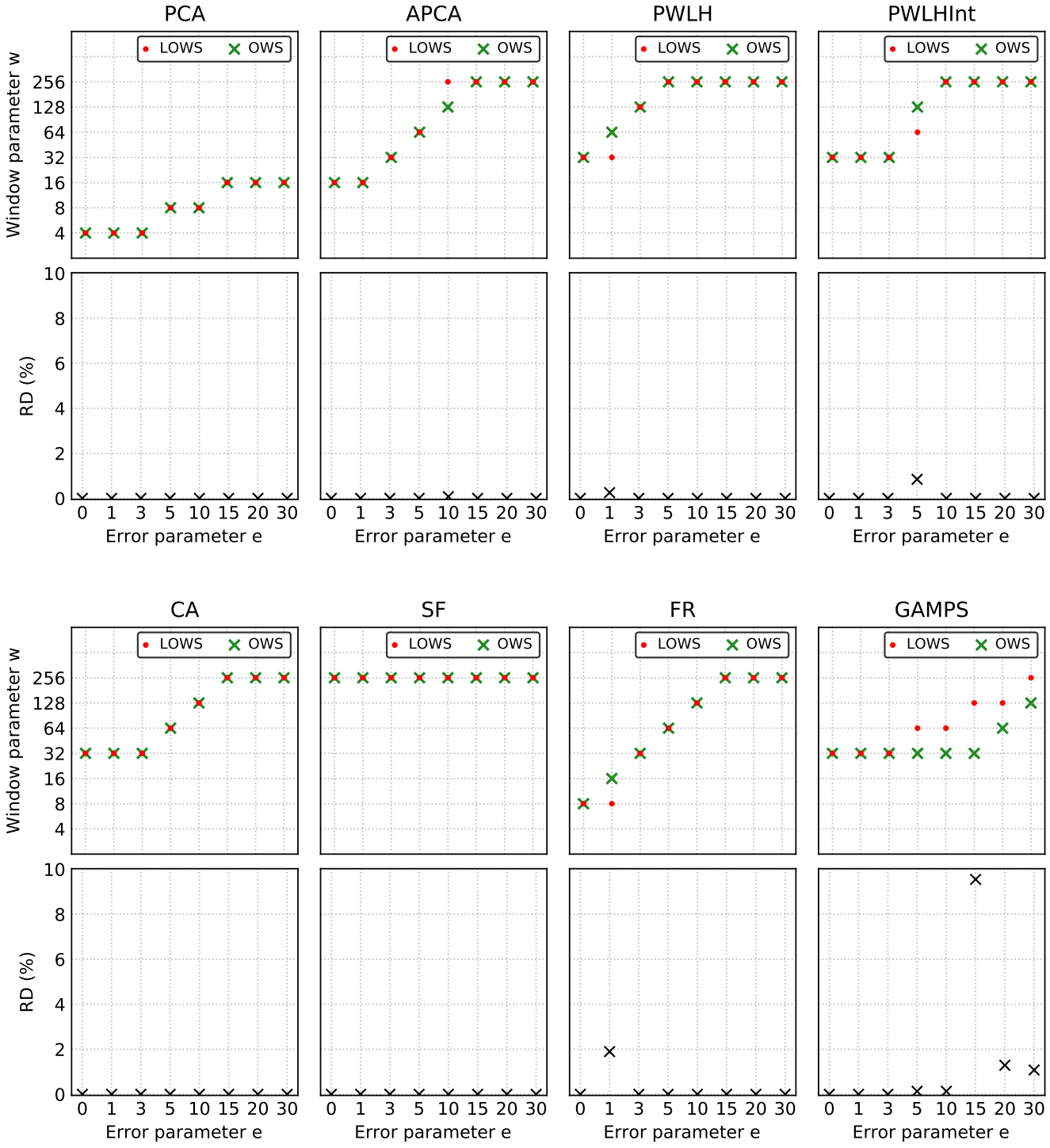

FIGURE B.7: Plots of w^*_{global}, w^*_{local}, and the RD between $c_{<a_v,w^*_{global},e>}$ and $c_{<a_v,w^*_{local},e>}$, as a function of the error parameter e, obtained for the data type "VWC" of the file "irkis-SLF2.csv" of the dataset IRKIS.

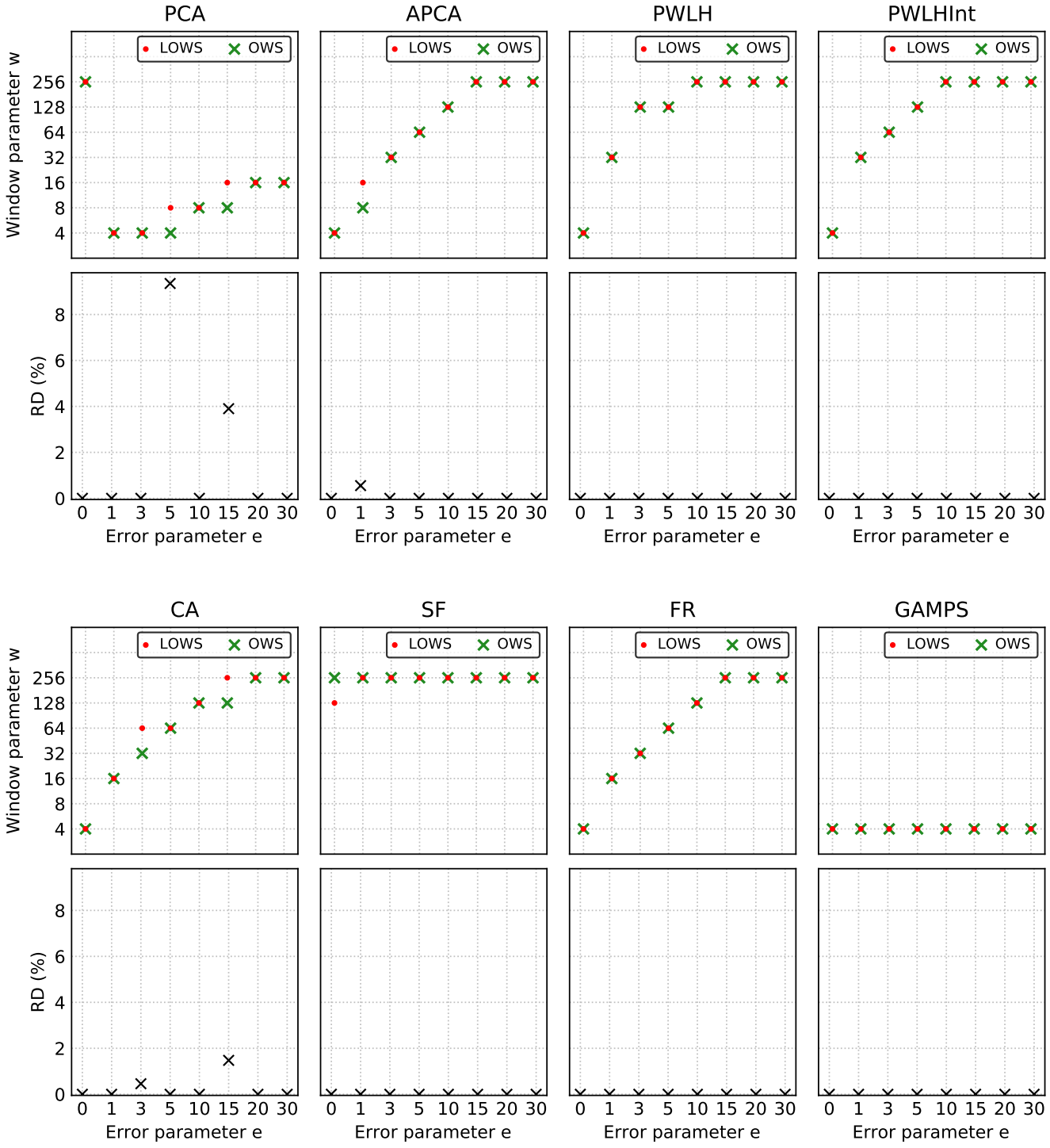

FIGURE B.8: Plots of w^*_{global}, w^*_{local}, and the RD between $c_{<a_v,w^*_{global},e>}$ and $c_{<a_v,w^*_{local},e>}$, as a function of the error parameter e, obtained for the data type "SST" of the file "sst-01-2017.csv" of the dataset SST.

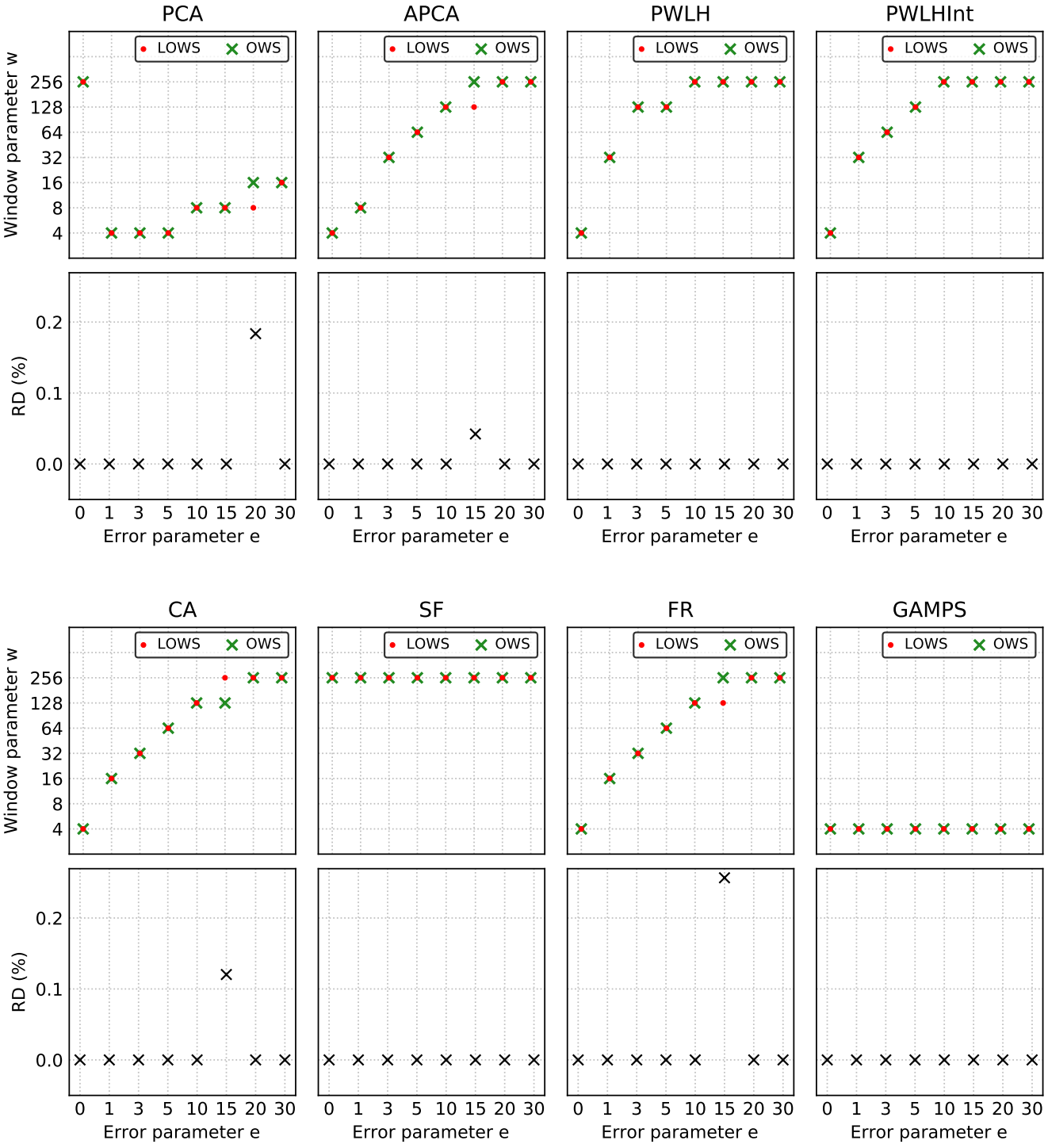

FIGURE B.9: Plots of w^*_{global}, w^*_{local}, and the RD between $c_{<a_v,w^*_{global},e>}$ and $c_{<a_v,w^*_{local},e>}$, as a function of the error parameter e, obtained for the data type "SST" of the file "sst-02-2017.csv" of the dataset SST.

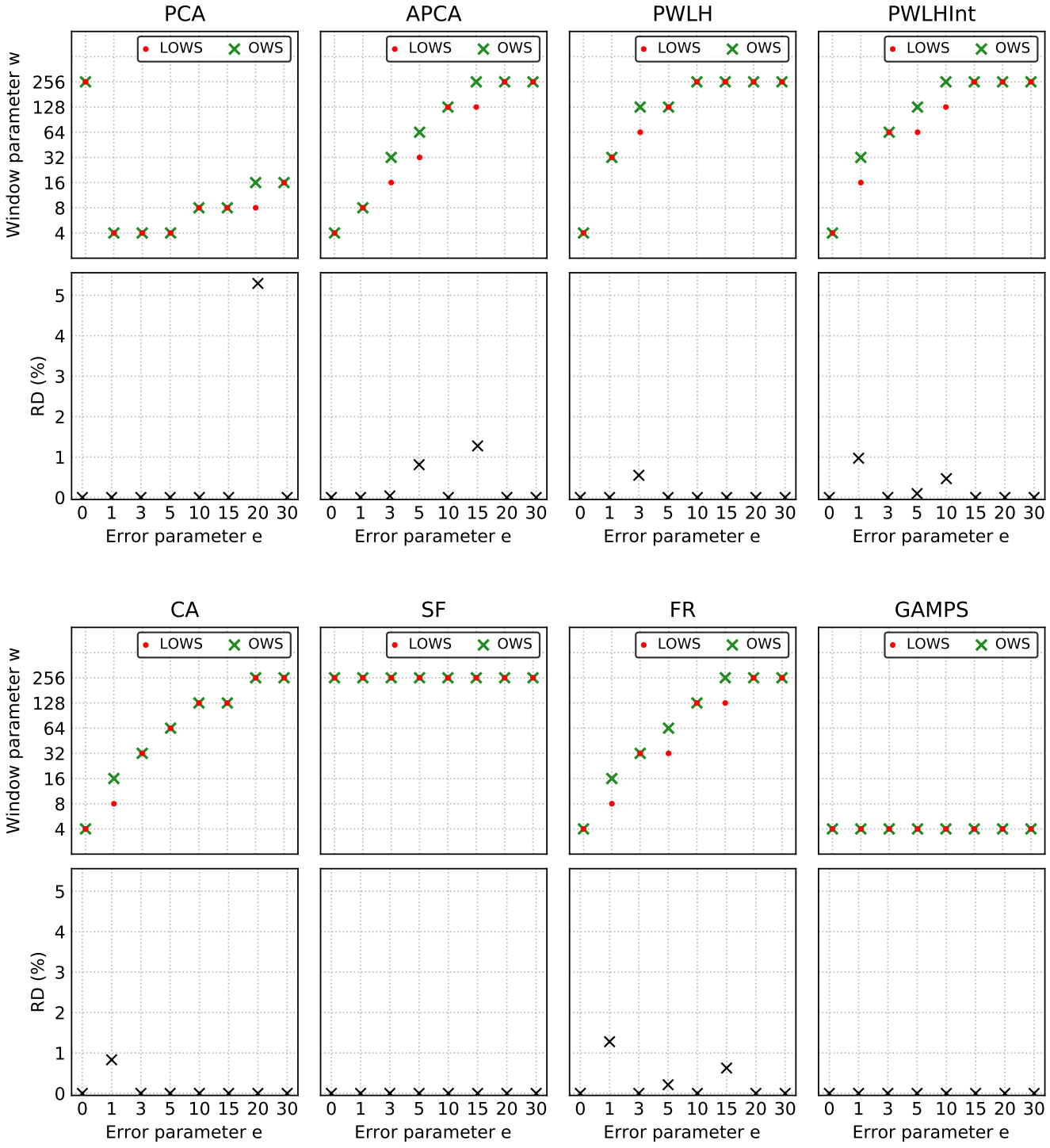

FIGURE B.10: Plots of w^*_{global}, w^*_{local}, and the RD between $c_{<a_v,w^*_{global},e>}$ and $c_{<a_v,w^*_{local},e>}$, as a function of the error parameter e, obtained for the data type "SST" of the file "sst-03-2017.csv" of the dataset SST.

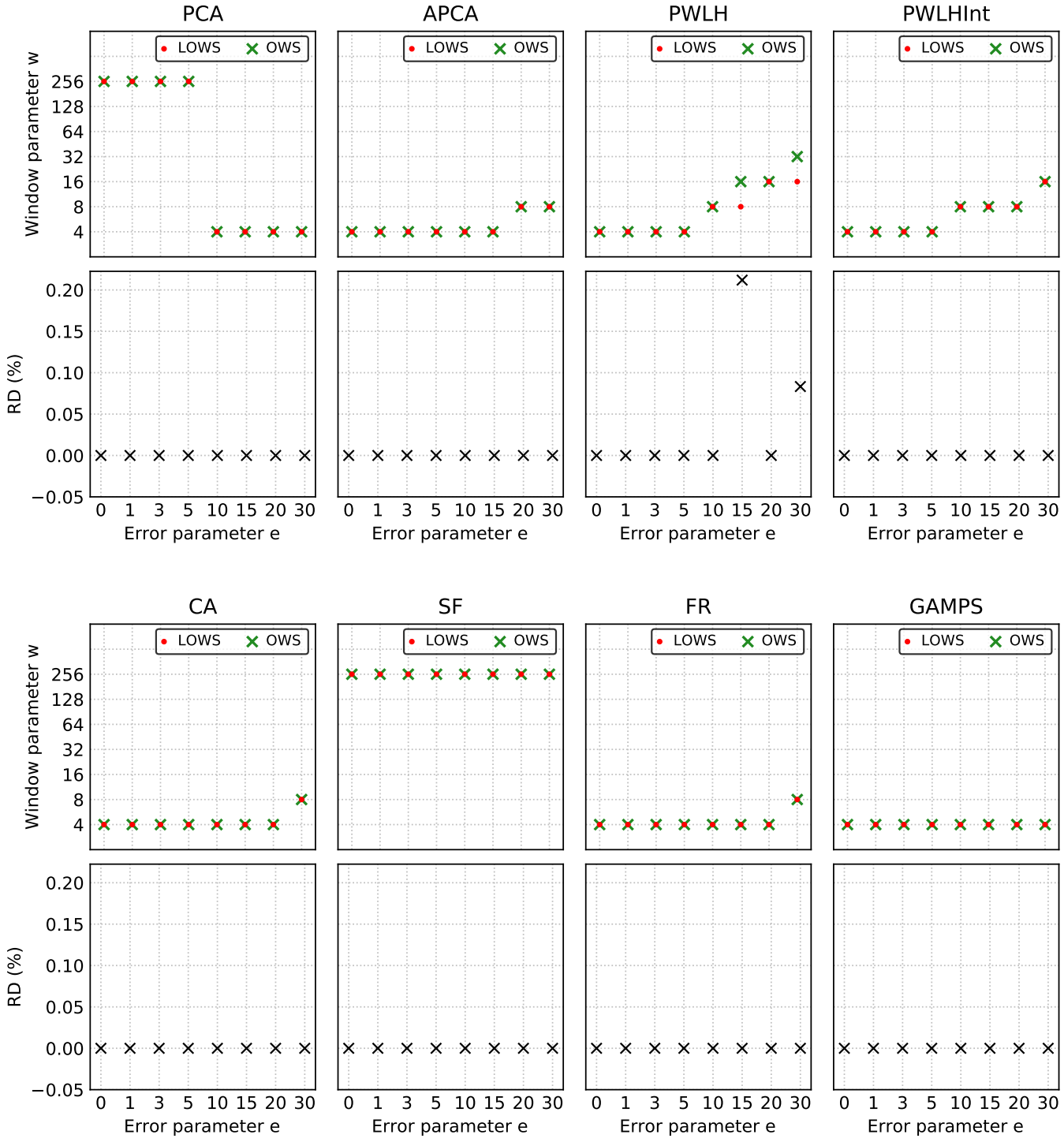

FIGURE B.11: Plots of w^*_{global}, w^*_{local}, and the RD between $c_{<a_v,w^*_{global},e>}$ and $c_{<a_v,w^*_{local},e>}$, as a function of the error parameter e, obtained for the data type "Velocity" of the file "adcp-01-2015.csv" of the dataset SST.

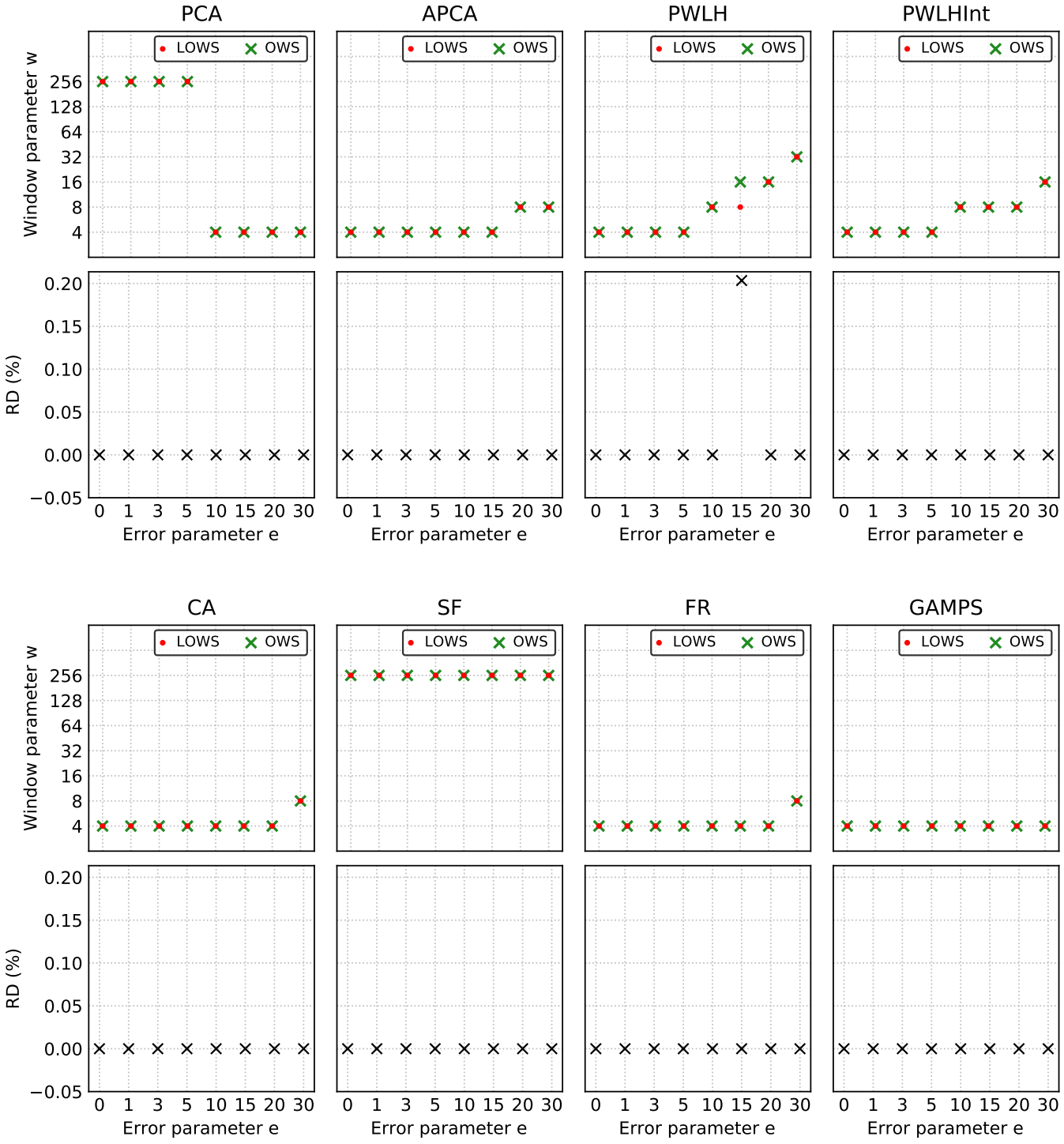

FIGURE B.12: Plots of w^*_{global}, w^*_{local}, and the RD between $c_{<a_v,w^*_{global},e>}$ and $c_{<a_v,w^*_{local},e>}$, as a function of the error parameter e, obtained for the data type "Velocity" of the file "adcp-02-2015.csv" of the dataset SST.

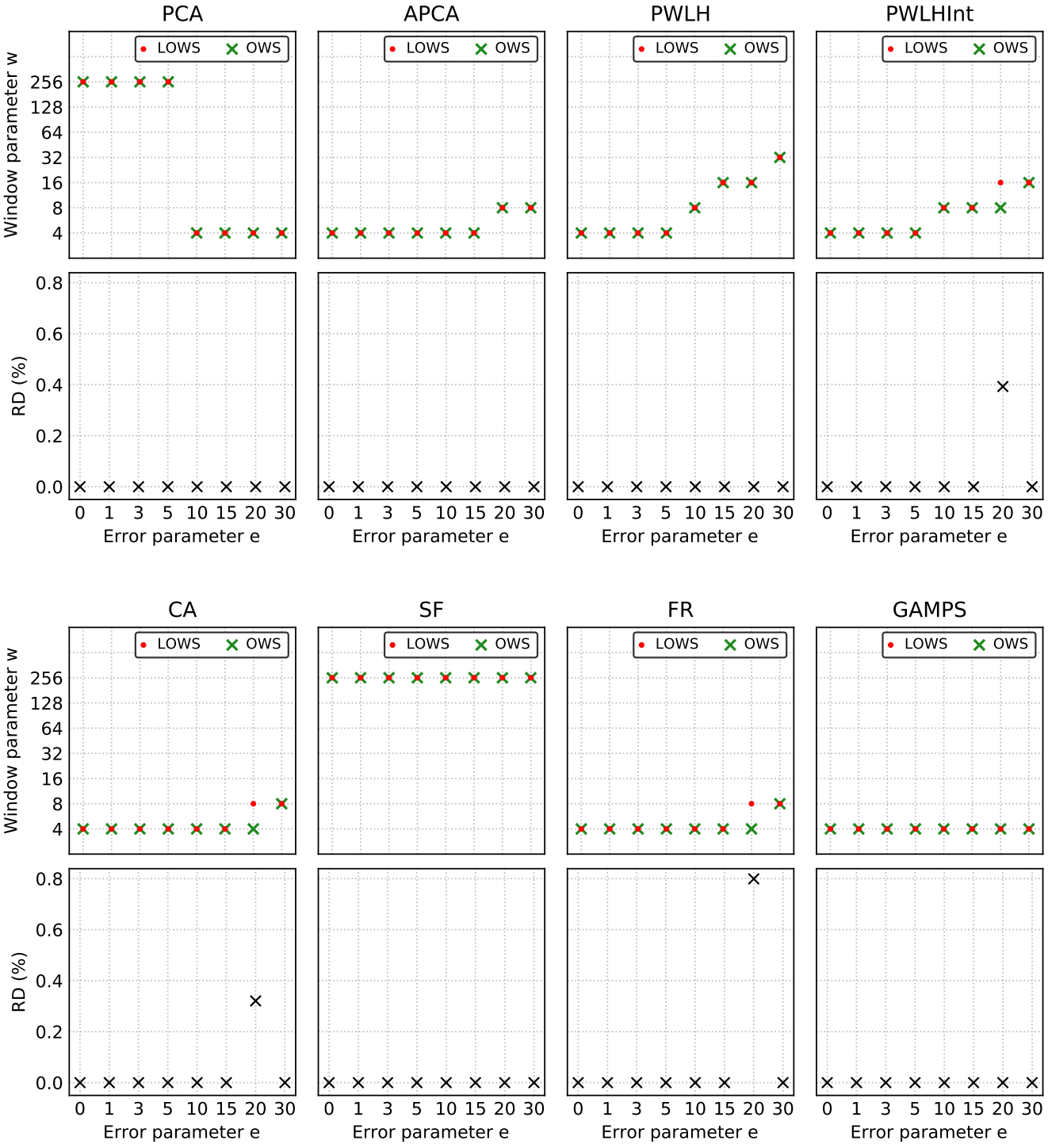

FIGURE B.13: Plots of w^*_{global}, w^*_{local}, and the RD between $c_{<a_v,w^*_{global},e>}$ and $c_{<a_v,w^*_{local},e>}$, as a function of the error parameter e, obtained for the data type "Velocity" of the file "adcp-03-2015.csv" of the dataset SST.

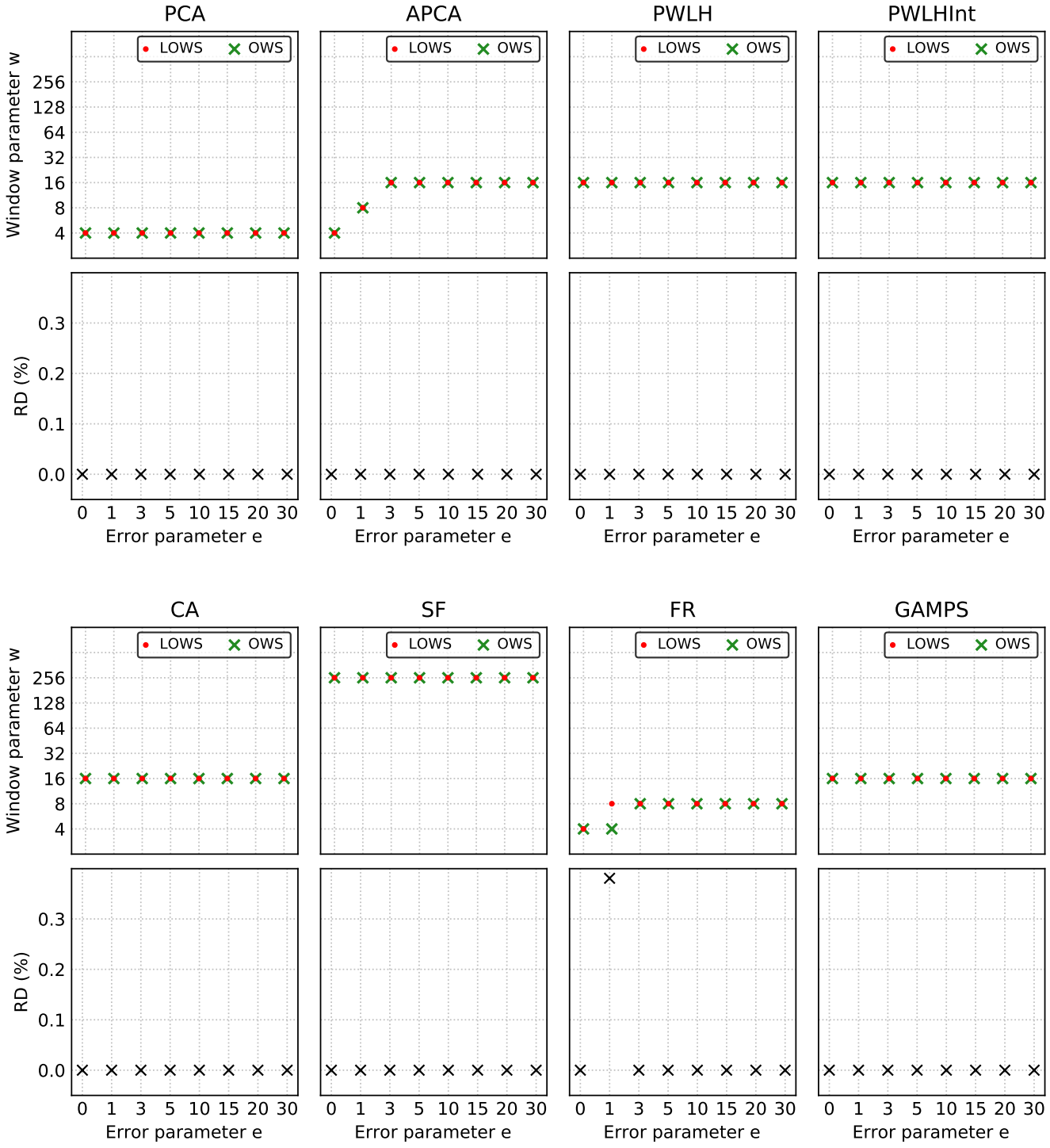

FIGURE B.14: Plots of w^*_{global}, w^*_{local}, and the RD between $c_{<a_v,w^*_{global},e>}$ and $c_{<a_v,w^*_{local},e>}$, as a function of the error parameter e, obtained for the data type "GHI" of the file "solar-2011.csv" of the dataset Solar.

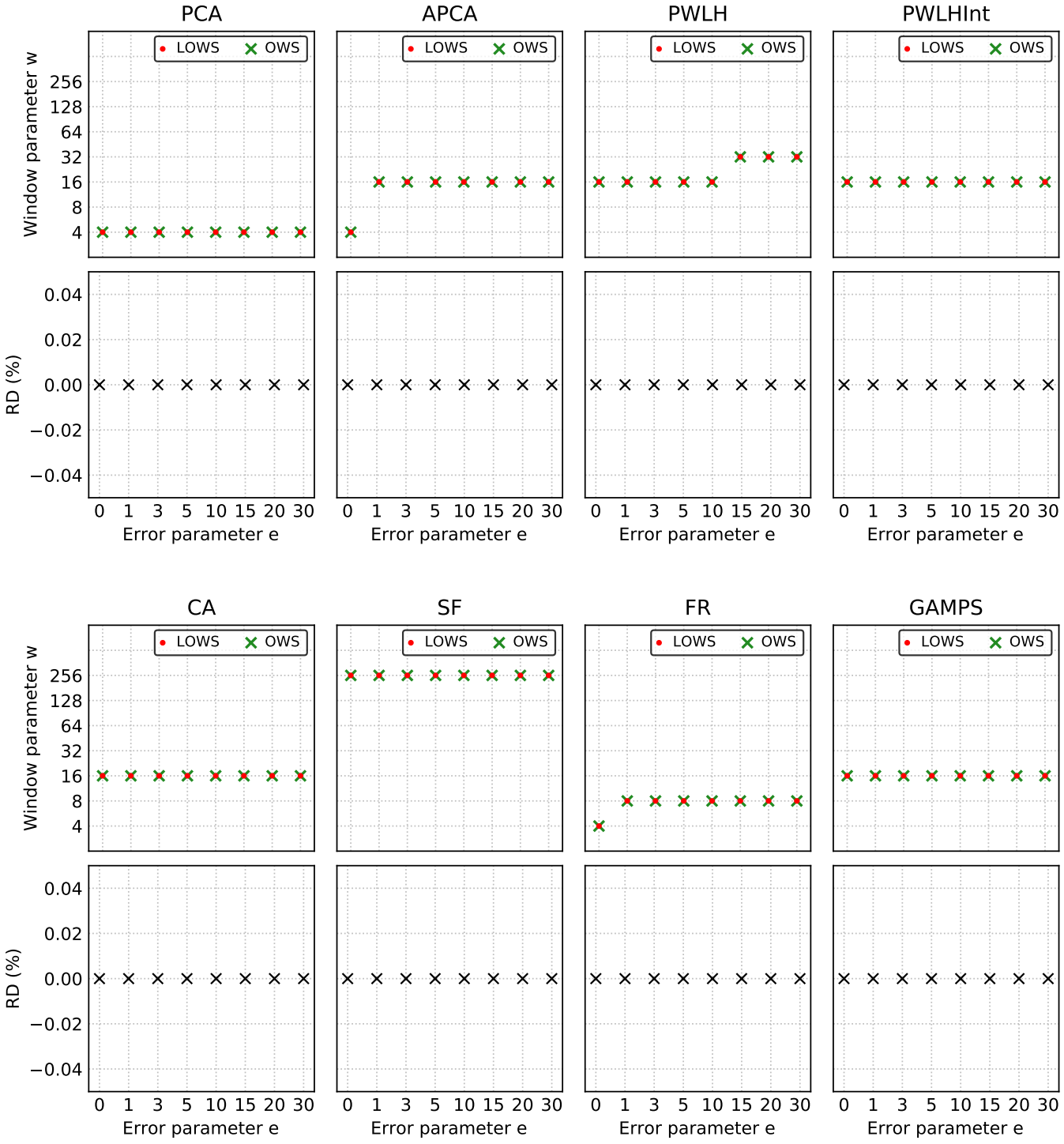

FIGURE B.15: Plots of w^*_{global}, w^*_{local}, and the RD between $c_{<a_v,w^*_{global},e>}$ and $c_{<a_v,w^*_{local},e>}$, as a function of the error parameter e, obtained for the data type "DNI" of the file "solar-2011.csv" of the dataset Solar.

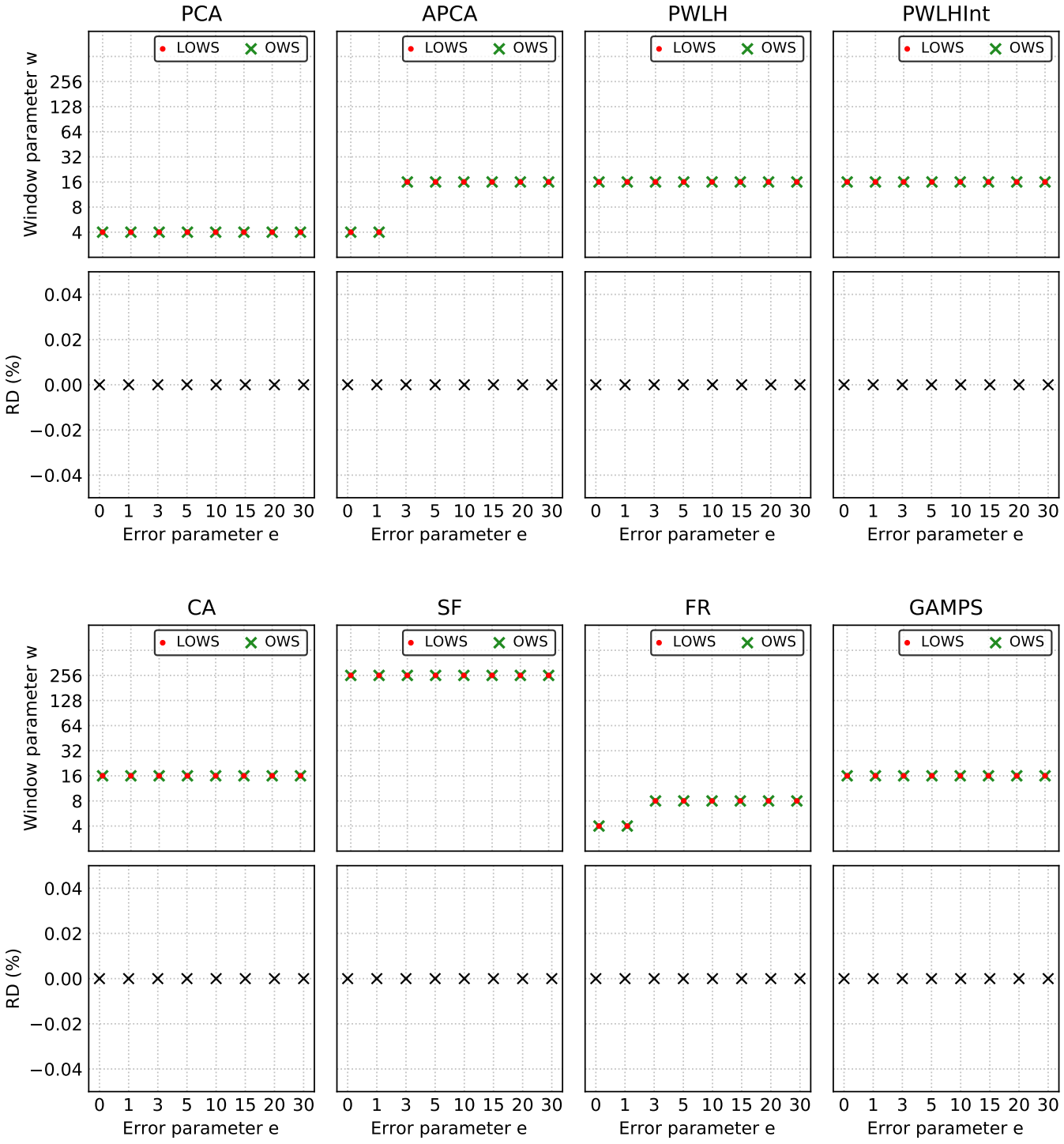

FIGURE B.16: Plots of w^*_{global}, w^*_{local}, and the RD between $c_{<a_v,w^*_{global},e>}$ and $c_{<a_v,w^*_{local},e>}$, as a function of the error parameter e, obtained for the data type "DHI" of the file "solar-2011.csv" of the dataset Solar.

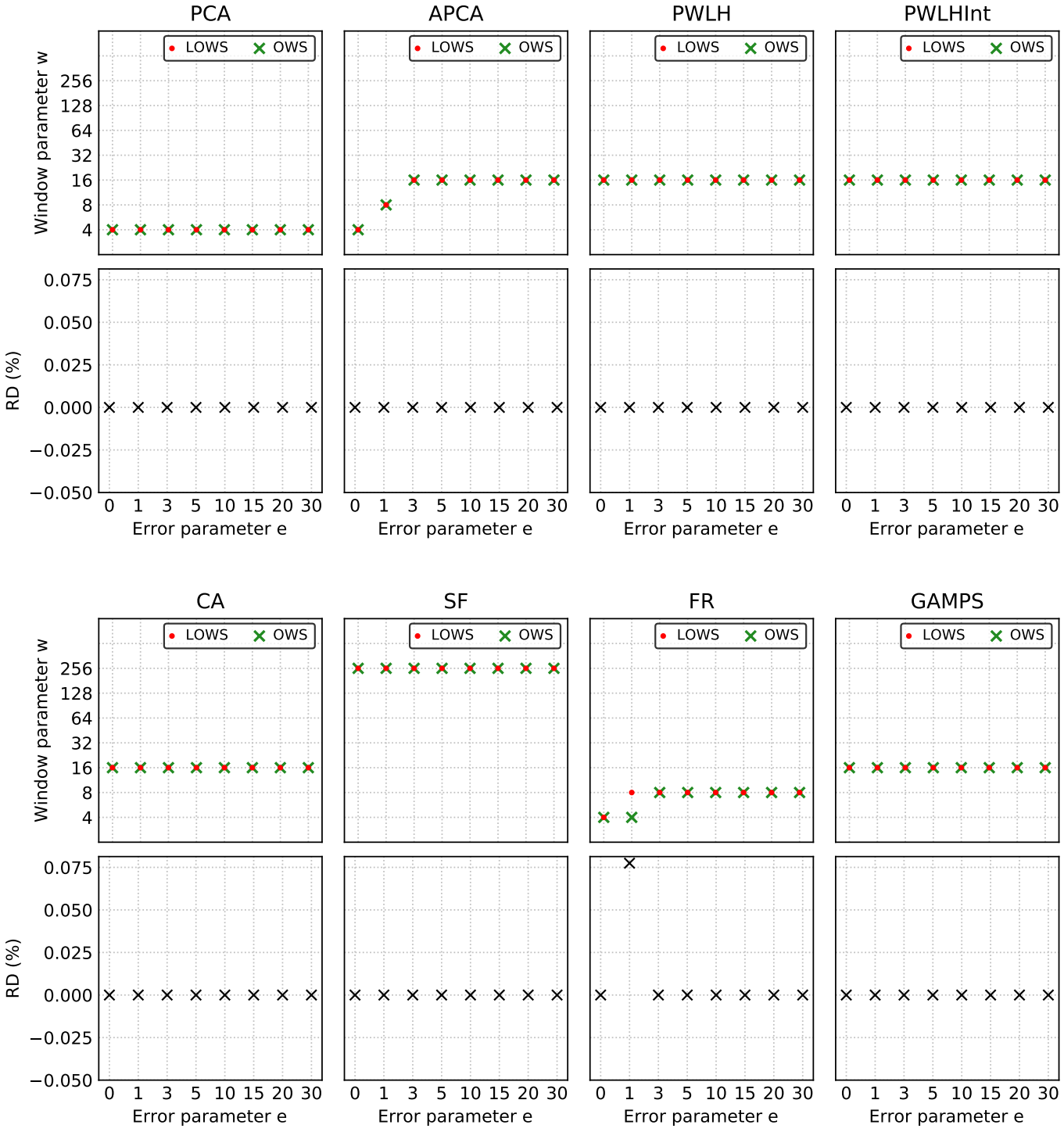

FIGURE B.17: Plots of w^*_{global}, w^*_{local}, and the RD between $c_{<a_v,w^*_{global},e>}$ and $c_{<a_v,w^*_{local},e>}$, as a function of the error parameter e, obtained for the data type "GHI" of the file "solar-2012.csv" of the dataset Solar.

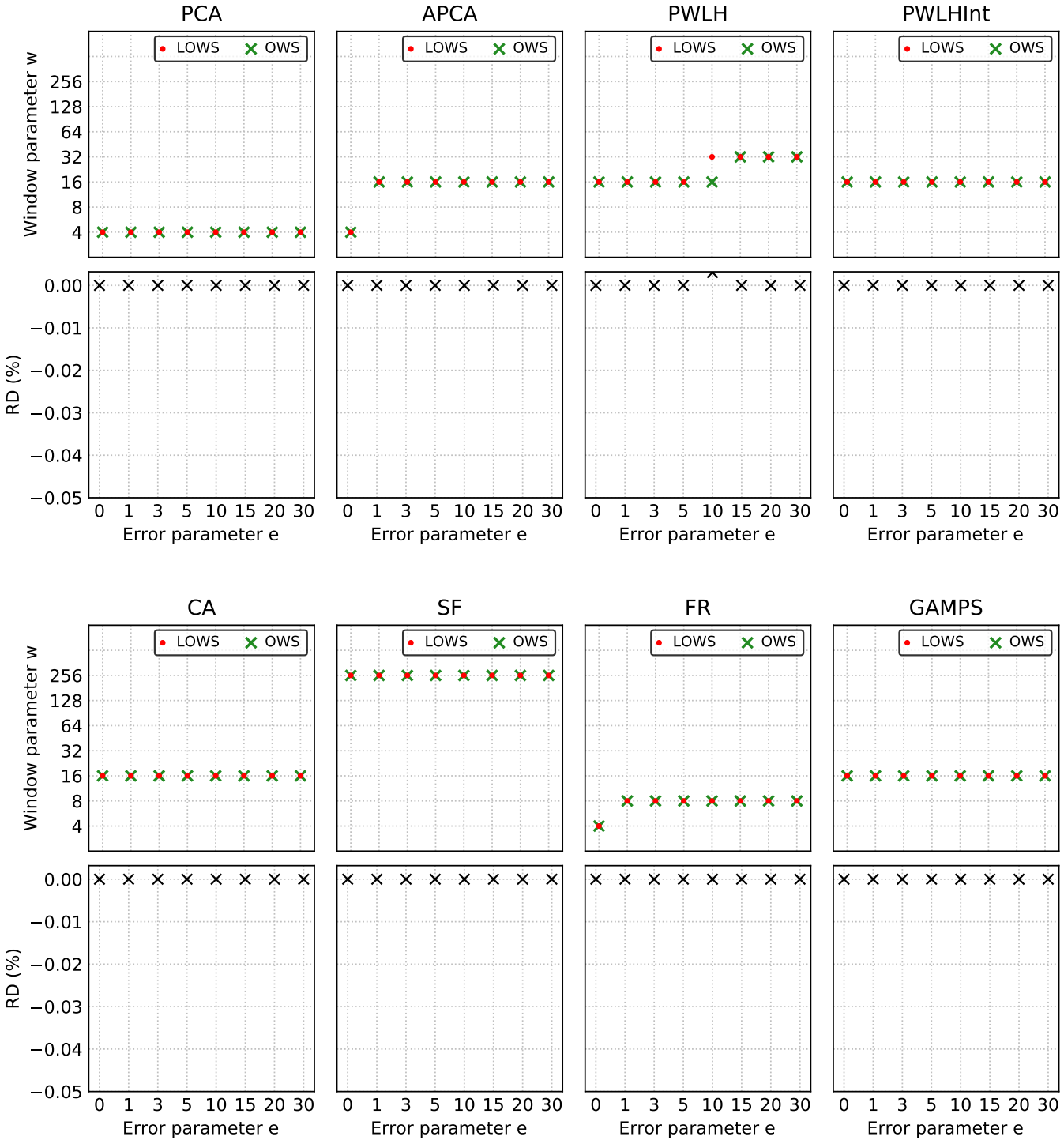

FIGURE B.18: Plots of w^*_{global}, w^*_{local}, and the RD between $c_{<a_v,w^*_{global},e>}$ and $c_{<a_v,w^*_{local},e>}$, as a function of the error parameter e, obtained for the data type "DNI" of the file "solar-2012.csv" of the dataset Solar.

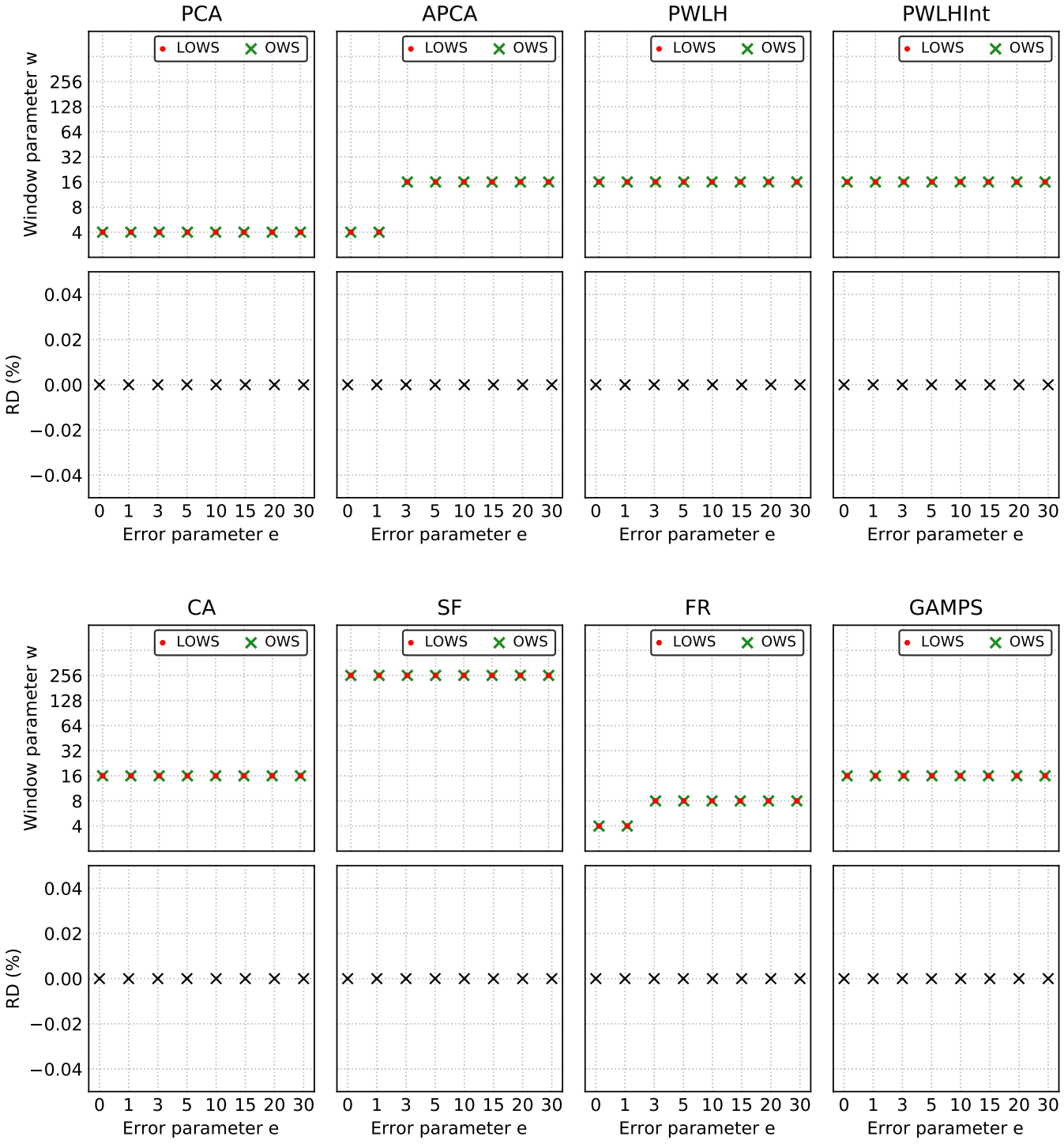

FIGURE B.19: Plots of w^*_{global}, w^*_{local}, and the RD between $c_{<a_v,w^*_{global},e>}$ and $c_{<a_v,w^*_{local},e>}$, as a function of the error parameter e, obtained for the data type "DHI" of the file "solar-2012.csv" of the dataset Solar.

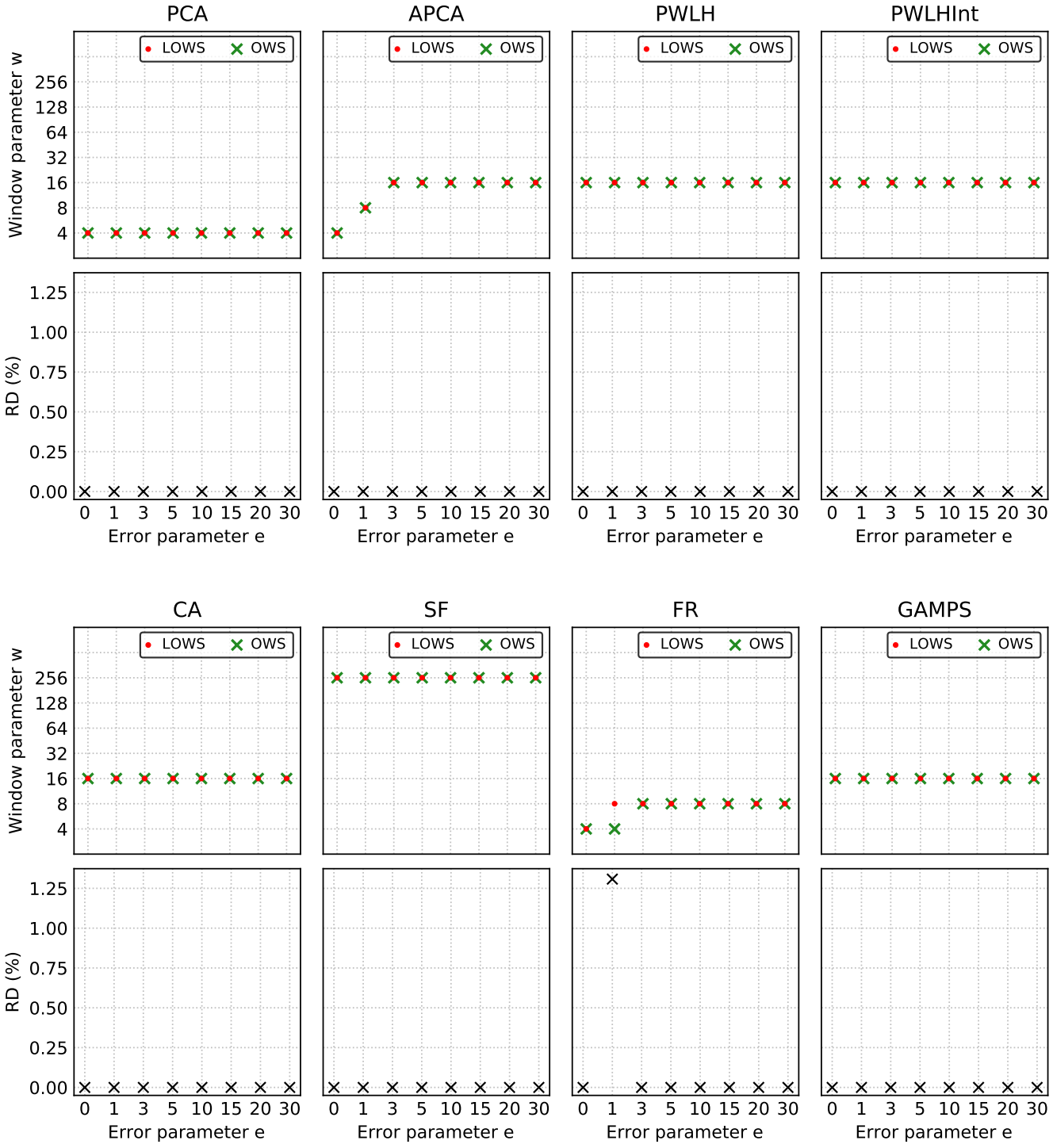

FIGURE B.20: Plots of w^*_{global}, w^*_{local}, and the RD between $c_{<a_v,w^*_{global},e>}$ and $c_{<a_v,w^*_{local},e>}$, as a function of the error parameter e, obtained for the data type "GHI" of the file "solar-2013.csv" of the dataset Solar.

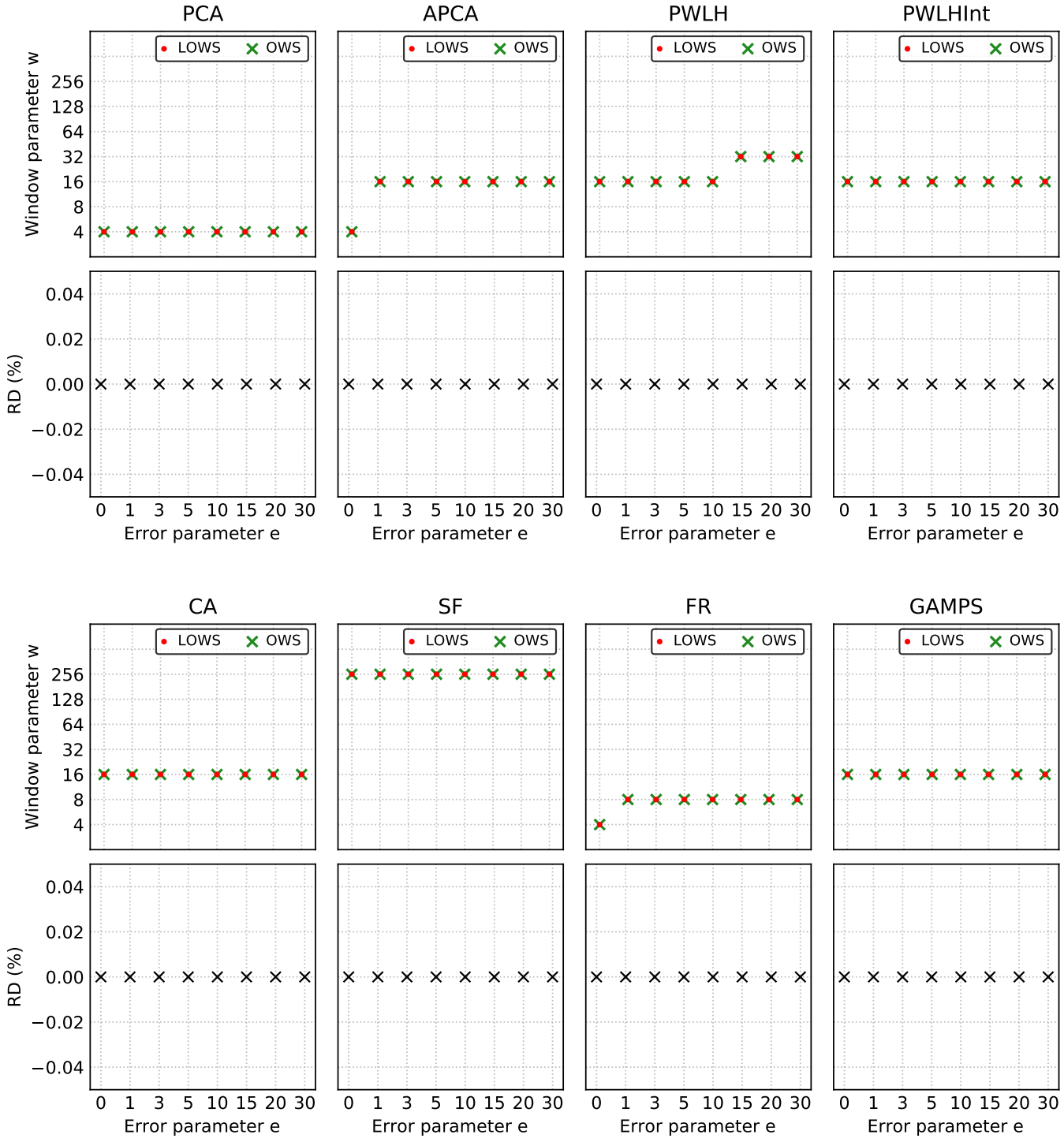

FIGURE B.21: Plots of w^*_{global}, w^*_{local}, and the RD between $c_{<a_v,w^*_{global},e>}$ and $c_{<a_v,w^*_{local},e>}$, as a function of the error parameter e, obtained for the data type "DNI" of the file "solar-2013.csv" of the dataset Solar.

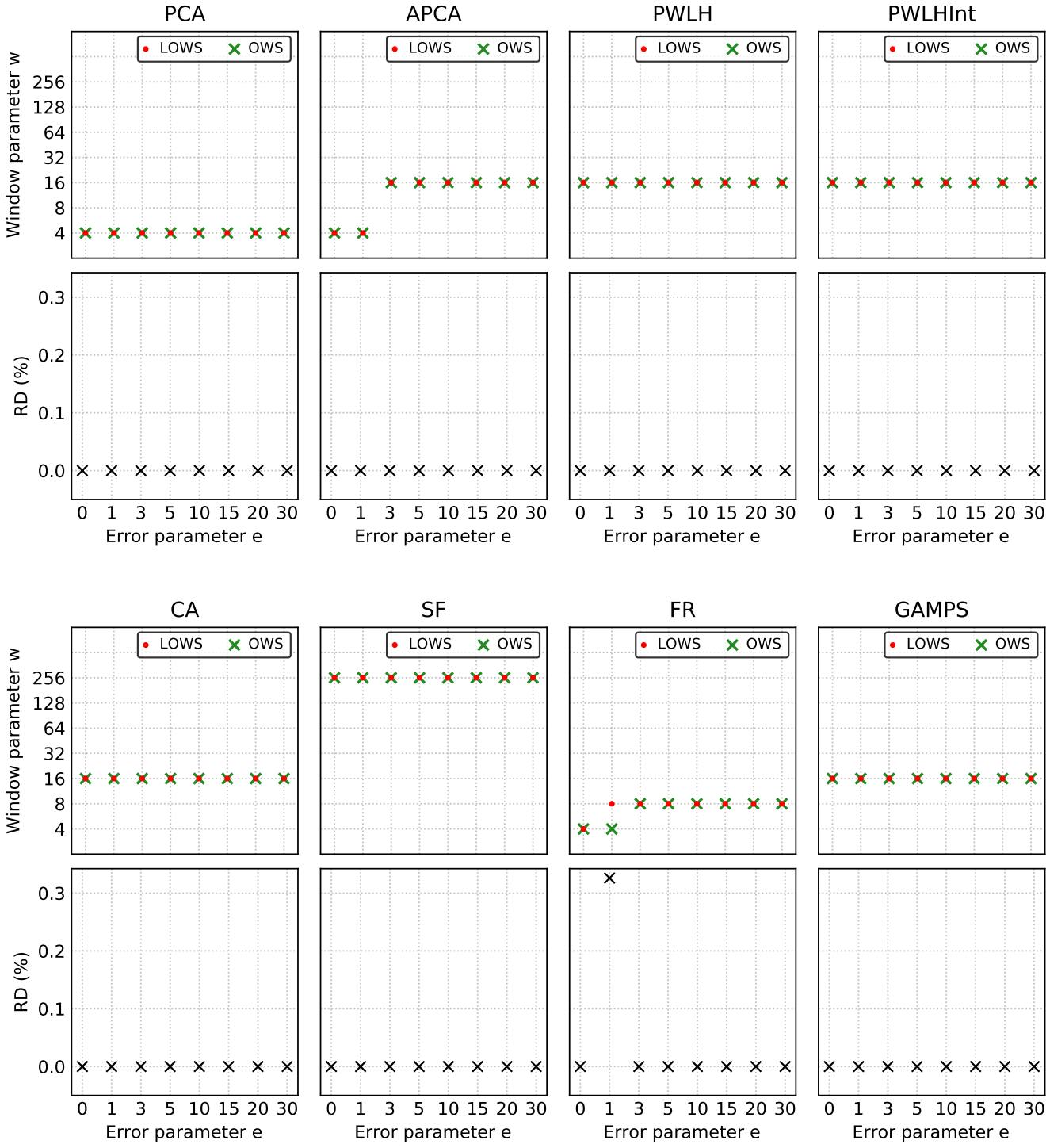

FIGURE B.22: Plots of w^*_{global}, w^*_{local}, and the RD between $c_{<a_v,w^*_{global},e>}$ and $c_{<a_v,w^*_{local},e>}$, as a function of the error parameter e, obtained for the data type "DHI" of the file "solar-2013.csv" of the dataset Solar.

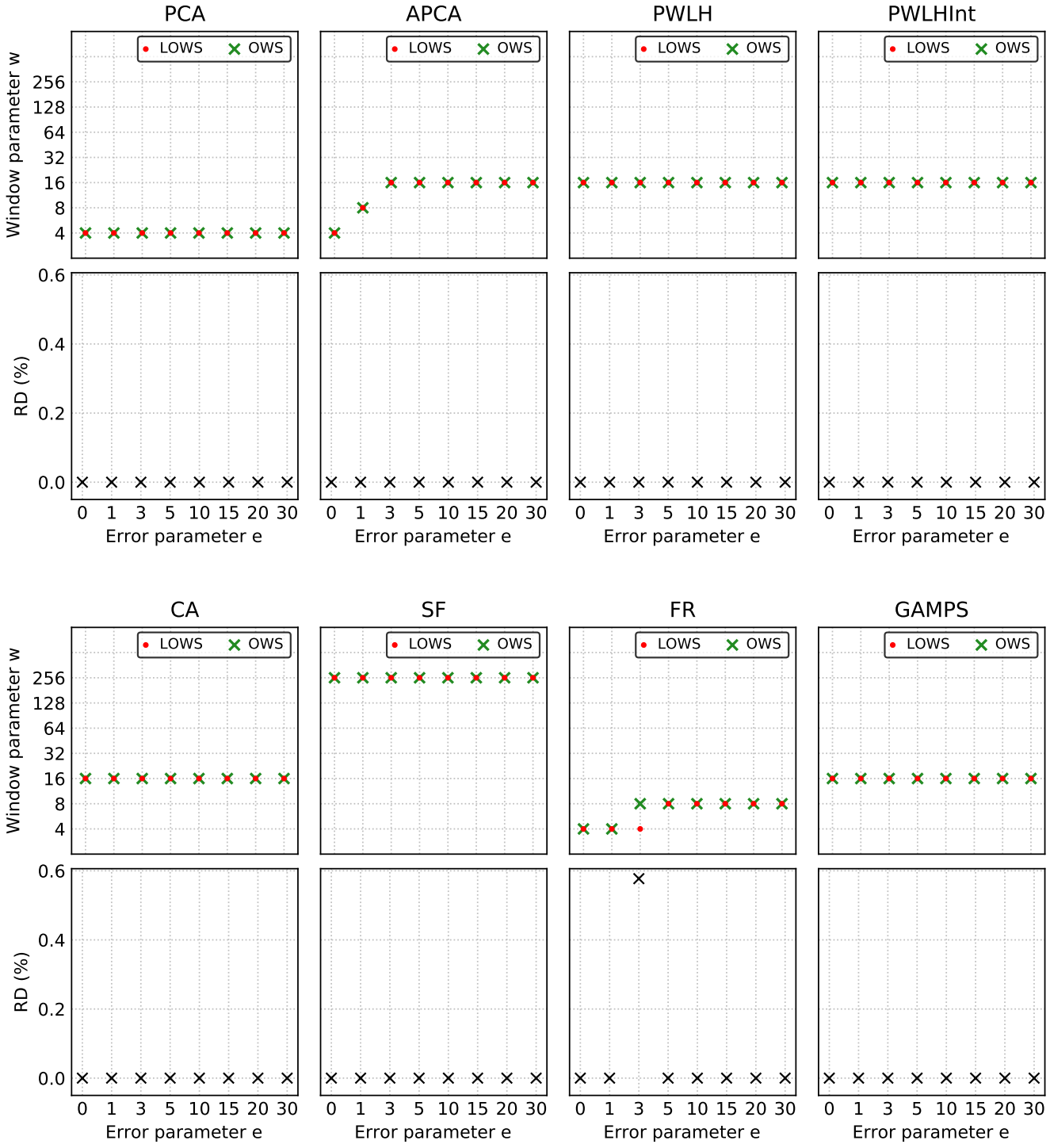

FIGURE B.23: Plots of w^*_{global}, w^*_{local}, and the RD between $c_{<a_v,w^*_{global},e>}$ and $c_{<a_v,w^*_{local},e>}$, as a function of the error parameter e, obtained for the data type "GHI" of the file "solar-2014.csv" of the dataset Solar.

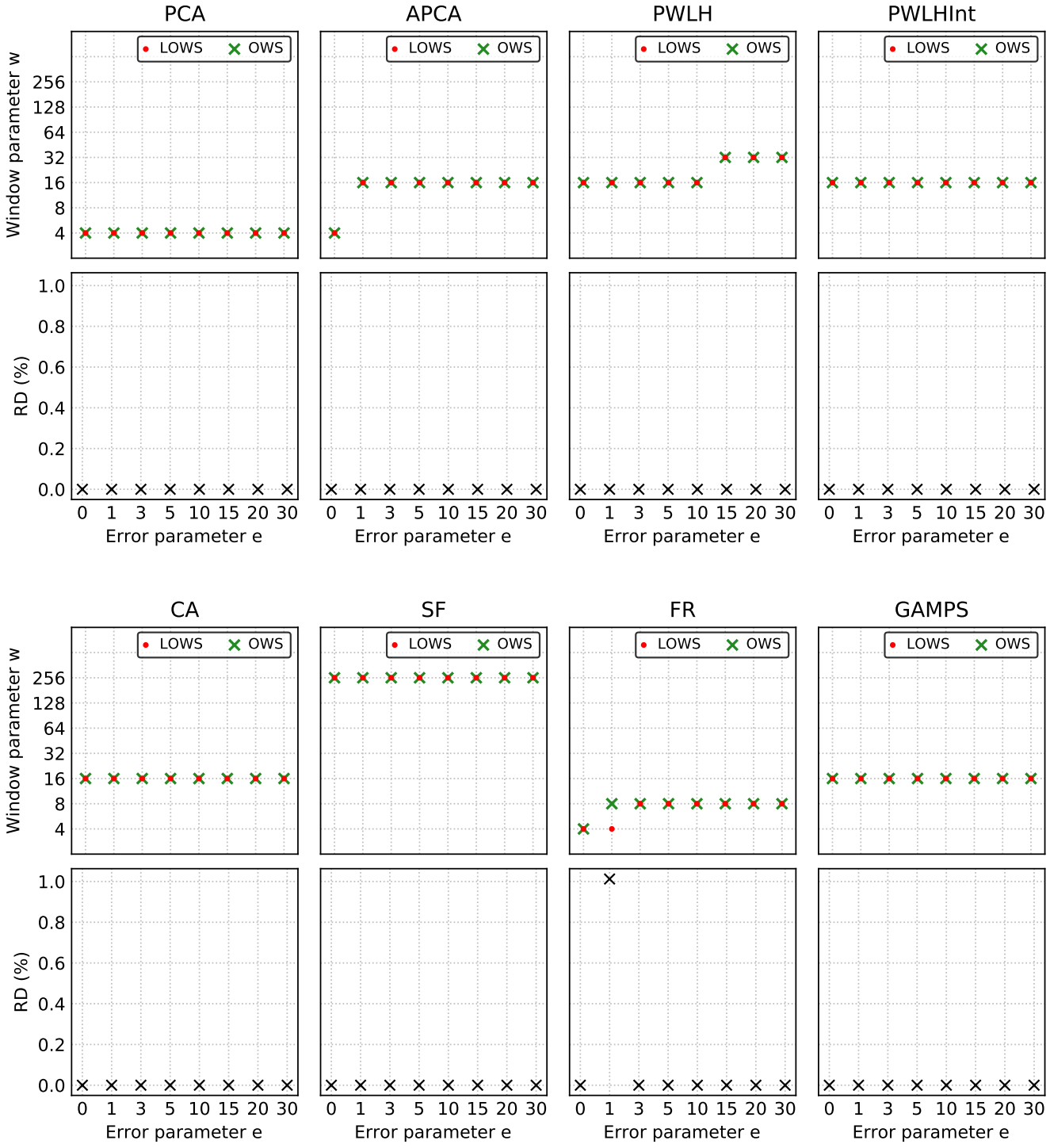

FIGURE B.24: Plots of w^*_{global}, w^*_{local}, and the RD between $c_{<a_v,w^*_{global},e>}$ and $c_{<a_v,w^*_{local},e>}$, as a function of the error parameter e, obtained for the data type "DNI" of the file "solar-2014.csv" of the dataset Solar.

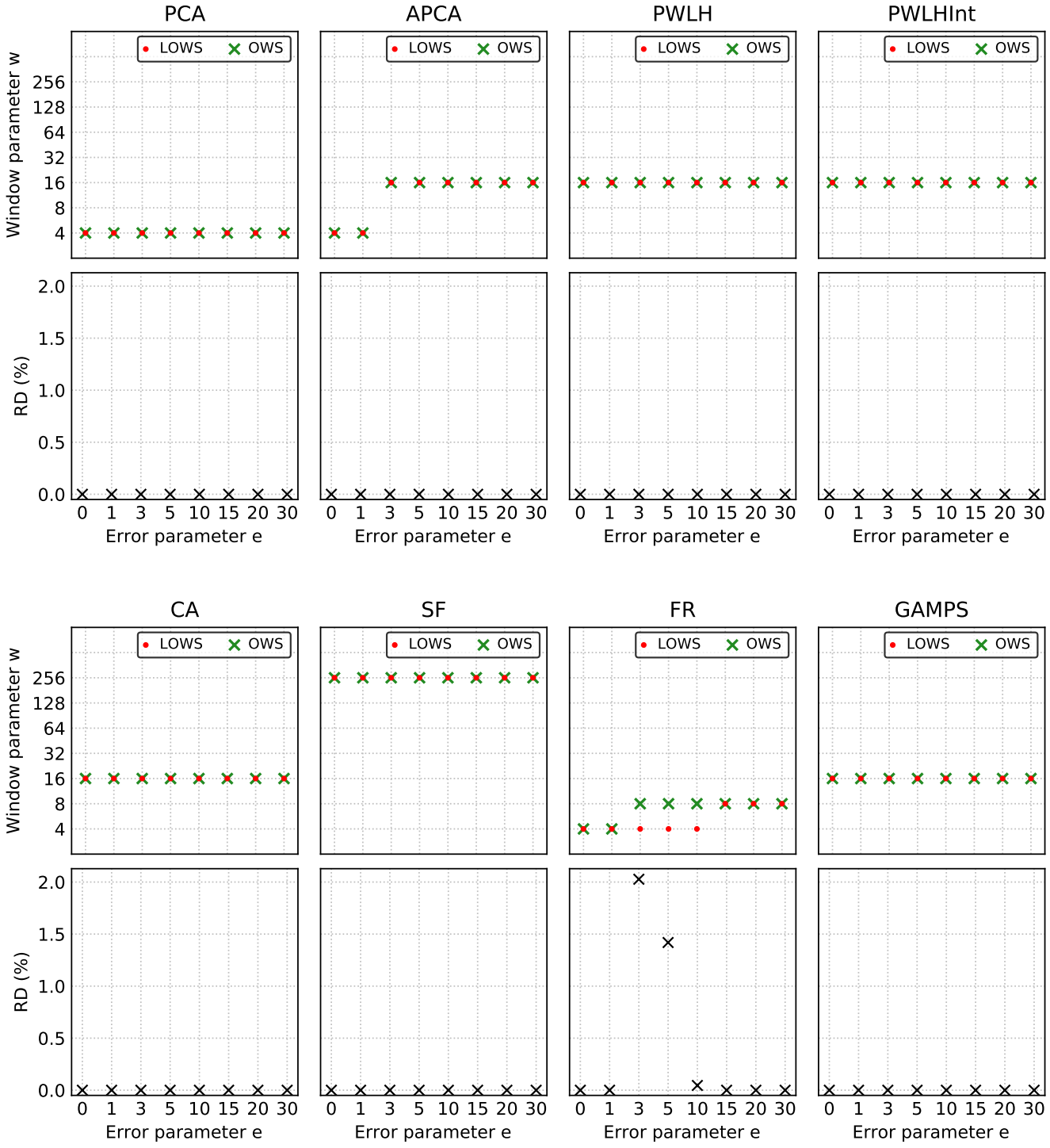

FIGURE B.25: Plots of w^*_{global}, w^*_{local}, and the RD between $c_{<a_v,w^*_{global},e>}$ and $c_{<a_v,w^*_{local},e>}$, as a function of the error parameter e, obtained for the data type "DHI" of the file "solar-2014.csv" of the dataset Solar.

Appendix C

Figures: Algorithm Compression Performance

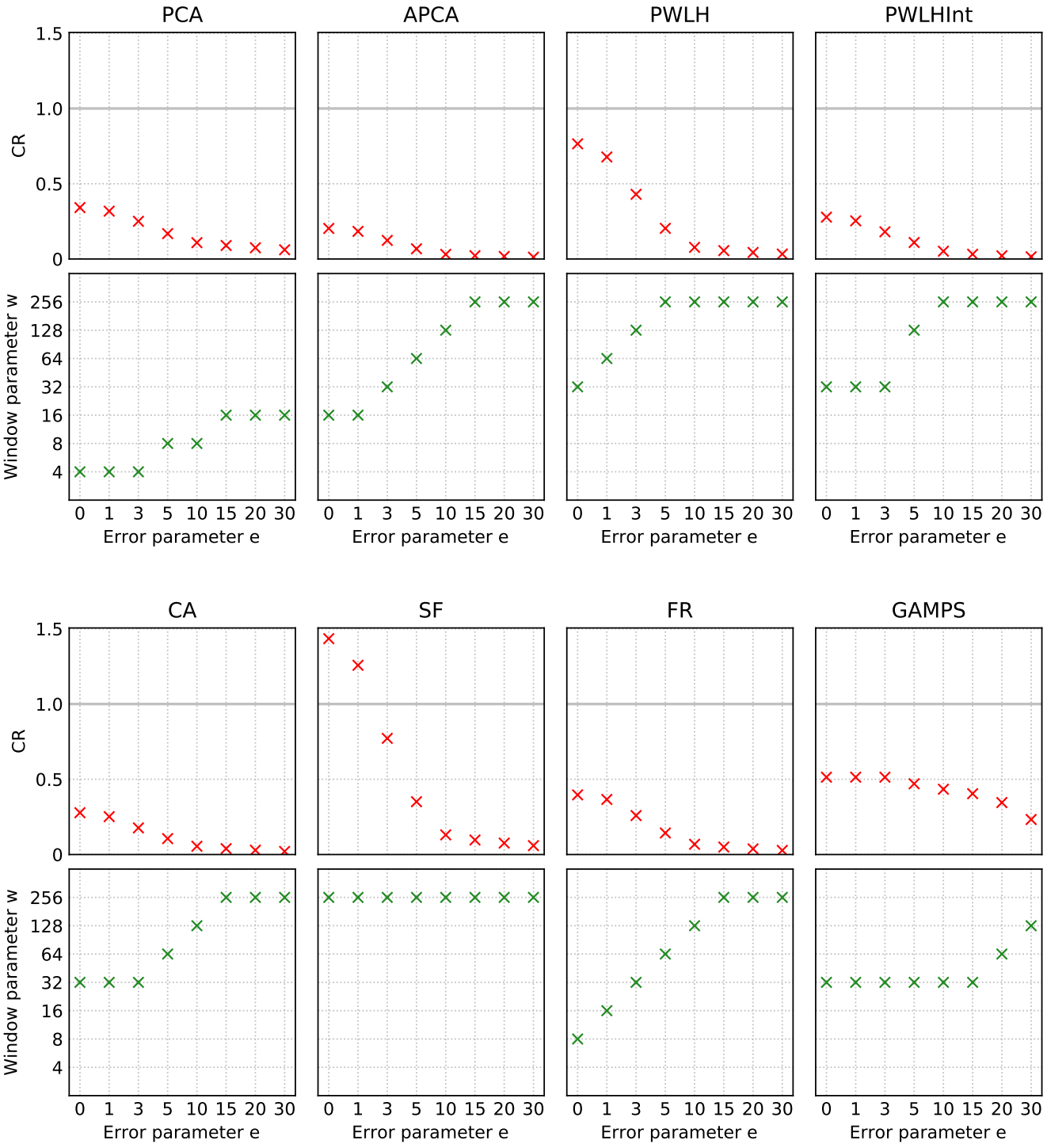

FIGURE C.1: CR and window size parameter plots for every evaluated algorithm, for the data type "VWC" of the dataset IRKIS.

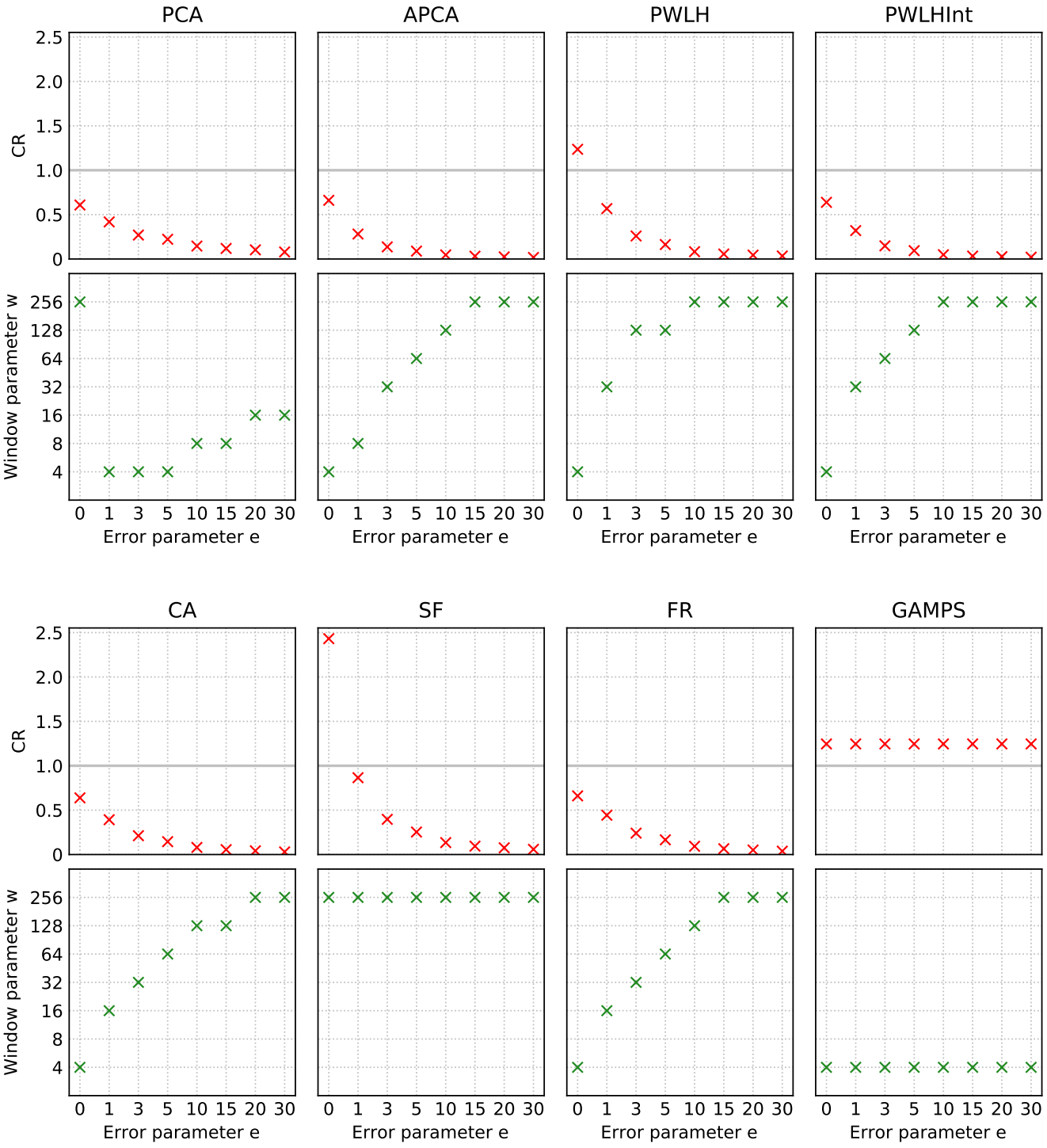

FIGURE C.2: CR and window size parameter plots for every evaluated algorithm, for the data type "SST" of the dataset SST.

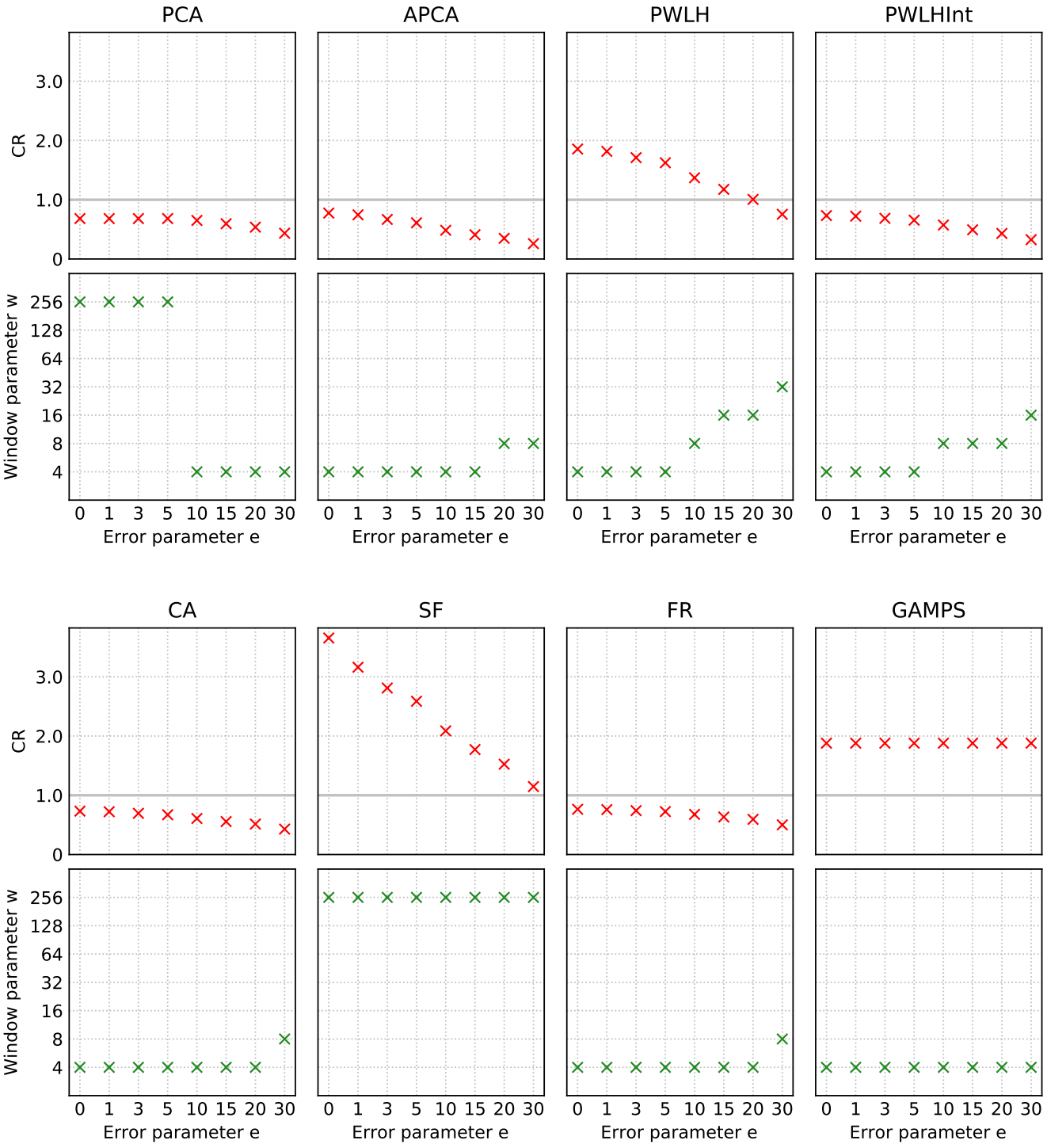

FIGURE C.3: CR and window size parameter plots for every evaluated algorithm, for the data type "Velocity" of the dataset ADCP.

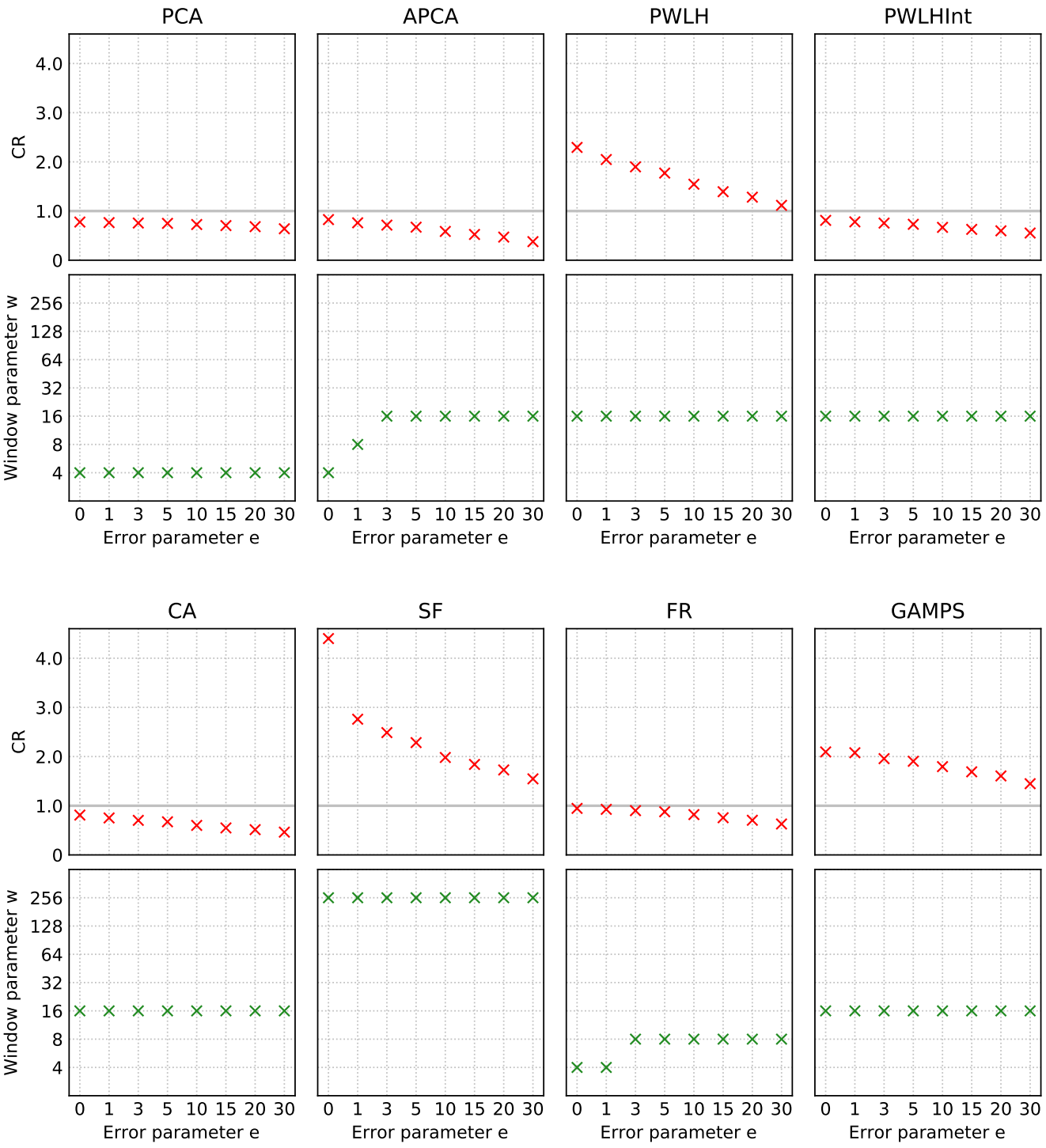

FIGURE C.4: CR and window size parameter plots for every evaluated algorithm, for the data type "GHI" of the dataset Solar.

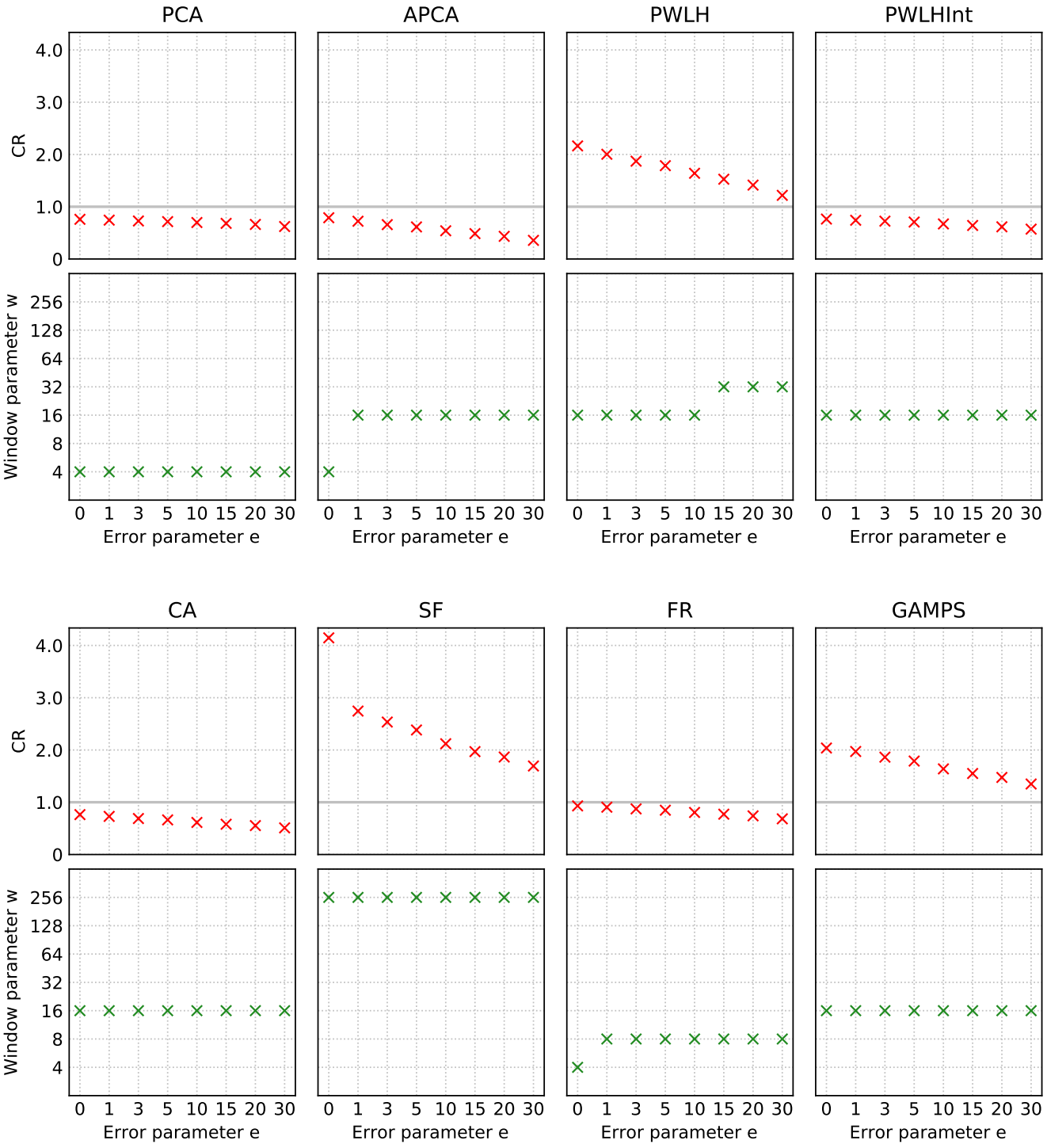

FIGURE C.5: CR and window size parameter plots for every evaluated algorithm, for the data type "DNI" of the dataset Solar.

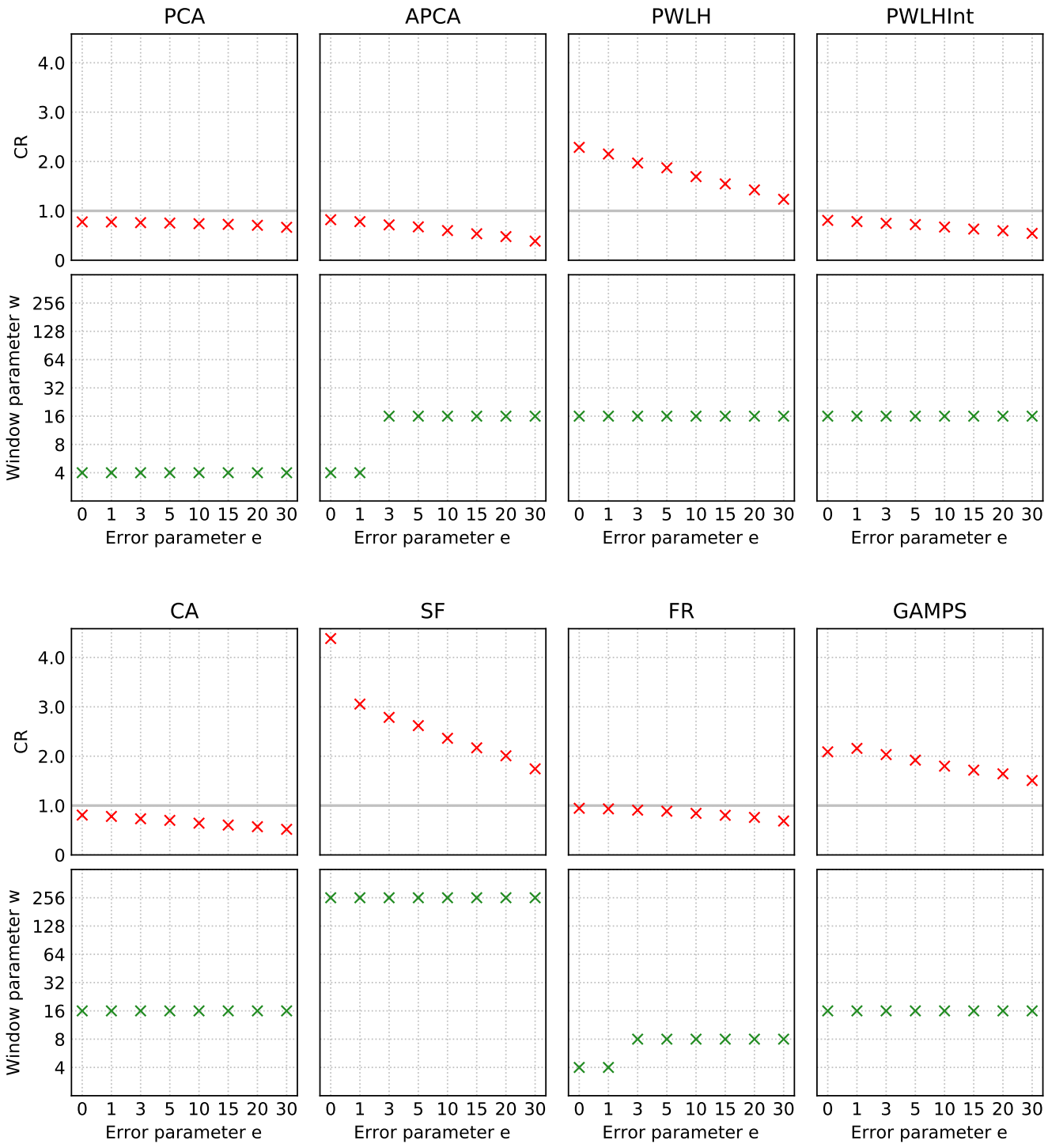

FIGURE C.6: CR and window size parameter plots for every evaluated algorithm, for the data type "DHI" of the dataset Solar.

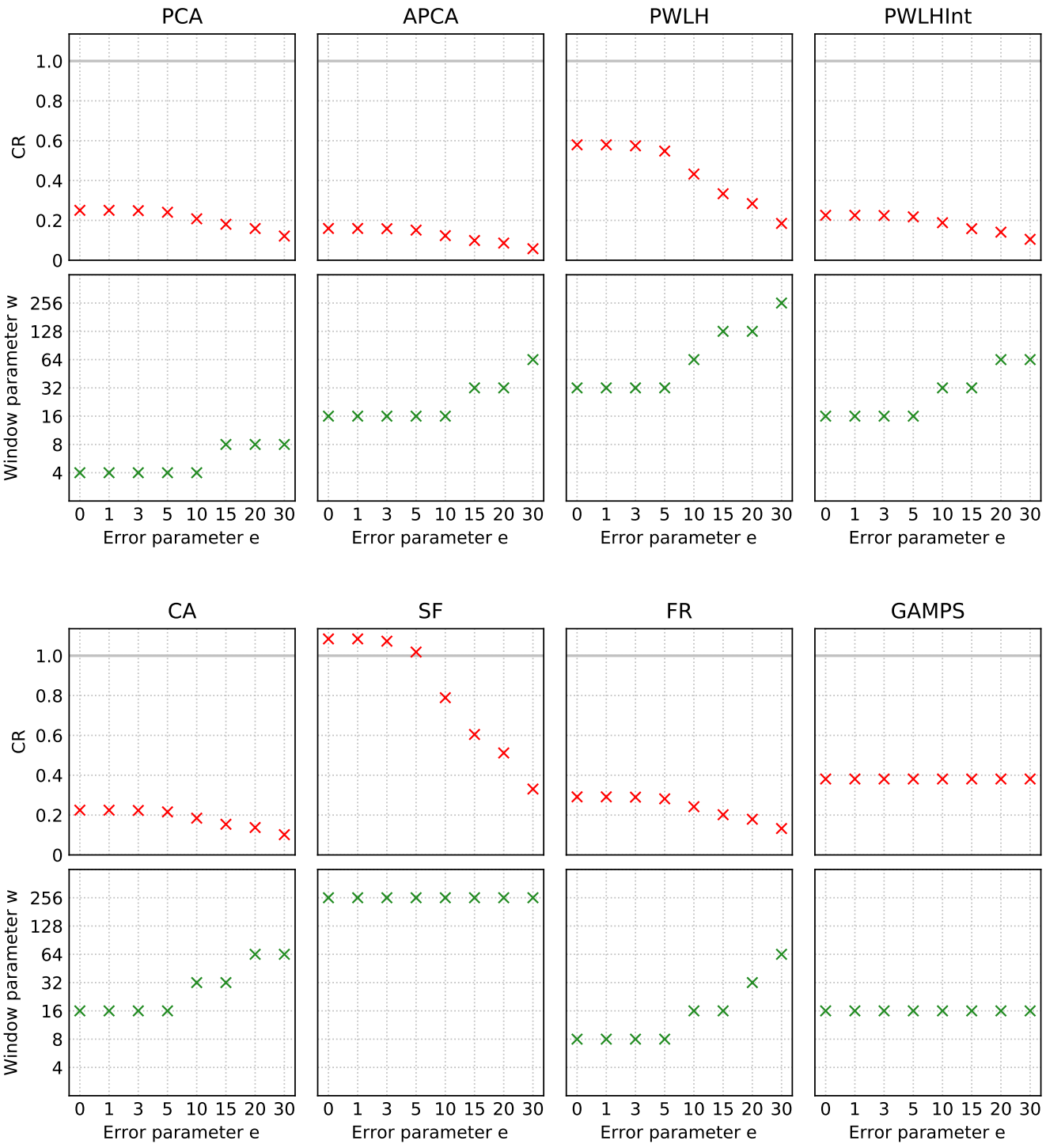

FIGURE C.7: CR and window size parameter plots for every evaluated algorithm, for the data type "Latitude" of the dataset ElNino.

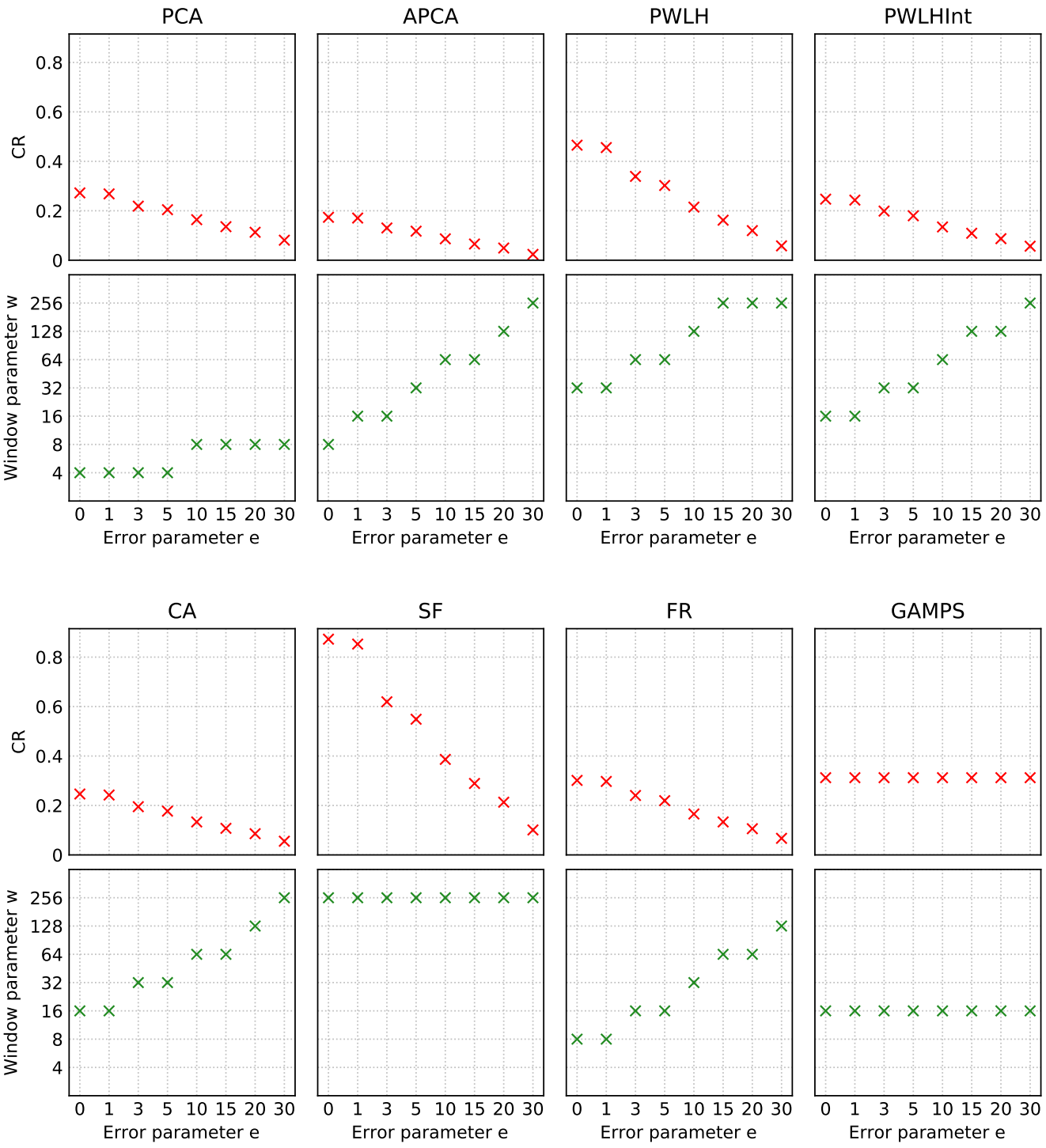

FIGURE C.8: CR and window size parameter plots for every evaluated algorithm, for the data type "Longitude" of the dataset ElNino.

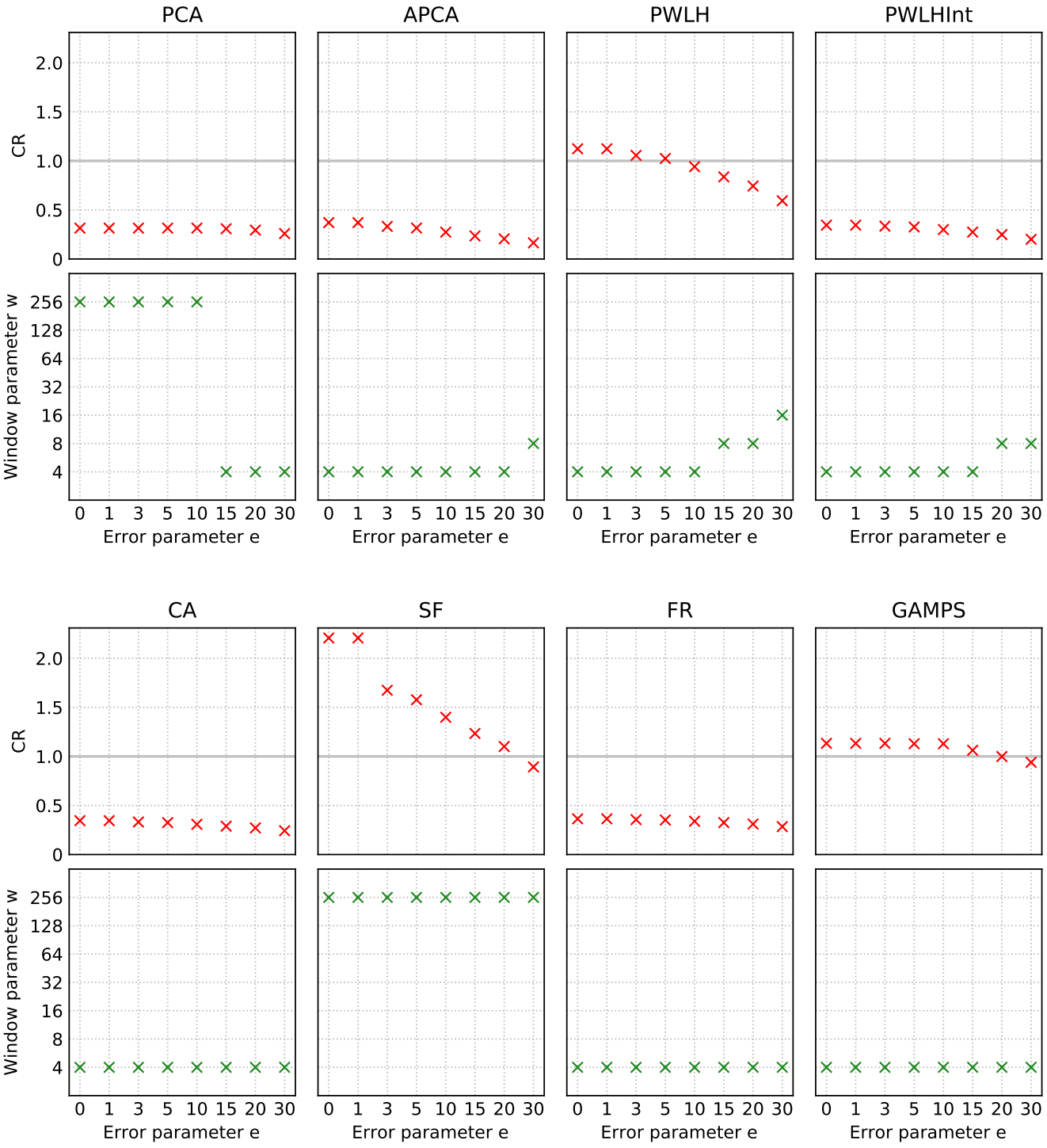

FIGURE C.9: CR and window size parameter plots for every evaluated algorithm, for the data type "Zon. Wind" of the dataset ElNino.

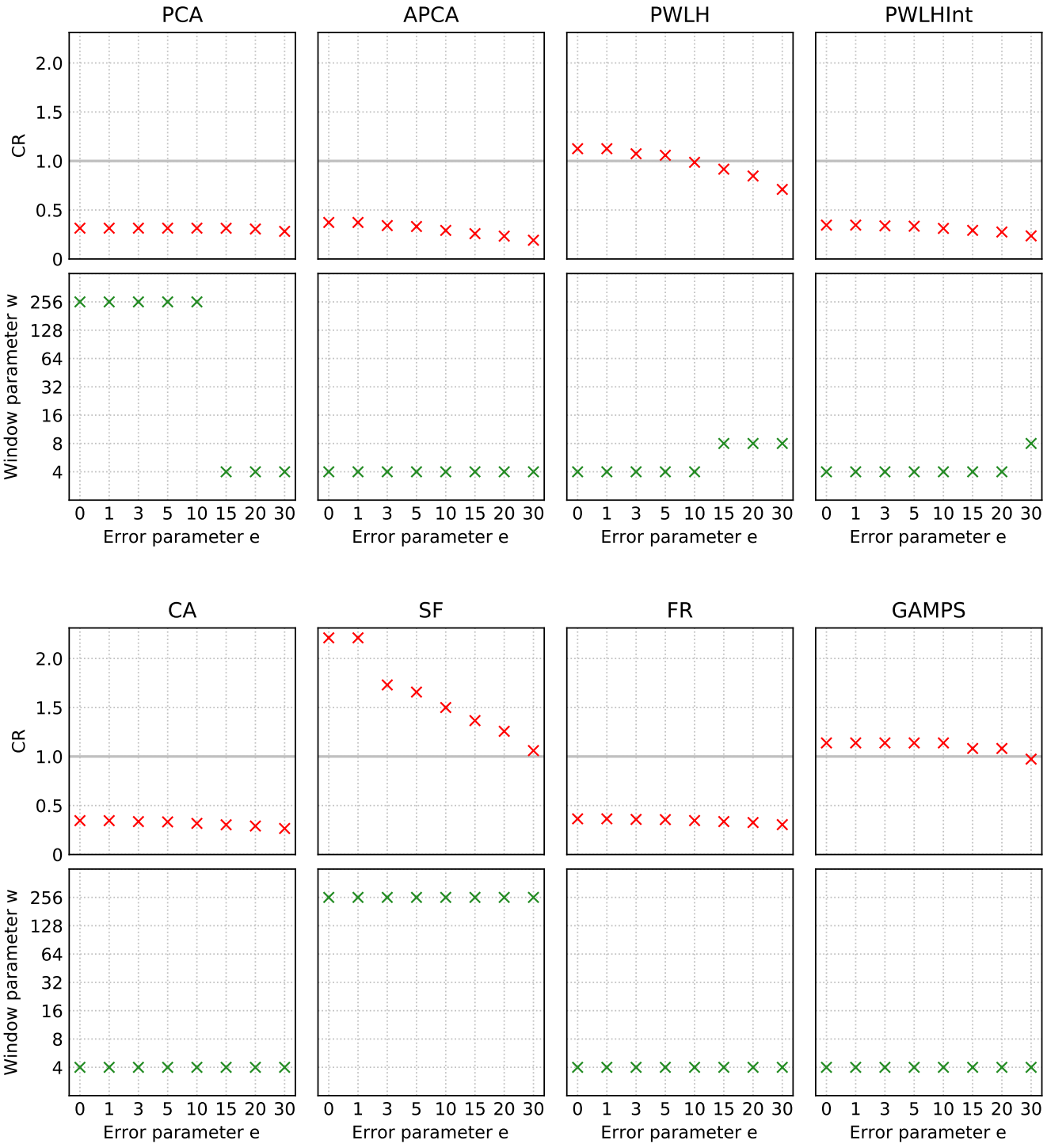

FIGURE C.10: CR and window size parameter plots for every evaluated algorithm, for the data type "Mer. Wind" of the dataset ElNino.

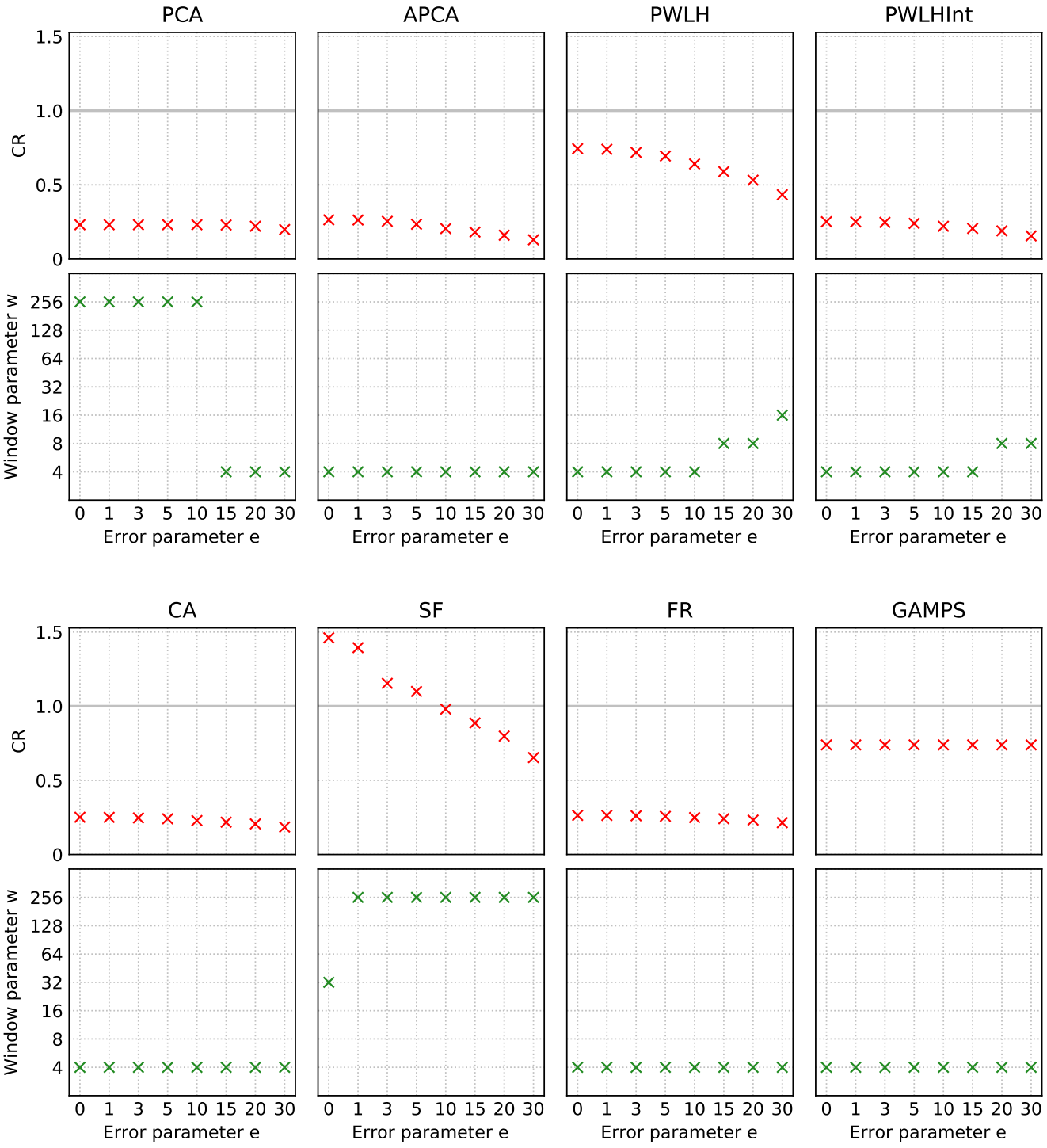

FIGURE C.11: CR and window size parameter plots for every evaluated algorithm, for the data type "Humidity" of the dataset ElNino.

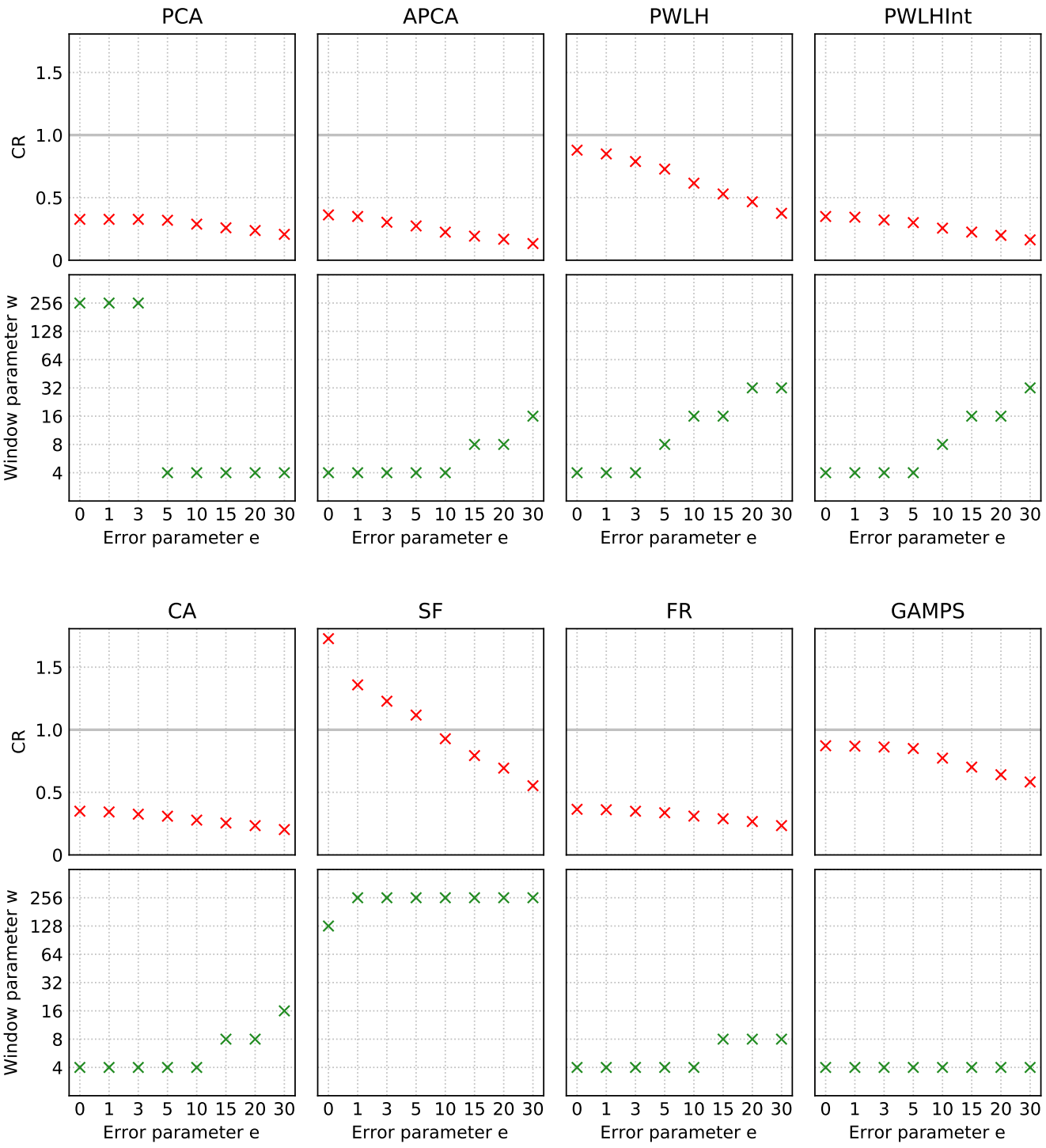

FIGURE C.12: CR and window size parameter plots for every evaluated algorithm, for the data type "Air Temp." of the dataset ElNino.

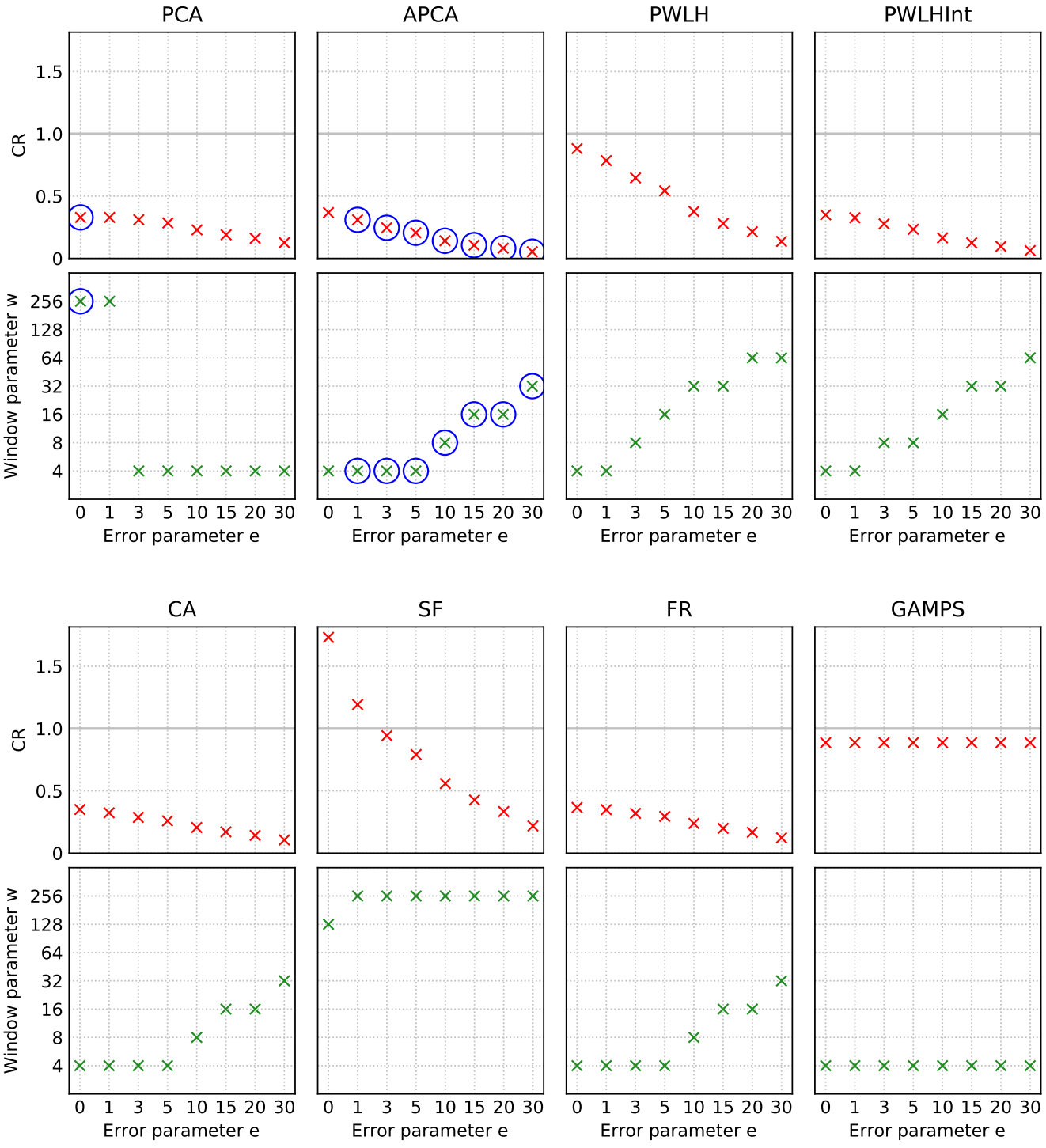

FIGURE C.13: CR and window size parameter plots for every evaluated algorithm, for the data type "Sea Temp." of the dataset ElNino. For each error parameter $e \in E$, we use blue circles to highlight the markers for the minimum CR value and the best window size (in the respective plots corresponding to the best coding variant).

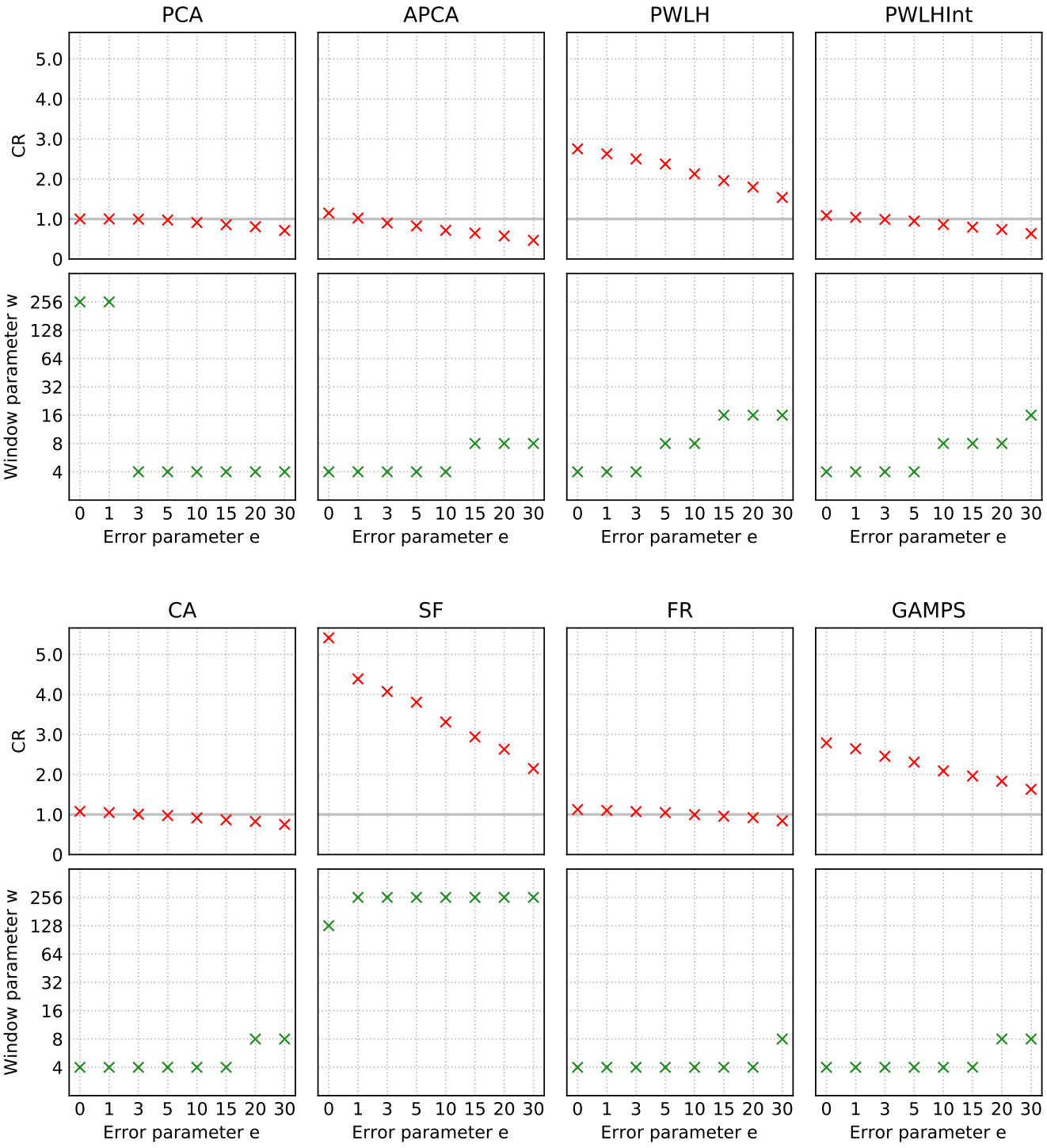

FIGURE C.14: CR and window size parameter plots for every evaluated algorithm, for the data type "Latitude" of the dataset Hail.

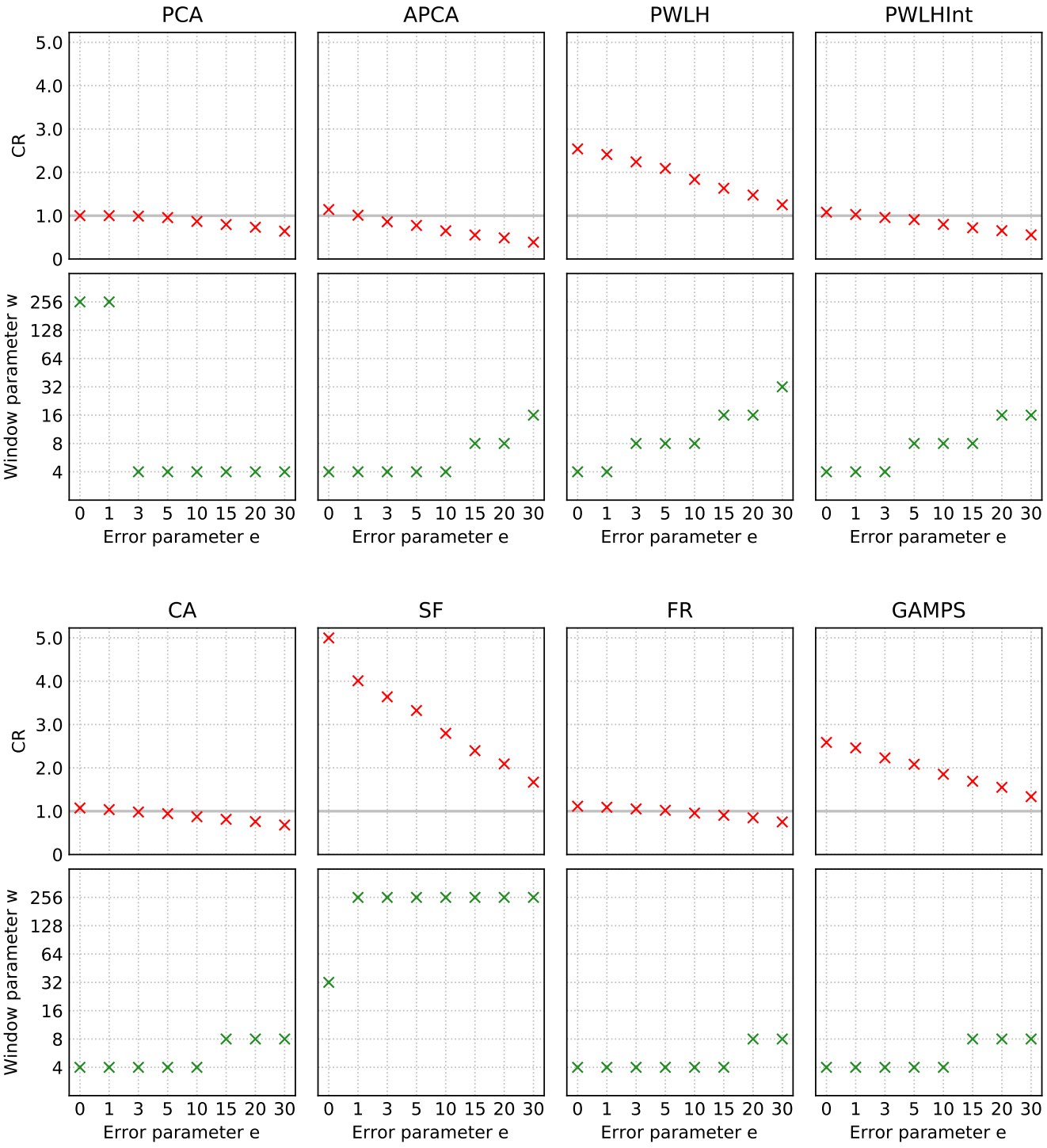

FIGURE C.15: CR and window size parameter plots for every evaluated algorithm, for the data type "Longitude" of the dataset Hail.

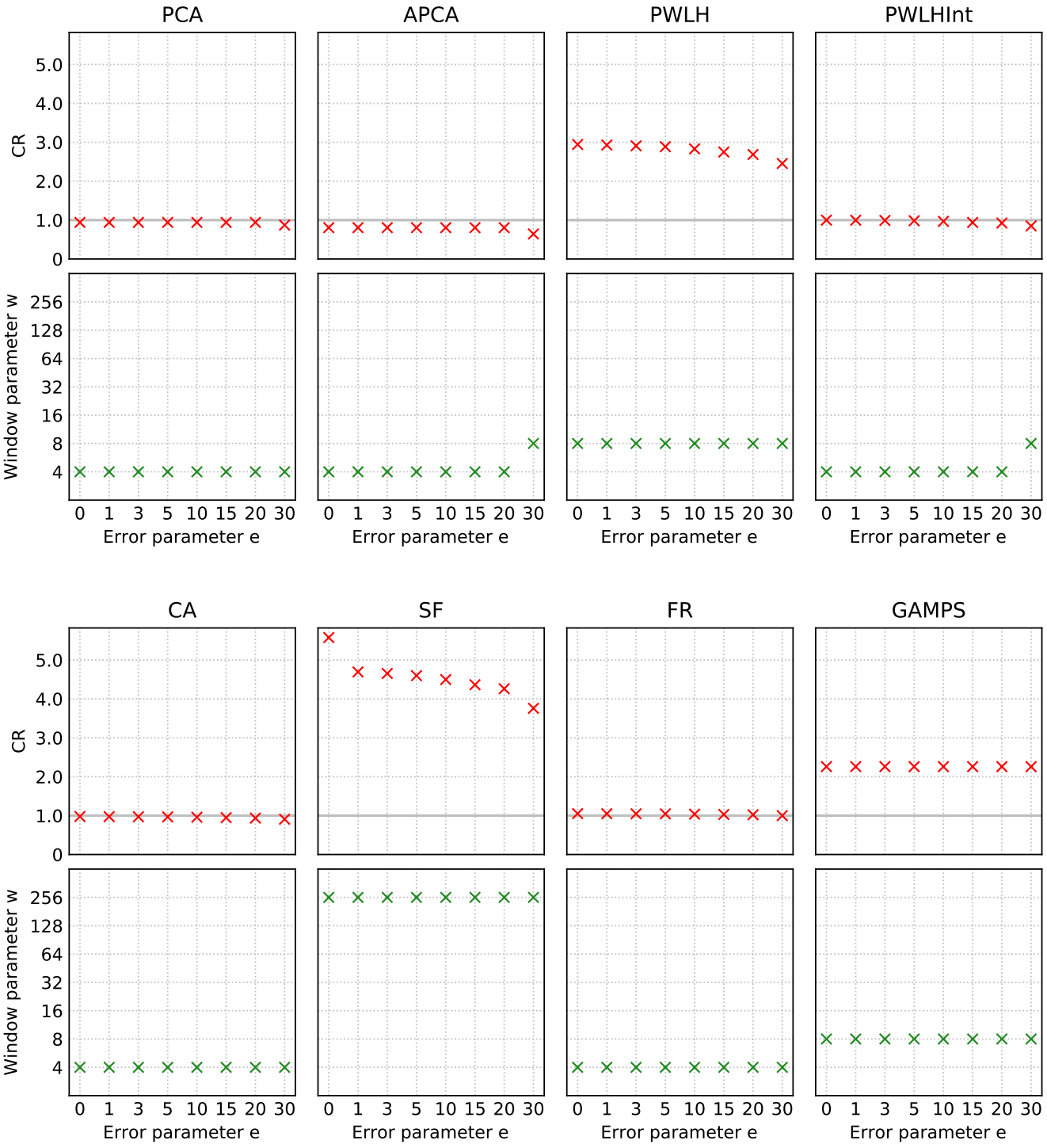

FIGURE C.16: CR and window size parameter plots for every evaluated algorithm, for the data type "Size" of the dataset Hail.

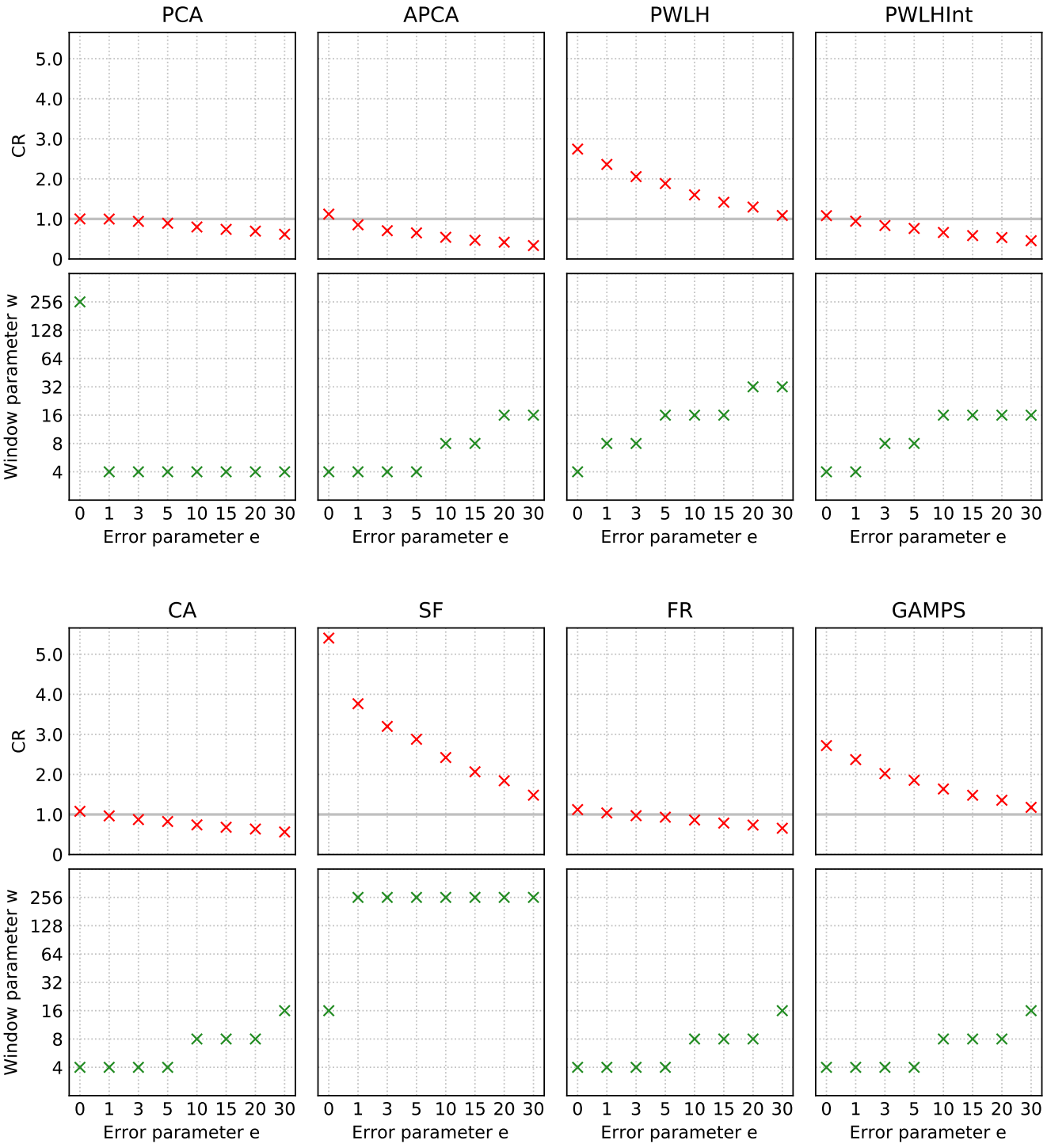

FIGURE C.17: CR and window size parameter plots for every evaluated algorithm, for the data type "Latitude" of the dataset Tornado.

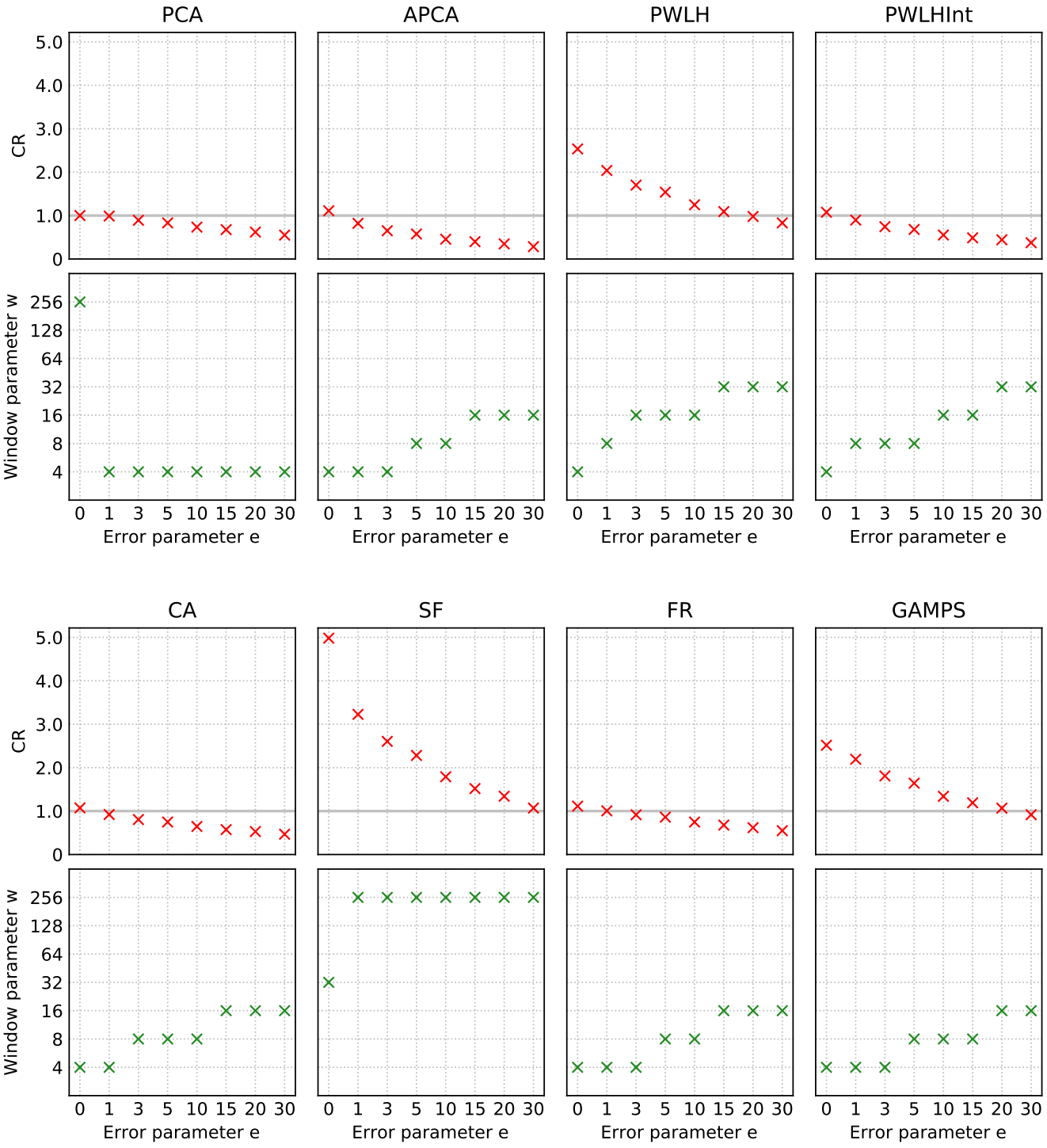

FIGURE C.18: CR and window size parameter plots for every evaluated algorithm, for the data type "Longitude" of the dataset Tornado.

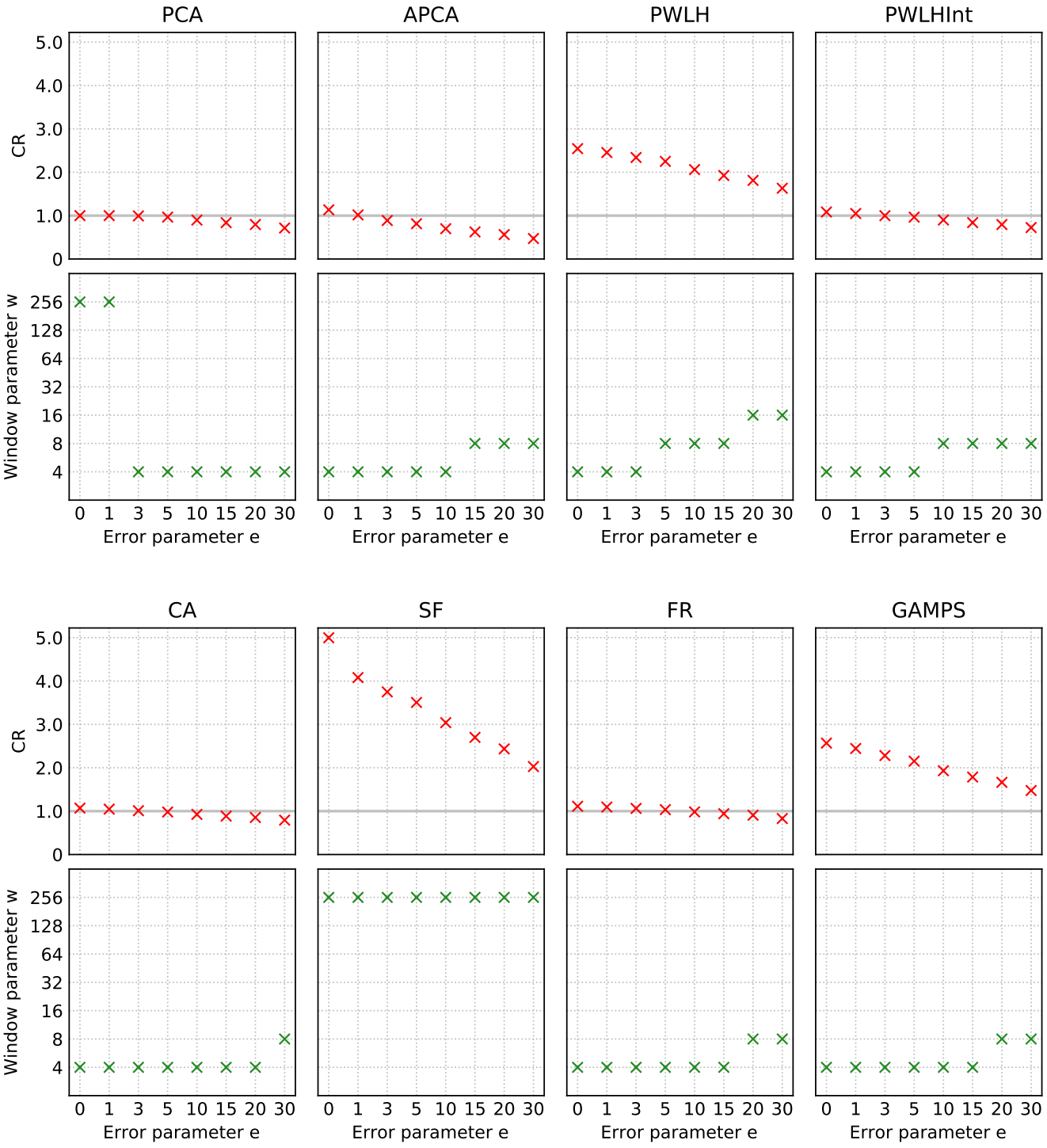

FIGURE C.19: CR and window size parameter plots for every evaluated algorithm, for the data type "Latitude" of the dataset Wind.

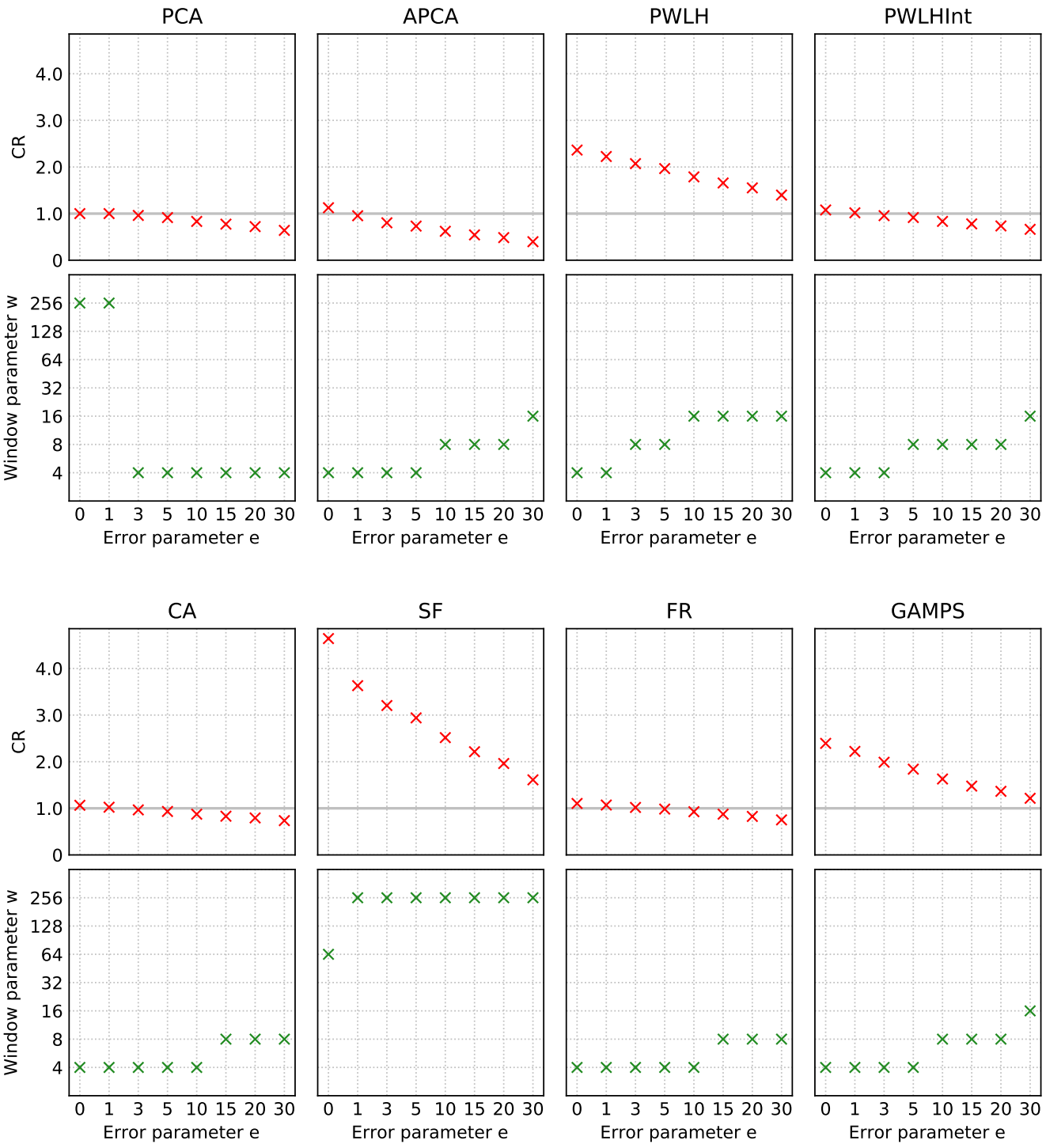

FIGURE C.20: CR and window size parameter plots for every evaluated algorithm, for the data type "Longitude" of the dataset Wind.

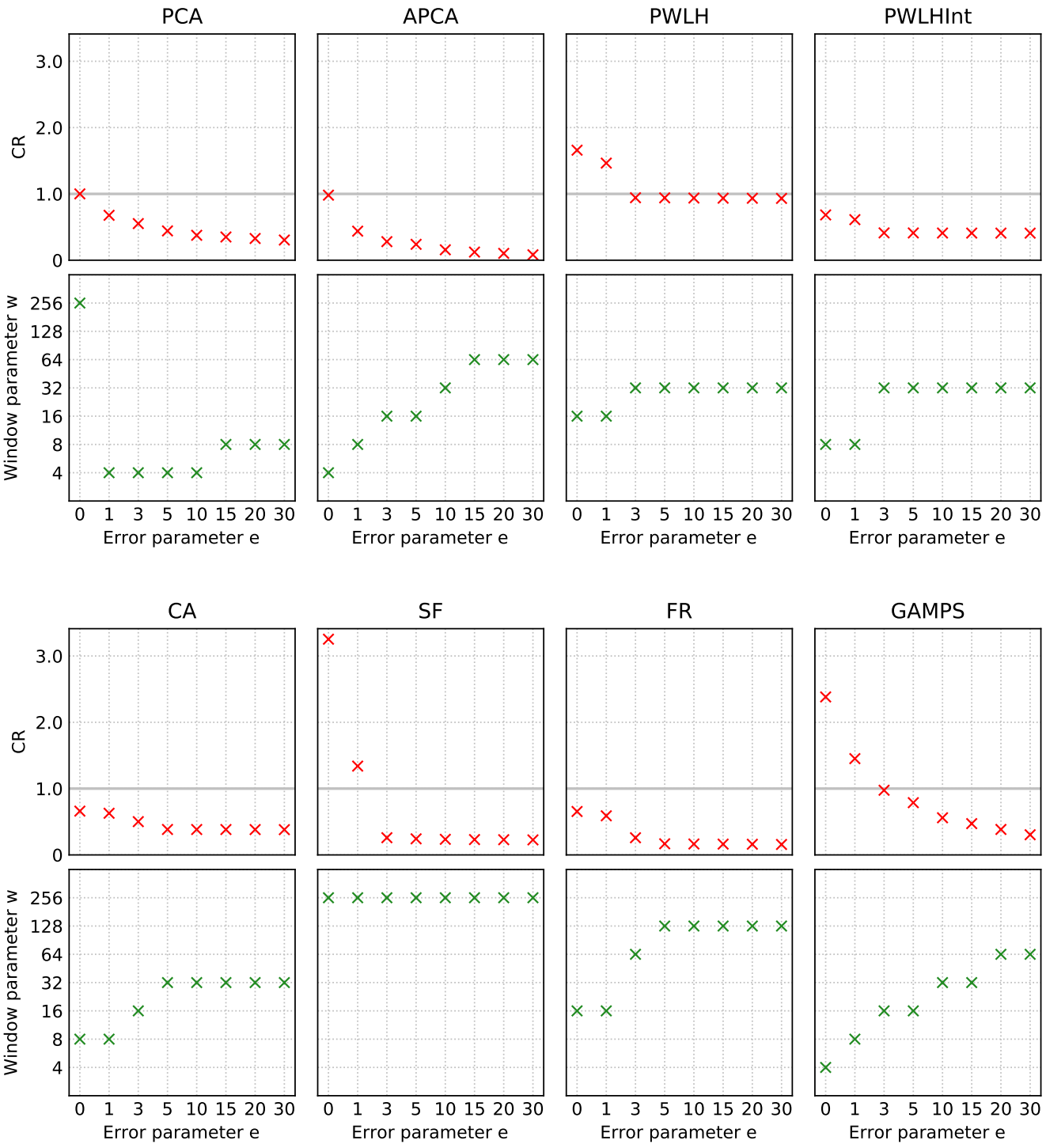

FIGURE C.21: CR and window size parameter plots for every evaluated algorithm, for the data type "Speed" of the dataset Wind.